

Jordan Journal of
P H Y S I C S

An International Peer-Reviewed Research Journal

Volume 4, No. 1, 2011, 1432 H

Jordan Journal of Physics (JJP): An International Peer-Reviewed Research Journal established by the Higher Research Committee, Ministry of Higher Education & Scientific Research, Jordan, and published quarterly by the Deanship of Research & Graduate Studies, Yarmouk University, Irbid, Jordan.

EDITOR-IN-CHIEF:

Ibrahim O. Abu Al-Jarayesh

Department of Physics, Yarmouk University, Irbid, Jordan.

ijaraysh@yu.edu.jo

EDITORIAL BOARD:

Dia-Eddin M. Arafah

Department of Physics, University of Jordan, Amman, Jordan.

darafah@ju.edu.jo

Nabil Y. Ayoub

Department of Physics, Yarmouk University, Irbid, Jordan.

nayoub@yu.edu.jo

Hisham B. Ghassib

Princess Sumaya University for Technology, Amman, Jordan.

ghassib@psut.edu.jo

Jamil M. Khalifeh

Department of Physics, University of Jordan, Amman, Jordan.

jkalifa@ju.edu.jo

Sami H. Mahmood

Department of Physics, University of Jordan, Amman, Jordan.

s.mahmood@ju.edu.jo

Marwan S. Mousa

Department of Physics, Mu'tah University, Al-Karak, Jordan.

mmousa@mutah.edu.jo

Nihad A. Yusuf

Department of Physics, Yarmouk University, Irbid, Jordan.

nihadyusuf@yu.edu.jo

Khalaf A. Al-Masaid

Department of Applied Physical Sciences, Jordan University Of Science And Technology, Irbid, Jordan.

khalaf@just.edu.jo

EDITORIAL SECRETARY: Majdi Al-Shannaq.

Manuscripts should be submitted to:

Prof. Ibrahim O. Abu Al-Jarayesh
Editor-in-Chief, Jordan Journal of Physics
Deanship of Research and Graduate Studies
Yarmouk University-Irbid-Jordan
Tel. 00 962 2 7211111 Ext. 2075
E-mail: jjp@yu.edu.jo
Website: <http://Journals.yu.edu.jo/jjp>

Jordan Journal of
P H Y S I C S

An International Peer-Reviewed Research Journal

Volume 4, No. 1, 2011, 1432 H

INTERNATIONAL ADVISORY BOARD

Prof. Dr. Ahmad Saleh

Department of Physics, Yarmouk University, Irbid, Jordan.
salema@yu.edu.jo

Prof. Dr. Aurore Savoy-Navarro

LPNHE Université de Paris 6/IN2P3-CNRS, Tour 33, RdC 4,
Place Jussieu, F 75252, Paris Cedex 05, France.
auore@lpnhep.in2p3.fr

Prof. Dr. Bernard Barbara

Laboratoire Louis Neel, Salle/Room: D 108, 25, Avenue des
Martyrs BP 166, 38042-Grenoble Cedex 9, France.
Barbara@grenoble.cnrs.fr

Prof. Dr. Bruno Guiderdoni

Observatoire Astronomique de Lyon, g, avenue Ch. Antre-F-69561,
Saint Genis Laval Cedex, France.
Bruno.guiderdoni@olos.univ-lyon1.fr

Prof. Dr. Buford Price

Physics Department, University of California, Berkeley, CA 94720,
U. S. A.
bprice@berkeley.edu

Prof. Dr. Colin Cough

School of Physics and Astronomy, University of Birmingham, B15
2TT, U. K.
c.cough@bham.ac.uk

Prof. Dr. Desmond Cook

Department of Physics, Condensed Matter and Materials Physics
Research Group, Old Dominion University, Norfolk, Virginia
23529, U. S. A.
Dcook@physics.odu.edu

Prof. Dr. Evgeny Sheshin

MIPT, Institutskij per. 9, Dogoprudnyi 141700, Russia.
sheshin@lafaet.mipt.ru

Prof. Dr. Hans Ott

Laboratorium Fuer Festkorperphysik, ETH Honggerberg, CH-
8093 Zurich, Switzerland.
ott@solid.phys.ethz.ch

Prof. Dr. Herwig Schopper

President SESAME Council, Chairman Scientific Board UNESCO
IBSP Programme, CERN, 1211 Geneva, Switzerland.
Herwig.Schopper@cern.ch

Prof. Dr. Humam Ghassib

Department of Physics, Jordan University, Amman, Jordan.
humam@atf.org.jo

Prof. Dr. Ingo Hofmann

GSI Darmstadt, Planckstr. 1, 64291, Darmstadt, Germany.
i.hofmann@gsi.de

Prof. Dr. Jozef Lipka

Department of Nuclear Physics and Technology, Slovak University
of Technology, Bratislava, Ilkovicova 3, 812 19 Bratislava,
Slovakia.
Lipka@elf.stuba.sk

Prof. Dr. Khalid Tougan

Chairman of Jordan Atomic Energy Commission, Amman, Jordan.

Prof. Dr. Mark J. Hagmann

Desert Electronics Research Corporation, 762 Lacey Way, North
Salt Lake 84064, Utah, U. S. A.
MHagmann@NewPathResearch.Com

Prof. Dr. Nasr Zubeidey

President: Al-Zaytoonah University of Jordan, Amman, Jordan.
President@alzaytoonah.edu.jo

Prof. Dr. Patrick Roudeau

Laboratoire de l'Accelérateur, Lineaire (LAL), Université Paris-
Sud 11, Batiment 200, 91898 Orsay Cedex, France.
roudeau@mail.cern.ch

Prof. Dr. Paul Chu

Department of Physics, University of Houston, Houston, Texas
77204-5005, U. S. A.
Ching-Wu.Chu@mail.uh.edu

Prof. Dr. Peter Dowben

Nebraska Center for Materials and Nanoscience, Department of
Physics and Astronomy, 255 Behlen Laboratory (10th and R
Streets), 116 Brace Lab., P. O. Box 880111, Lincoln, NE 68588-
0111, U. S. A.
pdowben@unl.edu

Prof. Dr. Peter Mulser

Institute fuer Physik, T.U. Darmstadt, Hochschulstr. 4a, 64289
Darmstadt, Germany.
Peter.mulser@physik.tu-darmstadt.de

Prof. Dr. Rasheed Azzam

Department of Electrical Engineering, University of New Orleans
New Orleans, Louisiana 70148, U. S. A.
razzam@uno.edu

Dr. Richard G. Forbes

University of Surrey, FEPS (X1), Guildford, Surrey GU2 7XH,
U. K.
R.Forbes@surrey.ac.uk

Prof. Dr. Roy Chantrell

Physics Department, York University, York, YO10 5DD, U. K.
Rc502@york.ac.uk

Prof. Dr. Shawqi Al-Dallal

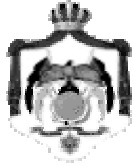
Department of Physics, Faculty of Science, University of Bahrain,
Manamah, Kingdom of Bahrain.

Prof. Dr. Susamu Taketomi

Matsumoto Yushi-Seiyaku Co. Ltd., Shibukawa-Cho, Yao City,
Osaka 581-0075, Japan.
staketomi@hotmail.com

Prof. Dr. Wolfgang Nolting

Institute of Physics / Chair: Solid State Theory, Humboldt-
University at Berlin, Newtonstr. 15 D-12489 Berlin, Germany
Wolfgang.nolting@physik.hu-berlin.de



The Hashemite Kingdom of Jordan



Yarmouk University

Jordan Journal of
PHYSICS

An International Peer-Reviewed Research Journal

Volume 4, No. 1, 2011, 1432 H

Instructions to Authors

Instructions to authors concerning manuscript organization and format apply to hardcopy submission by mail, and also to electronic online submission via the Journal homepage website (<http://jjp.yu.edu.jo>).

Manuscript Submission

1- **Hardcopy:** The original and three copies of the manuscript, together with a covering letter from the corresponding author, should be submitted to the Editor-in-Chief:

Professor Ibrahim O. Abu Al-Jarayesh
Editor-in-Chief, Jordan Journal of Physics
Deanship of Scientific Research and Graduate Studies
Yarmouk University, Irbid, Jordan.
Tel: 00962-2-7211111, Ext. 2075
Fax: 00962-2-7211121
E-mail: jjp@yu.edu.jo

2- **Online:** Follow the instructions at the journal homepage website.

Original *Research Articles*, *Communications* and *Technical Notes* are subject to critical review by minimum of two competent referees. Authors are encouraged to suggest names of competent reviewers. *Feature Articles* in active Physics research fields, in which the author's own contribution and its relationship to other work in the field constitute the main body of the article, appear as a result of an invitation from the Editorial Board, and will be so designated. The author of a *Feature Article* will be asked to provide a clear, concise and critical status report of the field as an introduction to the article. *Review Articles* on active and rapidly changing Physics research fields will also be published. Authors of *Review Articles* are encouraged to submit two-page proposals to the Editor-in-Chief for approval. Manuscripts submitted in *Arabic* should be accompanied by an Abstract and Keywords in English.

Organization of the Manuscript

Manuscripts should be typed double spaced on one side of A4 sheets (21.6 x 27.9 cm) with 3.71 cm margins, using Microsoft Word 2000 or a later version thereof. The author should adhere to the following order of presentation: Article Title, Author(s), Full Address and E-mail, Abstract, PACS and Keywords, Main Text, Acknowledgment. Only the first letters of words in the Title, Headings and Subheadings are capitalized. Headings should be in **bold** while subheadings in *italic* fonts.

Title Page: Includes the title of the article, authors' first names, middle initials and surnames and affiliations. The affiliation should comprise the department, institution (university or company), city, zip code and state and should be typed as a footnote to the author's name. The name and complete mailing address, telephone and fax numbers, and e-mail address of the author responsible for correspondence (designated with an asterisk) should also be included for official use. The title should be carefully, concisely and clearly constructed to highlight the emphasis and content of the manuscript, which is very important for information retrieval.

Abstract: A one paragraph abstract not exceeding 200 words is required, which should be arranged to highlight the purpose, methods used, results and major findings.

Keywords: A list of 4-6 keywords, which expresses the precise content of the manuscript for indexing purposes, should follow the abstract.

PACS: Authors should supply one or more relevant PACS-2006 classification codes, (available at <http://www.aip.org/pacs/pacs06/pacs06-toc.html>)

Introduction: Should present the purpose of the submitted work and its relationship to earlier work in the field, but it should not be an extensive review of the literature (e.g., should not exceed 1 ½ typed pages).

Experimental Methods: Should be sufficiently informative to allow competent reproduction of the experimental procedures presented; yet concise enough not to be repetitive of earlier published procedures.

Results: should present the results clearly and concisely.

Discussion: Should be concise and focus on the interpretation of the results.

Conclusion: Should be a brief account of the major findings of the study not exceeding one typed page.

Acknowledgments: Including those for grant and financial support if any, should be typed in one paragraph directly preceding the References.

References: References should be typed double spaced and numbered sequentially in the order in which they are cited in the text. References should be cited in the text by the appropriate Arabic numerals, enclosed in square brackets. Titles of journals are abbreviated according to list of scientific periodicals. The style and punctuation should conform to the following examples:

1. Journal Article:

- a) Heisenberg, W., *Z. Phys.* 49 (1928) 619.
- b) Bednorz, J. G. and Müller, K. A., *Z. Phys.* B64 (1986) 189
- c) Bardeen, J., Cooper, L.N. and Schrieffer, J. R., *Phys. Rev.* 106 (1957) 162.
- d) Asad, J. H., Hijjawi, R. S., Sakaji, A. and Khalifeh, J. M., *Int. J. Theor. Phys.* 44(4) (2005), 3977.

2. Books with Authors, but no Editors:

- a) Kittel, C., "Introduction to Solid State Physics", 8th Ed. (John Wiley and Sons, New York, 2005), chapter 16.
- b) Chikazumi, S., C. D. Graham, JR, "Physics of Ferromagnetism", 2nd Ed. (Oxford University Press, Oxford, 1997).

3. Books with Authors and Editors:

- a) Allen, P. B. "Dynamical Properties of Solids", Ed. (1), G. K. Horton and A. A. Maradudin (North-Holland, Amsterdam, 1980), p137.
- b) Chantrell, R. W. and O'Grady, K., "Magnetic Properties of Fine Particles" Eds. J. L. Dormann and D. Fiorani (North-Holland, Amsterdam, 1992), p103.

4. Technical Report:

Purcell, J. "The Superconducting Magnet System for the 12-Foot Bubble Chamber", report ANL/HEP6813, Argonne Natl. Lab., Argonne, III, (1968).

5. Patent:

Bigham, C. B., Schneider, H. R., US patent 3 925 676 (1975).

6. Thesis:

Mahmood, S. H., Ph.D. Thesis, Michigan State University, (1986), USA (Unpublished).

7. Conference or Symposium Proceedings:

Blandin, A. and Lederer, P. *Proc. Intern. Conf. on Magnetism, Nottingham* (1964), P.71.

8. Internet Source:

Should include authors' names (if any), title, internet website, URL, and date of access.

9. Prepublication online articles (already accepted for publication):

Should include authors' names (if any), title of digital database, database website, URL, and date of access.

For other types of referenced works, provide sufficient information to enable readers to access them.

Tables: Tables should be numbered with Arabic numerals and referred to by number in the Text (e.g., Table 1). Each table should be typed on a separate page with the legend above the table, while explanatory footnotes, which are indicated by superscript lowercase letters, should be typed below the table.

Illustrations: Figures, drawings, diagrams, charts and photographs are to be numbered in a consecutive series of Arabic numerals in the order in which they are cited in the text. Computer-generated illustrations and good-quality digital photographic prints are accepted. They should be black and white originals (not photocopies) provided on separate pages and identified with their corresponding numbers. Actual size graphics should be provided, which need no further manipulation, with lettering (Arial or Helvetica) not smaller than 8 points, lines no thinner than 0.5 point, and each of uniform density. All colors should be removed from graphics except for those graphics to be considered for publication in color. If graphics are to be submitted digitally, they should conform to the following minimum resolution requirements: 1200 dpi for black and white line art, 600 dpi for grayscale art, and 300 dpi for color art. All graphic files must be saved as TIFF images, and all illustrations must be submitted in the actual size at which they should appear in the journal. Note that good quality hardcopy original illustrations are required for both online and mail submissions of manuscripts.

Text Footnotes: The use of text footnotes is to be avoided. When their use is absolutely necessary, they should be typed at the bottom of the page to which they refer, and should be cited in the text by a superscript asterisk or multiples thereof. Place a line above the footnote, so that it is set off from the text.

Supplementary Material: Authors are encouraged to provide all supplementary materials that may facilitate the review process, including any detailed mathematical derivations that may not appear in whole in the manuscript.

Revised Manuscript and Computer Disks

Following the acceptance of a manuscript for publication and the incorporation of all required revisions, authors should submit an original and one more copy of the final disk containing the complete manuscript typed double spaced in Microsoft Word for Windows 2000 or a later version thereof. All graphic files must be saved as PDF, JPG, or TIFF images.

Allen, P.B., “.....”, in: Horton, G.K., and Muradudin, A. A., (eds.), “Dynamical.....”, (North.....), pp....

Reprints

Twenty (20) reprints free of charge are provided to the corresponding author. For orders of more reprints, a reprint order form and prices will be sent with the article proofs, which should be returned directly to the Editor for processing.

Copyright

Submission is an admission by the authors that the manuscript has neither been previously published nor is being considered for publication elsewhere. A statement transferring copyright from the authors to Yarmouk University is required before the manuscript can be accepted for publication. The necessary form for such transfer is supplied by the Editor-in-Chief. Reproduction of any part of the contents of a published work is forbidden without a written permission by the Editor-in-Chief.

Disclaimer

Opinions expressed in this Journal are those of the authors and neither necessarily reflects the opinions of the Editorial Board or the University, nor the policy of the Higher Scientific Research Committee or the Ministry of Higher Education and Scientific Research. The publisher shoulders no responsibility or liability whatsoever for the use or misuse of the information published by JJP.

Indexing

JJP is currently applying for indexing and abstracting to all related International Services.

Jordan Journal of
P H Y S I C S

An International Peer-Reviewed Research Journal

Volume 4, No. 1, 2011, 1432 H

Table of Contents:

Review Articles	Pages
Aggregation of Magnetic Fluids under an External Field: Micelle Formation: A Review Susamu Taketomi	1-37
<hr/>	
English Articles	Pages
Motion of a Charged Particle in a Strong Magnetic Field as a Lagrangian Linear in Velocities Khaled I. Nawafleh	39-42
<hr/>	
Two-Segment Electrophysiological Model of Excitable Membrane of <i>Paramecium</i> Abdul-Rahman A. Al-Rudainy	43-49
<hr/>	
IBM-1 Calculations of Low-Lying Excited Levels and Electric Transition Probabilities B(E2) on the Even-Even $^{174-180}\text{Hf}$ Isotopes" K. A. Al-Maqtary, M. H. Al-Zuhairy, M. N. Al-Sharaby and N. A. Shamlan	51-58

Jordan Journal of Physics

REVIEW ARTICLE

Aggregation of Magnetic Fluids under an External Field: Micelle Formation: A Review

Susamu Taketomi

Matsumoto Yushi-Seiyaku Co. Ltd., Yao, Osaka 581-0075, Japan.

Received on: 5/8/2010; Accepted on: 21/10/2010

Abstract: Soon after the invention of the magnetic fluid (MF), it was found that needle-like agglomerates (macro-clusters) were generated in some kind of MFs under an external magnetic field by optical microscope observation. However, the macro-clusters disappeared when the external field was removed. Therefore, many theories were proposed whether or not the macro-clusters were simple precipitants of the colloidal particles, or one phase of the two-phase separation, or etc. On the other hand, MFs under an external magnetic field show many peculiar and interesting phenomena in acoustics and magneto-optics. In order to interpret these peculiar phenomena, an assumption that submicron-order agglomerates of the colloidal particles elongated along the field direction (micro-clusters) was necessary. However, this assumption contradicted the MF's phase transition of second order between the particles' monodispersed phase and the phase in which the agglomerates were generated (Landau criterion). In this paper, first, the macro-cluster's nature is explained. The experimental results of the time dependence of the MF shaft seal's burst pressure, the MF's acoustic properties and magneto-optical effects are explained followed by explaining the necessity of the micro-cluster assumption. Proton-NMR experiment of the water-solvent MF and the latent heat measurement of the MF phase transition by differential scanning calorimetry are explained. The conventional MF and a 1000-fold diluted MF were used for the magnetization curve measurement, temperature and AC magnetic field frequency dependence experiment of the initial complex susceptibility measurement and frozen MF's magnetic aftereffect experiment. From these experiments, the magnetic colloidal particles interaction in the MF is discussed. Finally, we show a physical model that the excess surfactant molecules which are isolated and freely dissolved in the MF's solvent make special micelles when the temperature is decreased or the external magnetic field is applied. The magnetic colloidal particles stick to the surface of the micelles and this micelle with the colloidal particles is the actual micro-cluster. We show that this special micelle model explains all the MF's peculiar phenomena without any contradictions, especially the contradiction between the anisotropical agglomeration and Landau criterion with respect to the phase transition of second order.

Keywords: Magnetic fluid; Ferrofluid; Aggregation; Magnetic colloidal particle; Magnetic nanoparticle; Micelle; Phase transition of second order; Landau criterion.

PACS: 75.50.Lk, 75.50.Mm, 82.70.Dd, 82.70.Kj

I. Introduction

A magnetic fluid (hereafter abbreviated MF) is a stable colloidal solution containing ferro- or ferri-magnetic colloidal particles coated with strong dispersive surfactant molecules to disperse the particles stably in solvent. However, soon after the invention of MFs and becoming

widely known in the world, it was found by optical microscope observation that needle-like clusters of magnetic colloidal particles were formed under an external magnetic field in some kinds of MFs of which surfactant's dispersing ability was slightly weak[1]. These needle-like

clusters, however, disappeared after the external field was removed. In addition, many other interesting phenomena of the MF were found which could not be explained without assuming the generation of these clusters in the MF.

To begin with, we would like to correct two common misunderstandings with regard to the cluster formation in the MF. Many researchers, even specialists in magnetism, make these misunderstandings.

The first misunderstanding is the confusion of Bitter pattern with the clusters in the MF. The Bitter pattern is the visualization of the magnetic domains on the surface of the ferromagnetic or ferrimagnetic sample [2, 3]. The Bitter pattern appears in the following procedure. Magnetite powder whose particle size is in the order of a micron is mixed with soapy water and they are stirred strongly. As soon as the stirring stops, the mixture is pored onto the surface of the ferromagnetic sample. As the magnetization directions of the neighboring magnetic domains are completely different, the magnetic field gradient in the domain boundary region is very huge. Therefore, the magnetite particles in the mixture are attracted to the boundary regions and finally deposited along the boundaries. The deposited magnetite particles draw the domain boundary lines. That is the Bitter pattern. However, the magnetic colloidal particles in the MF are not precipitated in the boundary even if the MF is coated on the surface of the same ferromagnetic samples. It is because the size of the particles in the MF is only in the order of 10 nanometers, and therefore the thermal agitation force is much stronger than the gravitational force acting on the magnetite colloidal particle. In conclusion, the magnetic colloidal particles in the MF do not make a Bitter pattern and thus the clusters in the MF are not similar to the aggregates of the Bitter pattern. In other words, the clusters in the MF are not simple precipitants of the magnetic colloidal particles.

The second misunderstanding is the confusion of magneto-rheological fluid (hereafter abbreviated MR fluid) with the MF. The MR fluid consists of ferro- or ferri-magnetic particles in the order of micron size dispersed in viscous oil with the aid of some surfactants. As the particles in MR fluid are micron-size, they are multi-magnetic-domain particles and they have no permanent magnetic moment. Consequently, there is no mutual magnetic

attractive force between the particles in the MR fluid under no external magnetic field and no particles coagulation occurs when no external field is applied. As the MR fluid's particle size is in the order of a micron, the gravitational force overcomes the thermal agitation force and all the particles in MR fluid are finally deposited in the bottom of a container though this process takes a considerably long time due to the viscous oil. On the contrary, as the particle size in MF is in the order of 10 nm, the magnetic colloidal particles in MFs are single magnetic domain and each particle has permanent magnetic moment. Therefore, there is mutual magnetic attraction force between the particles in MFs and they would coagulate and precipitate in the bottom of MF. However, due to special surfactant molecules which cover the surface of all the magnetic colloidal particles, the particles in the MF do not coagulate. That is the reason why the MF is a stable colloidal solution.

After stirring the MR fluid and when the magnetic particles are dispersed in the oil, an external magnetic field is applied to the MR fluid. Due to the particle's induced magnetic moments, the neighboring magnetic particles are attracted to each other and they make chains. For example, a similar phenomenon occurs for iron filings dispersed on a plane paper sheet. When an external magnetic field is applied to the iron filings, they make chain lines along the magnetic force lines on the sheet. In such a case, if the MR fluid is forced to flow, the magnetic particle chains make entangled networks in the solvent or oil of the MR fluid. This network prevents the flow of the oil. Therefore, the apparent viscosity of the MR fluid under the external field increased hundreds or thousands of times larger than that under no external field. On the other hand, the viscosity of an MF under an external field increased less than two times over that under no field [4].

In conclusion, the MFs are completely different from the MR fluids or the mixture of the magnetic powder and the soap water which is used for Bitter pattern drawing.

Now, we turn back to the discussion of the cluster formation in the MF. The assumption of cluster formation or aggregation of the magnetic colloidal particles in MF essentially contradicts to the fundamental characteristics of the MF. In fact, if the colloidal particles in the MF really coagulate, the origin of the coagulation should

be molecular forces between the colloidal particles. Therefore, the coagulation should be an irreversible process, or once the coagulation occurs, the reverse process of turning back to a monodispersed state from the clusters should not occur. In fact, in order to prevent such coagulation, the surface of all the magnetic colloidal particles is clad with surfactant molecules that limit the nearest distance that two neighboring particles can approach one another. In reality, the clusters disappear when the external field is removed.

However, cluster formation cannot be denied due to the many experimental results which we shall show in the following sections. This contradiction was a serious mystery until quite recently. Recently, this mystery was solved. It was made clear that the so called mysterious cluster is not really, agglomerate but a special micelle which consists of the magnetic colloidal particles and excess isolated surfactant molecules.

In the following, we show several experimental results which we cannot explain without the coagulation of the colloidal particles in the MF in §s II and III. In §IV, we show the experiments to investigate the mysterious clusters and in §V we explain the special micelle model and interpret all the experimental results of MF without any contradictions.

II. Direct Observation of Clusters by Microscopy

A. Direct Observation of Macro-Clusters by Optical Microscopy

In 1975, Hayes reported optical microscope observations indicating that clusters or aggregates of the magnetic colloidal particles in MFs occurred when an external magnetic field was applied [1]. The MF is an opaque liquid. But, when it is sandwiched by two glass slides and pressed to a thin film of a few tens of micron thickness, visible light is transmitted through the MF film. Therefore, this MF thin film was observed by the optical microscope. For example, Figs. 1(a) and (b) show the clusters in such experiments [5]. Many needle-like clusters

of a few micron diameter are generated along the external field direction. In Figs.1(a) and (b), MF sample A was used. The characteristics of the MF samples discussed in this paper are shown in Table I.

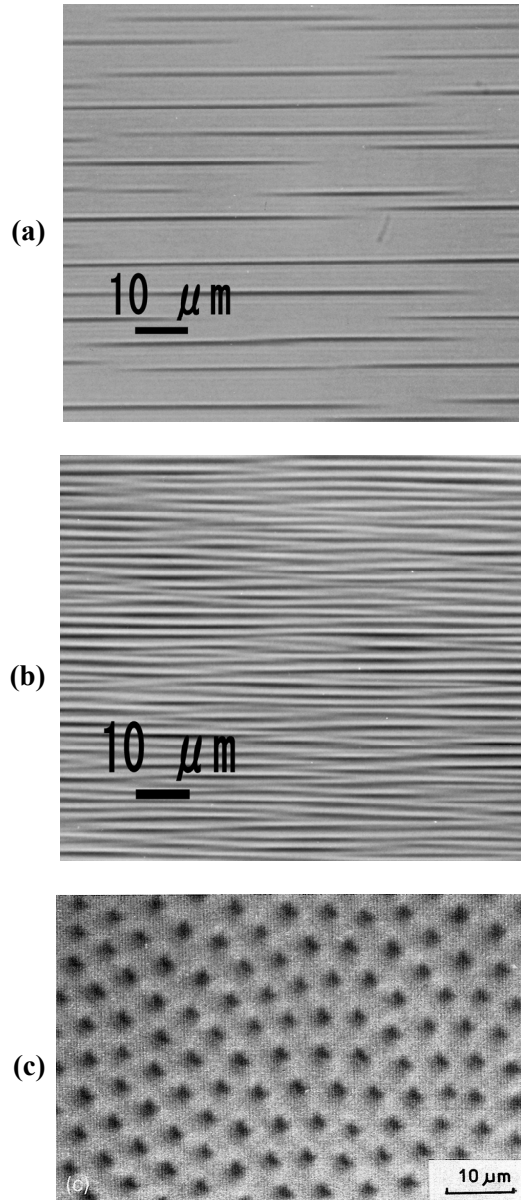


FIG. 1. Clusters in the MF thin film when an external magnetic field is applied parallel to the film ((a), (b)) [5] and perpendicular to the film (c) [8]. The field increase rate was very slow (a) and very rapid (b).

TABLE I. Characteristics of MF samples

Sample name	Colloidal particle	Solvent	Particles volume fraction	Dilution factor	Note
A	MnZn-ferrite	Paraffine	0.125	1	Mother MF
B	Magnetite	Alkyl naphthalene	0.104	1	Mother MF
C	Magnetite	Alkyl naphthalene	0.104	1	Sample B was under vacuum for 10 minutes and was obtained.
D	Magnetite	Alkyl naphthalene	0.052	1	two times dilution of sample B
E	Magnetite	Water	0.091	1	Mother MF
F	Magnetite	Paraffine and alkylbenzene	0.104	1	Mother MF
G	Magnetite	Water	0.003	30.3	30.3 times dilution of sample E
H	MnZn-ferrite	Paraffine	0.000051	2450	2450 times dilution of sample A
I	Magnetite	Alkyl naphthalene	0.000080	1300	1300 times dilution of sample B
J	Magnetite	Water	0.000074	1230	1230 times dilution of sample E
K	Magnetite	Alkyl naphthalene	0.0484	2.15	2.15 times Dilution of sample B
L	Magnetite	Alkyl naphthalene	0.00792	13.1	13.1 times dilution of sample B
M	Magnetite	Alkyl naphthalene	0.00066	158	158 times dilution of sample B
N	Magnetite	Alkyl naphthalene	0.104	1	Sample B was under vacuum for 1 hour and was obtained.
O	—	—	—	—	Mixing sample B and epoxy adhesive and stirring them fiercely, they were solidified.

A few theories were proposed with regard to the cluster formation in the MF. The simplest one was that the clusters were aggregates of the magnetic colloidal particles like iron filings' aggregation by a magnetic field. The iron filings dispersed on a plane paper sheet make aggregate lines along the magnetic force lines on the sheet when a magnetic field is applied. In the same scenario, the colloidal particles in the MF should coagulate along the magnetic force lines and that should be the clusters. However, this scenario contains a fatal contradiction. The colloidal particles in the MF do not coagulate by the high gradient magnetic field which is used in daily life. In fact, the magnetic colloidal solution in which the magnetic colloidal particles are easily coagulated and deposited in the bottom under the high gradient magnetic field which is used in our daily life should not be called MF. In addition, if the clusters in the MF are really the aggregates of the colloidal particles, they should remain aggregates after the field is removed. However, after the removal of the external field, the clusters in the MF disappeared and monodispersed state is again obtained in the MF. Unfortunately, in those days when it was not long since the MF was invented some, MFs had

poor dispersivity in the magnetic colloidal particles, i.e., some of the MFs in those days were not so good as those in the present days. When the external magnetic field was applied to such MF of bad quality, generated were some precipitants of the magnetic colloidal particles. Those phenomena led a considerable number of researchers in those days to the incorrect conclusion that the clusters in the MF were also the similar aggregates of the MFs of bad quality. However, the clusters in the MF and the precipitants in the bad MF are completely different substances.

Another theory is the-two phase separation model. According to this theory, when an external magnetic field is applied to the MF, the MF can no longer be one monodispersed phase, but separates into two phases of higher and lower particle volume concentration. The dense phase is looked upon as the clusters. This model was independently proposed by Sano and Doi [6] and Cebers [7]. Applying mean field theory, they obtained theoretical results that the MF can be separated into two phases when the external field is applied.

However, this theory contradicted experimental results. When the external field, H , which is applied to the MF at temperature, T , is increased from zero field, the clusters were generated at the threshold field strength, H_{th} . However, the clusters are no longer generated at any field strength, H , if the temperature, T , is higher than the threshold temperature, T_{Cl} . Cebers obtained the $H_{th} - T_{Cl}$ relation by his theory as:

$$H_{th} = \frac{1}{(T_{Cl} - T)} \quad (1)$$

This relation was contradicted by experiments [5]. Another experimental evidence which contradicts the two-phase separation model is the difference in the cluster formation by the different increase rate of the applied field. Figs. 1(a) and (b) are the optical micrographs of clusters under the magnetic fields. The temperature and the field strength of Fig. 1(a) were 300 K and 79.6 kA/m, respectively; while those of Fig. 1(b) were 302 K and 79.6 kA/m, respectively. The temperature and the field strength were almost the same in both experiments. However, the increasing field rate of Fig. 1(a) was 20 A/(m sec); while that of Fig. 1(b) was 8000 A/(m sec). In the case of rapid increasing rate, many clusters were generated densely, while in the case of slow increasing rate, the space intervals between the clusters are large but each cluster was thick. From this experimental result, the cluster generation seemed not to be in a thermodynamically stable state but rather in a transient state or quasi-stable state. Besides, one can easily find a white stripe accompanying a needle-like cluster, in which the colloidal particle density should be very low in this white stripe compared with the rest area. We discuss these white stripes in §IV. A of NMR experiment.

When the field is applied to the MF film perpendicular to the film, the needle-like clusters are generated, but directed perpendicular to the film. Therefore, the cluster images of the micrograph are dots [8], (Fig. 1(c)). As the direction of each cluster's magnetic moment is perpendicular to the film, the clusters mutually repel by a magnetic repulsive force. Therefore, the clusters make the pseudo-lattice structure in two dimensions. The MF's clusters' pseudo-lattice structure was first experimentally studied by Bar'yakhtar *et al.* [9]. The same subject was

experimentally studied by Jones *et al.* [10, 11] then by Cernak and Macko [8]. Especially Cernak and Macko showed beautiful pseudo-lattice micrographs one of which is Fig. 1(c). A long time later, a similar study was again conducted by Hong *et al.* [12].

From these studies, it is evident that the clusters are not simple aggregates of the colloidal particles in nature, because if they were simple aggregates, they would be merged to one large aggregate instead of making pseudo-lattice. There exists a positive surface tension on the boundary of the cluster. In fact, Rosensweig and Popplewel [13] made the following experiment. They observed the clusters in the MF by an optical microscope equipped with a video camera. The external field was applied to the MF film parallel to the film. Suddenly, the field was removed. They observed the decay of the cluster after the field was removed. First, the needle-like cluster collapsed to a linked sausage shape, then separated to spheres. By measuring the elapsed time of this collapse, they estimated the surface tension of the clusters. By measuring the elapsed time of the disappearance of the sphere, they estimated the diffusion constant of the colloidal particles and obtained the hydrodynamic diameter of the particles. From these experiments, we can confirm that the cluster in the MF is not a simple aggregate.

B. Strong Light Diffraction Image

As shown in the previous section, the MF thin film transmits visible light. Instead of observing the transmitted light by the optical microscope, the transmitted light is projected to a screen. Then a peculiar scattering light pattern is obtained when the MF film is under an external field parallel to the film. Haas and Adams [14] observed a peculiar projection of the transmitted light from the diluted MF film. When no field was applied to the sample, only a halo was obtained. However, when the field was applied to the sample perpendicular to the light propagation, the transmitted light is diffracted in the plane perpendicular to both the sample film and the external field. If one knew only this subsection's result, it would be very easy to conclude that this diffraction was induced by the needle-like clusters in the MF generated by the external field. However, Haas and Adams were not aware of these relations. Yusuf [15] correctly discussed the diffraction and the clusters relation. The needle-like clusters in the MF play

a role of gratings of an optical diffraction grating. The strong diffraction effect is caused due to the periodical spacing between the needle-like clusters. On the contrary, by measuring the diffraction light intensity as a function of the diffraction angle, one can calculate the spacing of the clusters by Fourier transform [5].

C. Cluster Observation by Electron Microscopy

The lower limit of an ordinary optical microscope's resolution is about a micron. Therefore, if the clusters in the MF are less far than the micron size, these clusters cannot be distinguished by the optical microscope. However, even nanometer-size objects are distinguished by an electron microscope. In fact, one can observe the magnetic colloidal particles in the MF by the electron microscope. Therefore, one can distinguish submicron-size clusters in the MF by the electron microscope. However, the electron microscope observation has a fatal disadvantage in observing the MF. When a sample is observed by the electron microscope, it is placed in an evacuated sample room. Therefore, before the observation, the MF droplet is put on a sustaining plastic film and the solvent is evaporated. We observe this dried MF or the colloidal particles on the sustaining plastic film by the electron microscope. During the drying process, the colloidal particles may move on the sustaining film and easily make aggregations. Therefore, the magnetic colloidal particles' aggregates in the electron micrograph which is obtained from the MF in this manner do not mean that there really exist aggregates in the MF. In fact, many electron micrographs in which aggregates of the MF were found were obtained by the above preparation method.

Donselaar *et al.* [16] succeeded in observing clusters of submicron scale in the MF by an electron microscope, in a different way. Quenching the MF, they obtained a frozen MF thin film fragment. They observed this frozen film fragment with the electron microscope and found these sub-micron clusters in the frozen sample. However, from a more critical viewpoint, even these sub-micron clusters might be formed during the quenching process.

III. Other Magnetic Fluid Physical Phenomena Which Cannot Be Explained Without Assuming Cluster Formation

In the previous section, we mainly mentioned the clusters of the MF, which can be observed by an optical microscope. This means that the size of the clusters is equal or larger than micron size. On the other hand, there are many MFs in which no such clusters are observed by the optical microscope even under a strong magnetic field of MA/m. These MFs, however, also show interesting physical phenomena which cannot be explained without assuming cluster formation in the MFs. It means that the clusters are formed in all the MF under the external field, and the difference is that for some MFs, the formed cluster size is micron size and for the rest of the MF, the formed cluster size is less than micron size. As no objects less than micron size are distinguished by the optical microscope, we could not see the clusters of sub-micron size in some MFs and we misunderstood that the clusters were not formed in those MFs. Hereafter, we call these clusters of submicron size micro-clusters and distinguish them from the clusters of micron size which we, hereafter, call macro-clusters. In the following, we enumerate the interesting experimental results of the MF which cannot be explained without assuming the micro- or macro-cluster formation.

A. Time Dependence of Magnetic Fluid Shaft Seal's Burst Pressure

One of the greatest successes in the applications of MF to industries is a magnetic fluid shaft seal, an important mechanical element [17–19]. In this paper, we briefly explain the mechanism of the MF shaft seal and explain the relation of the time dependence of the seal's burst pressure and the cluster formation in the MF in detail. Fig. 2 shows the schematic construction of the MF shaft seal. A rotational nonmagnetic shaft is set in a stationary cylindrical nonmagnetic housing with bearings. In the inner side of the housing, a cylindrical permanent magnet is sandwiched by two cylindrical pole-pieces which are made of magnetic material. A cylindrical sleeve which is also made of magnetic material is fixed on the outer surface of the shaft. The magnified cross-section of area A in Fig. 2 is shown in Fig. 3. A ring-like projection is attached on the outer surface of the cylindrical sleeve. The cross

section of the projection is a triangle (See Fig. 3). Therefore, a magnetic circuit is constructed through the permanent magnet, the magnetic pole-piece, the magnetic sleeve, the projection and the other pole-piece. A solid line arrow shows this magnetic circuit in Fig. 2. The gap between the projection's top and the inner surface of the pole-piece is usually a few tenth mm. The magnetic force lines concentrate to the top of the projection. Therefore, the magnetic field together with its gradient is huge compared with the rest of the area. When the MF is introduced into this area, it fills the gap between the top of the projection and the inner surface of the pole-piece which faces the top of the projection. The MF fills the gap like an O-ring and it separates the space into Space 1 and Space 2 in Fig. 3(a). The ring-like MF also hermetically seals the gas in Space 1 from Space 2 and *vice versa*. The MF shaft seal prevents even gas molecules from moving across the two spaces, 1 and 2. This is a brief explanation of the MF shaft seal. When the gas pressure, p_1 , of Space 1 is increased compared with the gas pressure, p_2 , of Space 2, the MF in the gap region shifts to the right due to the gas pressure difference, $\Delta p = p_1 - p_2$, in Fig. 3(b). However, it clings to the gap region by the magnetic force. A further gas pressure increase blows out the MF at a certain pressure difference Δp and the MF shaft seal is broken. Fig. 3(b) shows the MF's position just before the MF is blown out by the burst pressure, Δp . We call this maximum Δp "burst pressure" of the MF shaft seal. The burst pressure, Δp , is expressed in a good approximation by [18]:

$$\Delta p = \mu_0 M_S H, \quad (2)$$

where μ_0 is a magnetic permeability in vacuum, M_S is the saturation magnetization of the MF and H is the magnetic field strength at the boundary between Space 1 and the MF in Fig. 3(b)*. Strictly speaking, MF's magnetization strength, M , at the same boundary should be used instead of M_S . However, the field strength, H , at the boundary is so huge that M is almost M_S . The author carried out the following experiment nearly 30 years ago [18]. First, making the sealing area in the MF shaft seal empty in Fig. 3, the fresh MF was introduced in the seal region at

time $t = 0$. After leaving the MF shaft seal equipment at rest for time, t , we measured the burst pressure, Δp , of this equipment. In general, as M_S in Eq. (2) is constant with respect to time, t , Δp should be constant with respect to the elapsed time, t . We conducted this experiment with four different MF shaft seals. The four seals, I, II, III and IV were different in the gap, g , and projection height, h , in Fig. 3. Each seal's g and h are tabulated in Table II.

TABLE II. MF shaft seal's g and h

Seal	I	II	III	IV
Gap g (mm)	0.2	0.3	0.4	0.2
Height h (mm)	2.5	2.4	2.3	1.0

The experimental result is shown in Fig. 4. The burst pressure, Δp , is shown as a function of time, t . However, \sqrt{t} is scaled in abscissa. This experimental result leads to the conclusion that M_S , the MF's saturation magnetization at the boundary in Fig. 3, was not constant with respect to time, t , but expressed by:

$$M_S(t) = M_{S0} + C_2 \sqrt{t}, \quad (3)$$

where, M_{S0} is the MF's saturation magnetization at $t = 0$, or the ordinary MF's saturation magnetization, and C_2 is a positive constant. At that time, the present author tried to explain this effect as follows [18]. The magnetic colloidal particles in the MF moved to the top area B of the projection in Fig. 3(a) by the Brownian motion and the magnetic force. Once they reached area B, they were trapped in this area. In fact, by solving the special diffusion equation or Smoluchowski's equation, we obtained naturally the second term at the right hand side of Eq. (3).

In retrospect, the particles were not simply trapped in area B, but they made clusters and these clusters were not able to escape from this area. In fact, even after time, t , elapsed, if we rotated the shaft in high speed and measured the burst pressure, Δp , it decreased back to Δp at $t = 0$. It should be that the shaft's high speed rotation stirred the MF strongly and the clusters were broken leading the MF back to monodispersed state. However, we show the real meaning of the cluster in §V *Discussion*.

*In this paper, we define the relation among the magnetic field, H , the magnetization, M , and the magnetic flux density, B , as $B = \mu_0 (H + M)$.

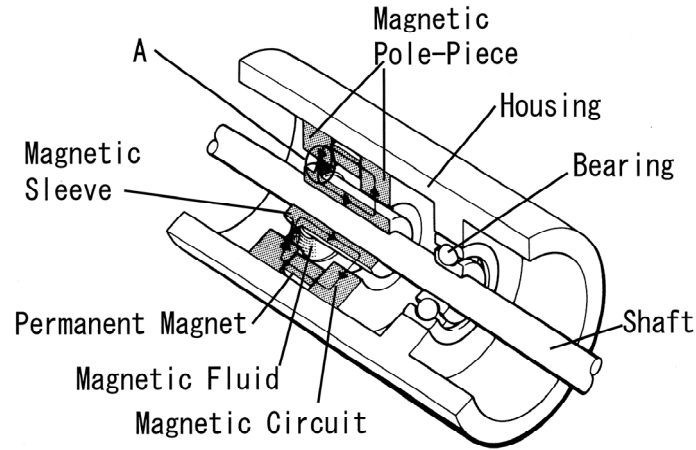


FIG. 2. Schematic figure of the MF shaft seal's construction.

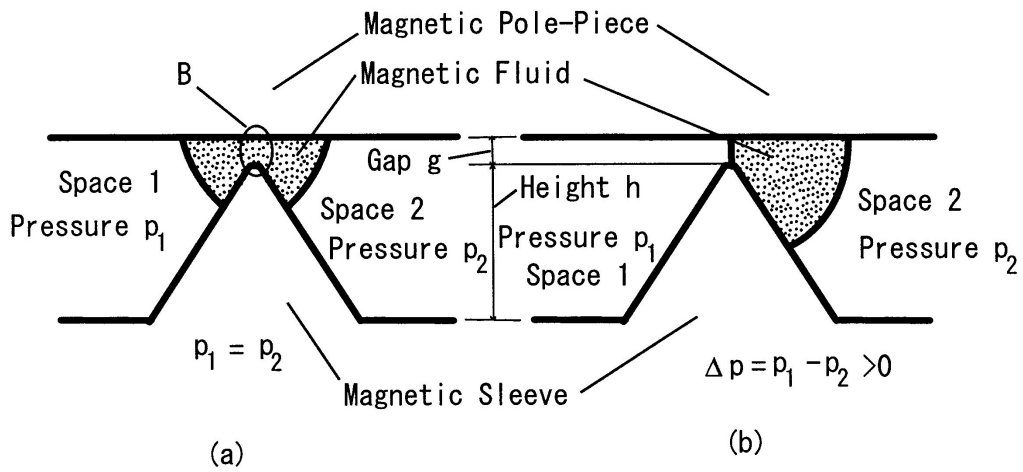


FIG. 3. Cross section of area A in Fig. 2, which is the most important section of the MF shaft seal. (a) There is no pressure difference. (b) The pressure difference is the burst pressure, Δp .

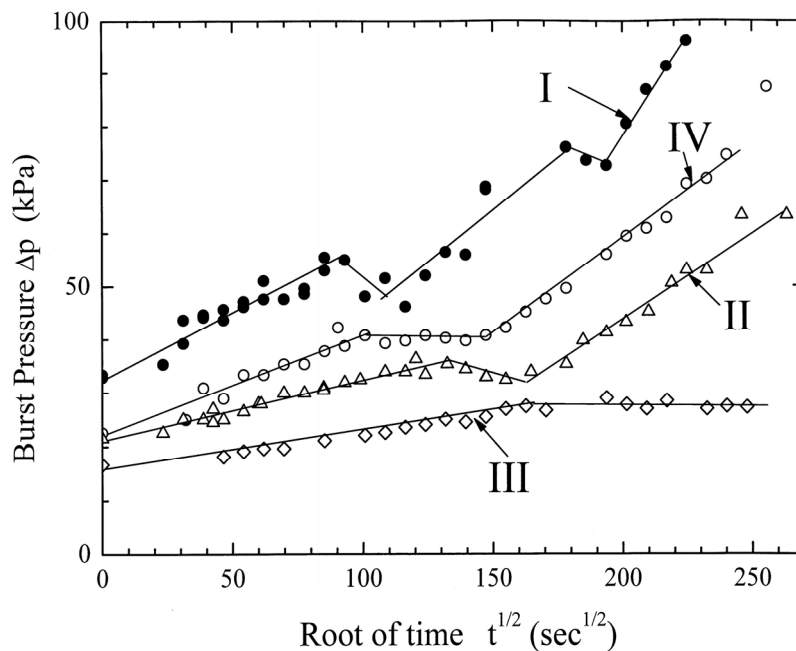


FIG. 4. The burst pressure, Δp , as a function of time, t . The time t is the elapsed time after the MF was introduced to the gap in the MF shaft seal. \sqrt{t} is scaled in abscissa [18].

B. Magnetic Fluid's Acoustic Effects

The acoustic properties of the MF under the magnetic field were first discussed theoretically by Parsons [20]. He discussed this subject assuming the MF as nematic liquid crystal with its molecules possessing gigantic magnetic moments. In fact, there exists an anisotropy in velocity and attenuation of the sound which propagates in the oriented liquid crystal with respect to the angle between the molecules' orientation direction and the sound propagation direction [21]. Parsons, however, naturally, did not take the MF's cluster formation into account in his theory. The experimental study of the acoustic properties of the MF under the external field was first conducted by Chung and Isler [22, 23]. They measured the velocity and attenuation of the sound which propagates in the MF under an external field and found an anisotropy in both the velocity and attenuation properties with regard to the angle between the applied field and sound propagation direction. They also found a poor reproducibility of the experimental data in this experiment. Gotoh and Chung [24] discussed their experimental result considering the MF a continuum. Not neglecting the nonlinear terms in the constitutive equations of the MF, but giving many suitable parameter values to the nonlinear terms, they obtained considerably good fitting theoretical curves for the experimental data. However, as the curve

fitting was the pure mathematical procedure, they obtained a poor physical meaning through their analysis. The present author checked whether or not the experimental data which were obtained by Chung and Isler could be interpreted by only the magnetic colloidal particles' orientation effect which Parsons derived [25]. Fig. 5 shows the sound attenuation coefficient, q_i , as a function of the angle, ϕ , between the applied field direction and the sound propagation direction. White empty circles are experimental data [23]. The $q_i^{(1)}$ curve was obtained by the theory taking only the effect of the colloidal particles' orientation into account after Parsons. Evidently, the $q_i^{(1)}$ curve does not fit to the experimental data. Therefore, we assumed the cluster formation in the MF and obtained the attenuation coefficient $q_i^{(2)}$ which is derived from the cluster formation [25]. The sum $q_i = q_i^{(1)} + q_i^{(2)}$ is the theoretical sound attenuation coefficient and its curve fits quite well to the experimental data. Later, assuming the periodic arrangement of the needle-like clusters in the MF, Kasparikova [26] discussed theoretically the acoustic properties of the MF under the magnetic field. The acoustic properties of the MF were also studied by Skumiel [27], and later by Motozawa and Sawada [28], actively. In conclusion, the cluster formation hypothesis is indispensable in discussing the acoustics of the MF under an applied magnetic field.

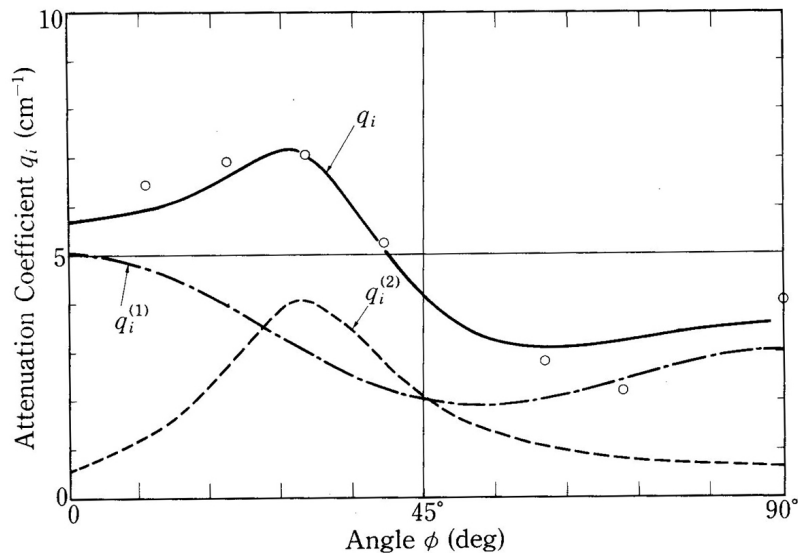


FIG. 5. The sound attenuation coefficient, q_i , as a function of the angle, ϕ , between the applied field direction and the sound propagation direction. Empty circles denote experimental data obtained by Chung and Isler [23]. The theoretical curve, $q_i^{(1)}$, is derived from the magnetic colloidal particles' orientation effect; while $q_i^{(2)}$ curve is derived from the cluster formation effect of the magnetic colloidal particles. $q_i = q_i^{(1)} + q_i^{(2)}$ [25].

C. Magneto-Optical Effect of Magnetic Fluid

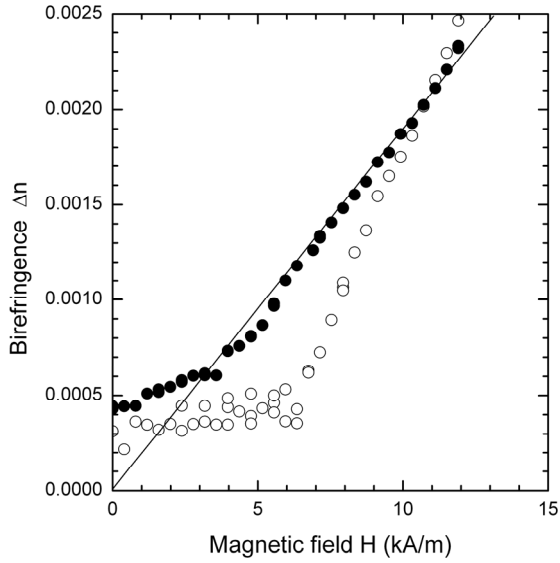
Recently, a review paper on the magneto-optical effects of the MF by Yusuf and Abu-Aljarayesh was published in the present journal [29]. In this paper here, we only discuss the magneto-optical effect of the MF in view of the cluster formation in the MF. Therefore, many important papers with respect to the magneto-optics of the MF but less related to the cluster formation are not referred to in this paper. These papers are referred to in the references of paper [29].

Majorana reported in 1902 that a colloidal solution which contained a very small amount of magnetic colloidal particles showed birefringence when light passed through the solution under a magnetic field directed perpendicular to the light propagation [30]. Therefore, this effect is now called Majorana effect. Here, the reason why we stressed that "the solution contained a very small amount of magnetic colloidal particles" is that it was long time before the MF was invented [31] when Majorana found this effect and only a very small amount of the magnetic colloidal particles was able to be dispersed in the solvent in those days. There were many studies on the magneto-optical effects of such solutions containing a very small amount of magnetic colloidal particles or magnetic ions [32]. However, what we discuss in the presenter paper is the magneto-optical effects of the colloidal solution which contains a considerable volume fraction of the magnetic colloidal particles, i.e., the MF. In conclusion, we have to distinguish the present MF's magneto-optical effect from the Majorana effect, rigorously.

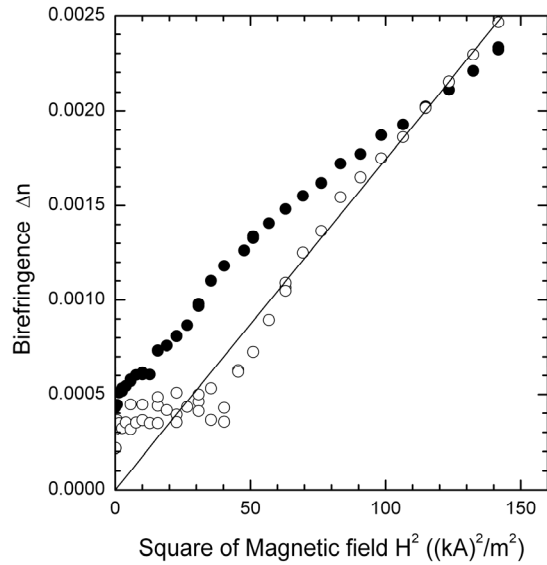
1. Field Dependence of Magnetic Fluid Magnetic Birefringence in a Weak Magnetic Field

To the best of my knowledge, Martinet first reported the magnetic birefringence of the MF [33]. There were two important properties in his paper. One is that the strength of the magnetic birefringence was huge compared with the ordinary Majorana effect. The other important property, which was more important than the former one in retrospect, was the field dependence of the birefringence, Δn . For ordinary magnetic birefringence called the Voigt effect [34] or the Cotton-Mouton effect [35], including the Majorana effect, the birefringence, Δn , is proportional to the square of the applied

magnetic field strength, H . However, Δn of the MF did not obey this law, but was rather proportional to H . This is very important, because if Δn is caused by each colloidal particle's independent contribution, Δn should be proportional to H^2 . In addition, what made this problem more complicated was that in some papers, the similar experiment showed that Δn was proportional to H^2 . Sakhnini and Popplewell [36] prepared very diluted MF not by dilution with solvent but by "magnetic filtering". The authors explained the "magnetic filtering" process as follows. By placing the mother MF under a huge magnetic gradient, the authors tried to remove the large magnetic colloidal particles and unstably dispersed particles from the MF by precipitating those particles with the huge magnetic force. By this magnetic filtering, 85 percent of the magnetic colloidal particles were removed from the mother MF and the diluted MF whose colloidal particles' volume concentration was 2×10^{-4} was obtained. They measured the magnetic birefringence, Δn , of this diluted MF and obtained H^2 dependence of Δn in the weak magnetic field. In fact, before their experiment, Davies and Llewellyn also reported the same H^2 dependence of Δn experiment in the weak magnetic field for the diluted MF with colloidal particles' volume concentration of 1×10^{-5} [37]. However, the present author speculates that there must be no interaction between the magnetic colloidal particles in such a diluted MF, and it was natural that the Majorana effect was obtained in such a diluted MF. Consequently, their experiments were not the real MF's magneto-optical effect. The next experimental result was more serious. The present author *et al.* conducted the similar experiment in the weak magnetic field region nearly 20 years ago [38]. In this experiment, we used two slightly different MF samples, the MF Samples B and C. Their characteristics are tabulated in Table I. Sample B was a very fresh MF when we made the experiment. Sample C was prepared as follows. We left the same MF as the Sample B's MF, under a vacuum for nearly 10 minutes. That was the MF sample, Sample C. The relative weight change of the MF before and after leaving it under a vacuum was less than 10^{-4} . Fig. 6 shows the birefringence, Δn , of Samples B and C as a function of the external field, H . The variables, H and H^2 , are scaled in abscissas of Figs. 6(a) and (b), respectively [38].



(a)



(b)

FIG. 6. The magnetic birefringence, Δn , of Samples, B (solid circle) and C (empty circle), as a function of the external magnetic field, H . The Sample B's MF was fresh; while the Sample C's MF was once under vacuum before the birefringence experiment. H and H^2 are scaled in abscissas of Figs. 6 (a) and (b), respectively [38].

The Sample B's Δn was proportional to H ; while proportional to H^2 was the Sample C's Δn in a weak field region. Why did such an eminent difference emerge even though both the MFs were almost the same except for the under-vacuum-experience? When we put the MF in a hermetically closed glass vessel and started air evacuation, the MF suddenly boiled fiercely and many bubbles were generated in the MF. However, this boiling continued only a few second, and the boiling ceased. It means that

some contaminant in the MF was evacuated by the pressure decrease though the removed contaminant's relative weight was less than 1×10^{-4} . In retrospect, this phenomenon was a very important clue to interpreting the MF's magneto-optical effect. We once again mention it in §V Discussion.

2. Temperature Dependence of Magnetic Fluid's Magnetic Birefringence

The second interesting property of MF's magnetic birefringence is its temperature dependence. Fig. 7 shows the experimental result of the MF's magnetic birefringence, Δn , as a function of the MF's temperature, T , under a constant magnetic field [39]. Δn plunges suddenly at a certain temperature, T , with the temperature decrease. This was due to the freezing of MF's solvent. In fact, the liquid state is necessary for the MF's magnetic birefringence. (In this experiment, the MF was first placed under a fixed magnetic field, then changing the temperature, the birefringence was measured as a function of temperature.) This sudden plunge of the birefringence due to the MF freezing was first observed by Abu-Safia *et al.* [39].

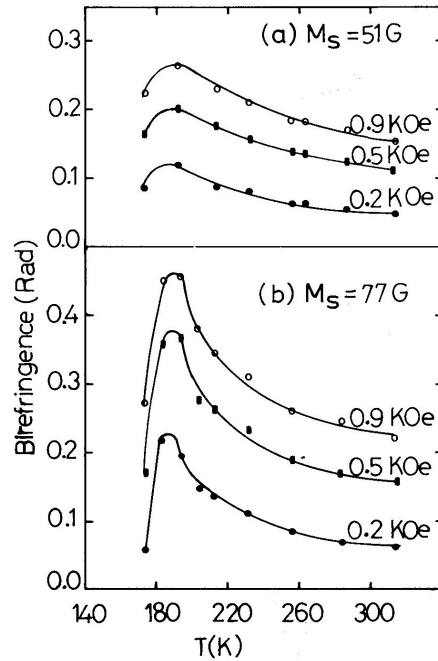


FIG. 7. The temperature dependence of the MF's magnetic birefringence, Δn , under a constant magnetic field. The MF's saturation magnetization was 51 Gauss ($= 5.1 \times 10^4$ A/m) in (a) and 77 Gauss ($= 7.7 \times 10^4$ A/m) in (b). The magnetic field strengths in the graph denote the constant magnetic field applied to the MF sample. There is a plunge in the birefringence, Δn , near the melting point of the MF [39].

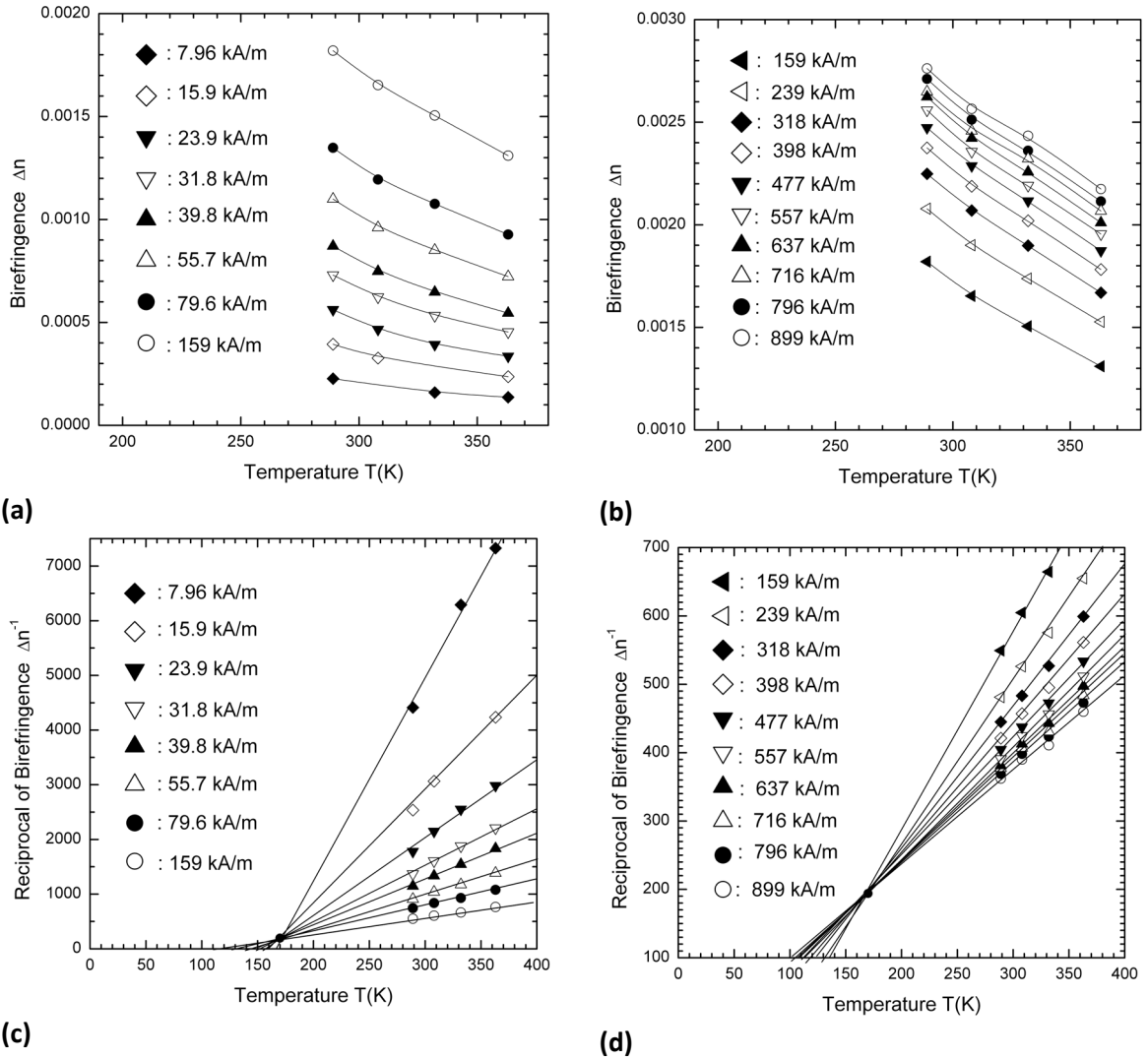


FIG. 8. The temperature dependence of the MF's magnetic birefringence, Δn , under many different external magnetic field strengths [40]. Marks in the graphs correspond to the different field strengths which are also shown in the graphs. (a) and (b): $\Delta n - T$ graphs, (c) and (d): $\frac{1}{\Delta n} - T$ graphs, (c) and (d) correspond to (a) and (b), respectively.

There is another interesting property of the temperature dependence of the MF's magnetic birefringence. Figs. 8(a), (b), (c) and (d) show the other experimental result of the MF's magnetic birefringence, Δn , as a function of the MF's temperature, T , under a constant magnetic field, H [40]. Here, the MF Sample D was used for this experiment, the characteristics of which are tabulated in Table I. The MF Sample D was under a constant external magnetic field during the temperature dependence measurement of Δn . We carried out the experiment with many different constant magnetic fields, H . The marks in the graphs denote the field strengths which are also shown in each graph. We show the birefringence, Δn , as a function of the sample temperature, T , in Figs. 8(a) and (b). We also

show the re-plotted graphs $\frac{1}{\Delta n} - T$, in Figs. 8(c) and (d), which correspond to Figs. 8(a) and (b), respectively. The experimental data under a fixed magnetic field strength falls on the straight line. In addition, the bundle of lines for different field strengths cross at one point in $\frac{1}{\Delta n} - T$ graph. These are mathematically expressed by:

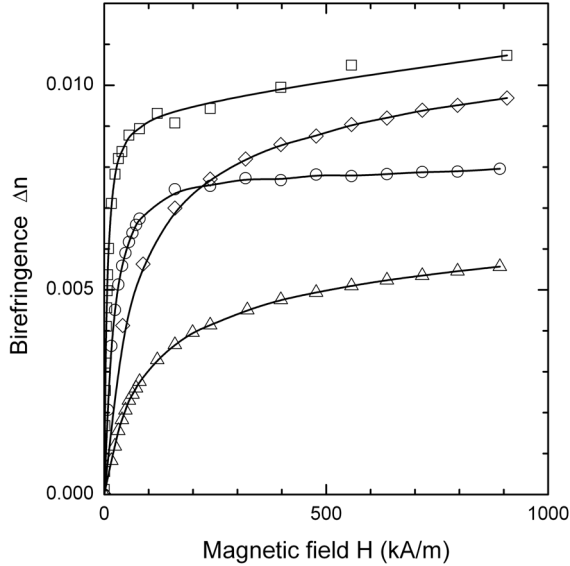
$$\Delta n = \frac{\Delta n_1 f(H)}{\frac{T}{T_1} - 1 + f(H)}, \quad (4)$$

where T_1 and Δn_1 are positive constants denoting the coordinates of the crossing point of lines in

Figs. 8(c) and (d). The function $f(H)$ is an increasing function of H . Formula (4) is the same form as the Curie-Weiss law. This implies that the MF's magnetic birefringence is a typical cooperative phenomenon, leading to the conclusion that the magnetic colloidal particles strongly interact with each other.

3. Scaling Law

The last interesting property of the MF's magnetic birefringence is an existence of scaling law [41]. The $\Delta n - H$ graphs of different MFs converge to one universal function f_u by scaling both Δn and H . Fig. 9(a) shows the experimental $\Delta n - H$ graph for four different MFs, Samples, A, B, E and F, respectively, whose solvents, colloidal particles and particles' concentrations differed from each other.

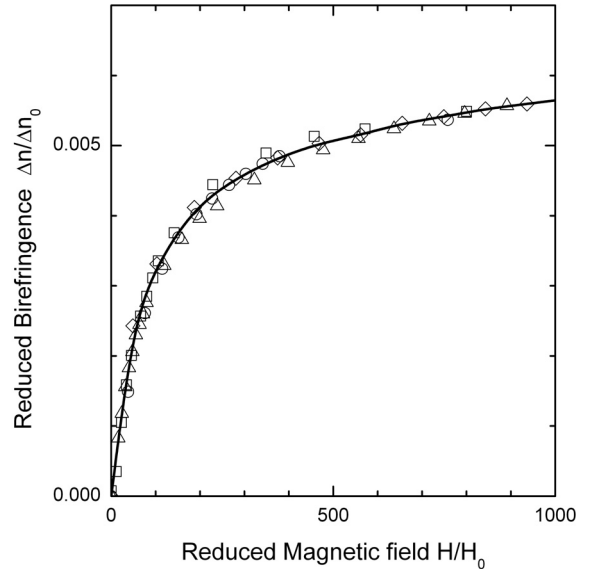


(a)

Their characteristics are tabulated in Table I. The scaled $\Delta n - H$ graphs of those in Fig. 9(a) are shown in Fig. 9(b). Here, the scaling means that Δn and H are divided by Δn_0 and H_0 , respectively, and $\frac{\Delta n}{\Delta n_0} - \frac{H}{H_0}$ graph is the scaled graph. The values, Δn_0 and H_0 , for each Sample are tabulated in Table III. Fig. 9(b) shows that four different $\Delta n - H$ graphs converged to one universal function f_u fairly well. We will discuss it in §V Discussion.

TABLE III. Scaling constants Δn_0 and H_0

MF Sample	A	B	E	F
Δn_0	1.39	1	1.6	1.7
H_0 (kA/m)	0.21	1	0.0696	0.85



(b)

FIG. 9. Scaling law of $\Delta n - H$ graphs [41]. (a): ordinary $\Delta n - H$ graphs, (b): scaled $\frac{\Delta n}{\Delta n_0} - \frac{H}{H_0}$ graphs.

○: Sample A, △: Sample B, □: Sample E, ◇: Sample F.

4. Origin of the Magnetic Fluid Magneto-Optical Effect

Mainly three hypotheses were proposed to explain the MF's magneto-optical effect when it was found [42]. The first hypothesis tried to explain the MF's magneto-optical effect assuming that there was anisotropy in electric susceptibility with respect to the permanent magnetic moment's direction in the colloidal particles in the MF. If there was no external magnetic field, the permanent magnetic moment

of the particles in the MF oriented randomly and the averaged electric susceptibility of all the colloidal particles in the MF was isotropic. However, if an external magnetic field is applied to the MF, the permanent magnetic moment of the colloidal particle was oriented to the external field and accordingly the electric susceptibility of the particles had anisotropy in the direction. This induced an anisotropy in permittivity of the MF in that direction. This is the origin of the MF's magnetic birefringence.

The second hypothesis assumed shape

anisotropy in the magnetic colloidal particles in the MF. For example, if the magnetic colloidal particle was elongated along the magnetic moment's axis and had a rugby ball shape, the particle had different electric polarizabilities in the long axis direction and the short axis direction due to different depolarization factors. If the colloidal particles' directions were randomly oriented in the MF, there was no anisotropy in the permittivity of the MF. However, if the external magnetic field was applied to the MF, the direction of each particle's magnetic moment was oriented along the field, and the particles' long axis directions were oriented to the field direction. Accordingly, there occurred an anisotropy in the MF's permittivity. If a few particles coagulated and made a rigid stick-like cluster, the particles need not be of elongated shape but be spherical [43]. The rigid stick-like clusters in the MF played the same role of the elongated particles. In conclusion, the shape anisotropy or the rigid stick-like cluster formation is the origin of the MF's magnetic birefringence.

The third hypothesis assumed the needle-like cluster formation of the magnetic colloidal particles in the MF when the external field is applied to the MF and the needle-like clusters were oriented in the field direction [41]. As the same manner in the second hypothesis, the electric polarizability of the needle-like cluster differs in the cluster axis direction and in the perpendicular direction, there occurred an anisotropy in the permittivity of the MF and that was the origin of the magnetic birefringence. The difference between the second and the third hypotheses is that the elongated particles or the stick-like clusters in the former theory made the Brownian rotation even under the external field, while the needle-like clusters in the latter theory did not make Brownian rotation but was just oriented to the field direction. Therefore, the Langevin function, $L(x)$, appeared in the mathematical formula of the magneto-optical properties in the second hypothesis model while $L(x)$ did not appear in the formula in the third hypothesis model [41, 43]. Here, $L(x)$ is expressed by:

$$L(x) = \coth x - \frac{1}{x} \quad (5)$$

The first hypothesis was denied by Abu-Safia *et al.*'s magnetic birefringence experiment at low temperature of the MF [39]. They measured the

MF's magnetic birefringence with decreasing the MF's temperature. The birefringence suddenly plunged near the MF's melting point with decreasing the temperature (See Fig. 7(b)). This was due to the fact that the colloidal particles could neither move nor rotate once the solvent froze. If the first hypothesis were correct, as the magnetic moment of the colloidal particle could freely rotate even if the particle was fixed by the frozen solvent, the birefringence plunge could not occur.

The second hypothesis was proposed to explain the Majorana effect [30] which was discovered well before the MF's magnetic birefringence was discovered [33]. However, it had a serious contradiction when applied to explain the MF's magnetic birefringence. The mathematical expression of the birefringence, Δn , derived from this hypothesis, contains a factor [43, 44],

$$\left[\frac{1}{3} - \frac{L\left(\frac{\nu M_s H}{k_B T}\right)}{\left(\frac{\nu M_s H}{k_B T}\right)} \right],$$

where ν and M_s are the colloidal particle's volume and the saturation magnetization, respectively. H , T and k_B are the external field strength, temperature and the Boltzmann's constant, respectively. Langevin's function, $L(x)$, is expressed by:

$$L(x) \approx \frac{x}{3} - \frac{x^3}{45} \quad \text{for } |x| \ll 1. \quad (6)$$

If we use Eq. (6), the birefringence, Δn , satisfies in a weak external field region ($\frac{\nu M_s H}{k_B T} \ll 1$),

$$\begin{aligned} \Delta n &\propto \left[\frac{1}{3} - \frac{L\left(\frac{\nu M_s H}{k_B T}\right)}{\left(\frac{\nu M_s H}{k_B T}\right)} \right] \\ &\propto \frac{\left(\frac{\nu M_s H}{k_B T}\right)^2}{45} \\ &\propto H^2. \end{aligned} \quad (7)$$

This is contradictory to the experimental result that the MF's Δn is proportional to H in a

weak field region:

$$\Delta n \propto H.$$

Once again, we stress that the relation $\Delta n \propto H$ for the MF is important, because for almost all the materials, the relation $\Delta n \propto H^2$ holds. This relation can be generally derived by linear response theory [45]. When the linear response theory is applicable, the diagonal components of the ordinary material's permittivity tensor, $\vec{\epsilon}$, can be expanded by:

$$\begin{aligned} \epsilon_{xx} &= \epsilon_1 + a_2 H^2 + a_4 H^4 + \dots \\ \epsilon_{yy} &= \epsilon_1 + b_2 H^2 + b_4 H^4 + \dots, \end{aligned} \quad (8)$$

where, ϵ_{xx} is the x, x components of $\vec{\epsilon}$ in a Cartesian coordinate system (x, y, z) . $\epsilon_1, a_2, a_4, b_2$ and b_4 are constants. Refer to the Appendix for deriving the relation of the Δn 's H^2 dependence. Eq. (8) holds for the ordinary material's ordinary state. However, it does not hold for the MF's magnetic birefringence: it implies that the MF is in an unstable state when it shows the magnetic birefringence. The condition that Eq. (8) holds is that the fluctuation of a physical quantity in a physical system is expressed by a linear combination of the physical quantities in that physical system [46]. It means that the fluctuation is small enough to be expressed by the linear combination of the physical quantities. However, if the fluctuation becomes large, it does not hold and consequently Eq. (8) does not hold. Therefore, the MF's magneto-optical effect is induced in the state in which large fluctuation exists or in a so-called critical state.

From the above discussion, it follows that the third hypothesis is the true physical picture. In the following, we prove that the MF's magneto-optical effect is a critical phenomenon of a second order phase transition.

The third hypothesis assumed that all the aggregates in the MF were the sufficiently elongated needle-like clusters the axes of which are all directed to the field direction. Accordingly, we can assume that the depolarization factor, N , of the needle-like cluster in the axis direction is zero. On the other hand, there still remains a considerable number of colloidal particles monodispersed in the solvent. As the particles are almost spherical, the depolarization factor, N , of these monodispersed particles is $\frac{1}{3}$. Accordingly, with weighing the

volume fraction, the average depolarization factor, $\langle N \rangle$, is expressed by:

$$\langle N \rangle = \frac{\left(\frac{1}{3} \right) \cdot \phi_{mon} + 0 \cdot \phi_{agg}}{\phi} \quad (9)$$

$$= \frac{1}{3} \cdot \frac{\phi_{mon}}{\phi}$$

where ϕ_{mon} is the volume fraction of the colloidal particles which are monodispersed in the MF and ϕ_{agg} is the volume fraction of the colloidal particles which aggregate and ϕ is the volume fraction of all the particles in the MF, satisfying:

$$\phi_{mon} + \phi_{agg} = \phi. \quad (10)$$

From Eqs. (9) and (10):

$$\langle N \rangle = \frac{1}{3} \cdot \left[1 - \frac{\phi_{agg}}{\phi} \right] \quad (11)$$

is obtained. On the other hand, though in this paper we do not explain [41, 47, 48], the MF's magnetic birefringence, Δn , is expressed by the average depolarization factor, $\langle N \rangle$, as:

$$\Delta n = \Delta n_0 (1 - 3 \langle N \rangle), \quad (12)$$

where Δn_0 is a positive constant. Inserting Eq. (11) into Eq. (12) yields:

$$\Delta n = \Delta n_0 \cdot \frac{\phi_{agg}}{\phi}. \quad (13)$$

Here, we heuristically introduce an order parameter, Δ , defined by:

$$\Delta \equiv \frac{\phi_{agg}}{\phi}. \quad (14)$$

The physical meaning of the order parameter, Δ , is that if all the colloidal particles in the MF are monodispersed, $\Delta = 0$; a completely disordered state. If all the particles make the needle-like clusters, $\Delta = 1$; a completely ordered state.

Now, we assume that the phase transition with regard to this order parameter, Δ , is of second order and prove that this assumption is consistent with the experimental result. The Gibbs energy, G , of the MF under the external magnetic field is Taylor-expanded with regard to Δ , under an external field, H , by:

$$G(T, H, \Delta) = G_0(T, H) + \frac{a}{2} \left(\frac{T}{T_a} - 1 + f(H) \right) \Delta^2 \left. \vphantom{G(T, H, \Delta)} \right\} + b\Delta^4 - cf(H)\Delta. \quad (15)$$

Here, there is no Δ^3 term due to the phase transition of second order, $G_0(T, H)$ is the Gibbs free energy, if there is no aggregation in the MF, a , b , c and T_a are positive constants, $f(H)$ is the monotonous increasing function of H [41, 47, 48]. Be careful that a and b in Eq. (15) are different from those in Eq. (8). The minimum condition of the free energy leads to:

$$\frac{\partial G(T, H, \Delta)}{\partial \Delta} = 0. \quad (16)$$

Inserting Eq. (15) into Eq. (16), we obtain:

$$\Delta = \frac{c}{a} \cdot \frac{f(H)}{\frac{T}{T_a} - 1 + f(H)}. \quad (17)$$

Now, Eq. (17) is equivalent with the empirical formula Eq. (4) if Eqs. (13) and (14) are taken into account. Thus we see that the peculiar MF's magnetic birefringence is consistently explained if we assume the third hypothesis physical model, the order parameter, Δ , defined by Eq. (14) and the phase transition of second order.

However, there remain two important contradictions with respect to the above interpretation. The first one is the contradiction to the Landau criterion [49]. If a phase transition of second order occurs, the two phases before and after the transition should belong to the same space symmetry group. As a typical example, the phase transition of nematic liquid crystal is of first order [50]. The nematic liquid crystal consists of stick-like molecules. In high temperature region, the direction of the stick-like molecule's axis is randomly oriented and it is an isotropic phase. With temperature decrease, all the axes of the molecules are suddenly oriented to one direction at temperature, T_C , which is the nematic phase. The two phases evidently belong to different space symmetry groups and consequently this phase transition is a first order transition. In the same way, as the MF's monodispersed phase and the needle-like cluster formed phase belong to the different space symmetry groups, this transition should not be a second order transition.

The second contradiction is related to the very definition of the MF; the MF is the colloidal solution in which the magnetic colloidal particles are stably dispersed in the solvent and they would not aggregate to make clusters. In fact, if they really make clusters, the clusters would not dissolve due to a short-distance molecular force and the MF should be no longer the stable colloidal solution. In truth, both contradictions are closely connected and they are solved in the last section, §V *Discussion*.

IV. Experimental Study of Cluster Formation in a Magnetic Fluid

In the previous sections, we argued the cluster micrographs in the MF and the several experiments which cannot be interpreted without assuming the existence of the clusters in the MF. In this section, we argue the direct experimental studies on the clusters in the MF.

A. Local Field in Magnetic Fluid (NMR Experiment)

When one studies the magnetic colloidal particle behavior in the MF, it is necessary to know how strong the magnetic field is at the particle position. The so-called local magnetic field at the particle position is different from an external field, H_0 , which is applied to the MF. For example, let us consider the local field, H_{loc} , at a certain particle location. In addition to H_0 , there are magnetic fields generated by the permanent magnetic moments of all the magnetic colloidal particles surrounding this particle. If the colloidal particles are uniformly distributed, the problem is not so difficult, but the existence of many clusters in the MF together with the magnetic colloidal particles in the MF make the problem more complicated. The local field, H_{loc} , inside the cluster should be much stronger than that at the rest of the system. However, as the cluster is micron size, as is shown in the micrograph of Fig. 1, it is difficult to measure H_{loc} with ordinary equipment although some researchers have tried to measure the local field of the MF [51]. We can make such measurement with the nuclear magnetic resonance (NMR) method. The following is the concrete technique [52]. We look upon one nucleus of hydrogen atom which composes a water molecule which belongs to the solvent of water-solvent MF. The magnetic spin of the hydrogen nucleus, or proton, makes a precession of angular frequency, ω_0 , under the local field, H_{loc} , satisfying:

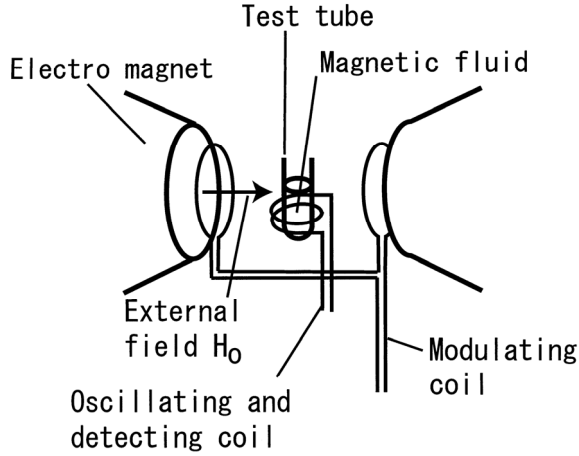


FIG. 10. Experimental setup of NMR measurement of water-solvent MF [52].

$$\omega_0 = \gamma H_{loc}, \quad (18)$$

where $\gamma = 3.36 \times 10^4 \text{ sec}^{-1} (\text{A/m})^{-1}$ for proton. Fig. 10 shows the experimental set up. In this experiment, a water-solvent MF, Sample *G*, was used. Its characteristics are tabulated in Table I. A static external field, H_0 , is applied to a glass tube which is filled with the MF Sample *G* perpendicular to the glass tube axis. An ac magnetic field, H_{ac} , of angular frequency, ω , is also applied to the sample in the direction perpendicular to H_0 and parallel to the glass tube axis. When the strength of H_0 is increased from zero, the local field strength, H_{loc} , also increases from zero. With the increase of H_{loc} , when ω_0 derived from Eq. (18) satisfies:

$$\omega_0 = \omega,$$

the hydrogen nucleus of the water molecule in the MF solvent begins a resonance with the ac field, H_{ac} , which induces huge energy absorption from the ac field generator. In real experiment, the resonance is detected by the AC field generating coil in Fig. 10 with an abrupt huge increase in the imaginary part, χ'' , of the complex magnetic susceptibility, χ^* , of the sample. Here, the complex magnetic susceptibility, χ^* is expressed by:

$$\chi^* = \chi' - i\chi'',$$

where χ' and χ'' are the real part and imaginary part of χ^* , respectively. Modulating coils in Fig. 10 amplifies the signal of $\frac{d\chi''}{dH}$. The local field, H_{loc} , consists of three terms: the external field, H_0 , the demagnetizing field, H_d , and the Lorentz

field, H_L , expressed by:

$$H_{loc} = H_0 + H_d + H_L. \quad (19)$$

The Lorentz field which a certain hydrogen nucleus feels is the sum of the magnetic fields induced by all the magnetic colloidal particles' permanent magnetic moments surrounding the nucleus. Here, the hydrogen nucleus is in a water solvent molecule in the MF. A simple approximation is as follows. We assume a virtual spherical cavity of radius a centered at the hydrogen nucleus, or proton. (See Fig. 11.) The radius a is a couple of nanometers, and there is no magnetic colloidal particle in this virtual cavity.

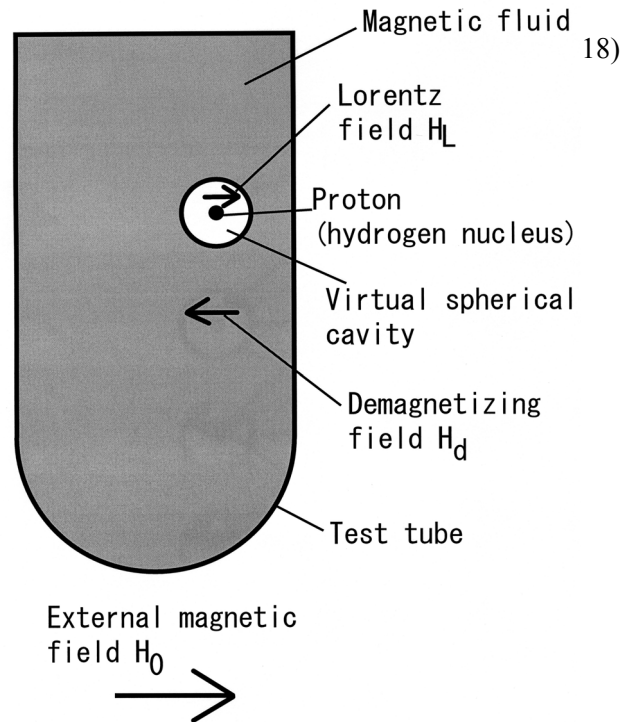


FIG. 11: The schematic figure to explain the local field, H_{loc} . The scale of the virtual cavity is in the order of a couple of nanometers, while the diameter of the glass test tube is a couple of centimeters.

Assuming the MF surrounding the cavity a continuum, there is a magnetic charge generated on the inner surface of the cavity, which induces the Lorentz field, H_L , given by:

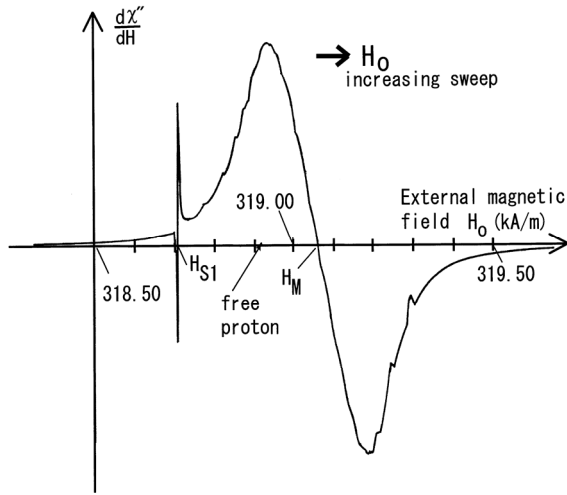
$$H_L = \frac{M}{3},$$

where M is the MF's magnetization [53]. On the other hand, the MF sample fills the cylindrical glass test tube and H_0 is applied perpendicular to the cylindrical axis, the demagnetizing field, H_d ,

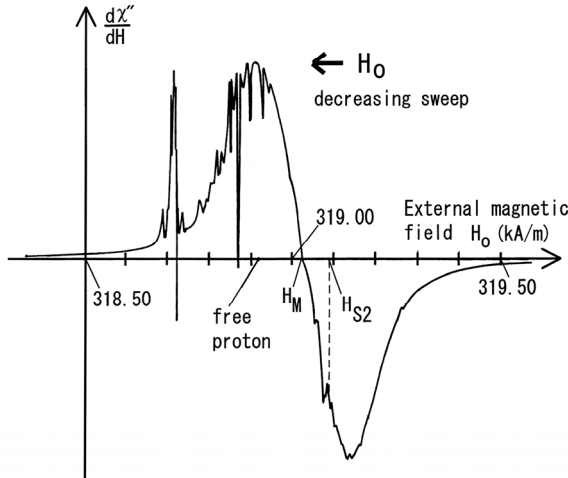
is $-\frac{M}{2}$. Inserting these values into Eq. (19), we obtain:

$$H_{loc} = H_0 - \frac{M}{2} + \frac{M}{3} = H_0 - \frac{M}{6} \quad (20)$$

Fig. 12 shows the experimental result obtained from the experimental setup in Fig. 10.



(a)



(b)

FIG. 12. The experimental differential derivative, $\frac{dx''}{dH_0}$, as a function of the external field, H_0 . (a): the increasing sweep of the H_0 , (b): the returning sweep, or decreasing sweep, of the H_0 .

The experimental differential derivative, $\frac{dx''}{dH_0}$, is shown as a function of the external field, H_0 , in Fig. 12. $\frac{dx''}{dH_0}$ in Fig. 12(a) was obtained with the increasing sweep of H_0 ; while

that in Fig. 2(b) was obtained with the returning sweep, or decreasing sweep of H_0 . The frequency of the ac field, H_{ac} , was 17.063 MHz. The corresponding resonant field, H_F , of the free proton is 318.915 kA/m. However, the experimental resonant field, H_M , was 319.046 kA/m, which was greater than H_F by 0.131 kA/m. It was due to the second term at the right hand side of Eq. (20). When H_0 amounts to as high as 300 kA/m, the MF's magnetization, M , is almost saturated and it can be replaced with the saturation magnetization, $M_S = 0.90$ kA/m. Then, Eq. (20) is written as:

$$H_M - H_F = \frac{M_S}{6}. \quad (21)$$

Inserting $M_S = 0.90$ kA/m into the right hand side of Eq. (21), the theoretical value of $(H_M - H_F)$ is estimated to be 0.15 kA/m, which is in fair agreement with the experimental value, 0.131 kA/m. In conclusion, the magnetic field which is applied to the proton in the water-solvent MF, is not only the external field, H_0 , but also $(-\frac{M_S}{6})$. Accordingly, the external field should be increased greater than H_F by $(\frac{M_S}{6})$, then the protons in the MF make the resonance.

The more important problem is other resonant fields' existence in Fig. 12. There are two very small resonant fields, one is less than H_M by 0.358 kA/m, and the other one whose resonance is much less than the former one, is greater than H_M by 0.064 kA/m. Hereafter, we call these resonant fields, H_{S1} and H_{S2} , respectively. By the way, there are many peaks between H_{S1} and H_M in Fig. 12(b). It is, however, due to wiggle which is the delayed resonant signal generated when the external field, H_0 , passes through H_M in the increasing field sweep [54]. The resonance at H_{S1} corresponds to the proton's precession resonance in the MF region, in which the magnetization is greater than that in the rest of the region. It means that the region was the cluster, i. e., the H_{S1} resonance corresponded the resonance of the protons in the clusters. Let the cluster's magnetization be M_1 , and the relation between H_F and H_{S1} be expressed by:

$$H_F = H_{S1} + \frac{1}{3}M_1 - \frac{1}{2}M_S. \quad (22)$$

If the cluster is of a needle-like shape and the demagnetizing field in the cluster is negligible,

then, from Eqs. (21) and (22):

$$\frac{1}{3}(M_1 - M_S) = H_M - H_{S1}, \quad (23)$$

holds and consequently, $M_1 = 1.97$ kA/m is obtained. Assuming the colloidal particles' volume fraction to be proportional to the magnetization of the MF, the volume fraction of the particles in the cluster was 0.66 %. In the same manner, the magnetization and the particles' volume concentration of the area in the MF corresponding to H_{S2} were 0.71 kA/m and 0.24 %, respectively. This area corresponds to the white stripes accompanying the clusters in Fig. 1(a). By the way, the initial volume fraction is 0.30 %.

In conclusion, by NMR experiment, not only the local fields of the MF were measured, but also the magnetization and particle concentration in the cluster can be obtained. We also confirmed that not only the cluster formation but also the thinner particles' concentration area existed accompanying with the clusters in the MF. Accordingly, the cluster is not simply a closely connected aggregate of the colloidal particles, but a group in which the particles have some distance from each other.

B. Nature of the Magnetic Fluid Phase Transition (Latent Heat Measurement)

In the previous section, we interpreted the MF's magneto-optical effect as the phase transition between the colloidal particles' monodispersed phase and the phase in which the clusters were formed. In addition, the experiment showed that this transition was a second order phase transition. However, from a theoretical viewpoint, this phase transition should be a first order phase transition. If two phases belong to different symmetry groups, the phase transition from one phase to the other should be a first order phase transition [49]. In fact, the colloidal particles' monodispersed phase and the phase in which the needle-like clusters were formed and directed to the external field, apparently belong to different space symmetry groups. Therefore, the phase transition of the MF accompanying the magneto-optical effect should be the phase transition of first order from the theoretical viewpoint. However, the theoretical conjecture sometimes implicitly assumes a physical system too simplified and misleads to an incorrect conclusion. This contradiction is easily solved by an experiment. If this phase transition is

accompanied with a latent heat or heat discharge, the phase transition should be of first order, and if not, it is not a first order phase transition. We performed an experiment to test whether or not the phase transition of the MF was accompanied with heat charge or discharge.

Differential Scanning Calorimeter (DSC)

We used a differential scanning calorimeter (DSC) to carry out this experiment [55]. The measuring method is as follows. Fig. 13 shows the schematic construction of the DSC. We used two completely similar sample holders made of aluminum [48]. The first holder was filled with the MF and hermetically sealed with an aluminum lid. The other one was also sealed with the same lid leaving the inside empty (See Fig. 13(a)).

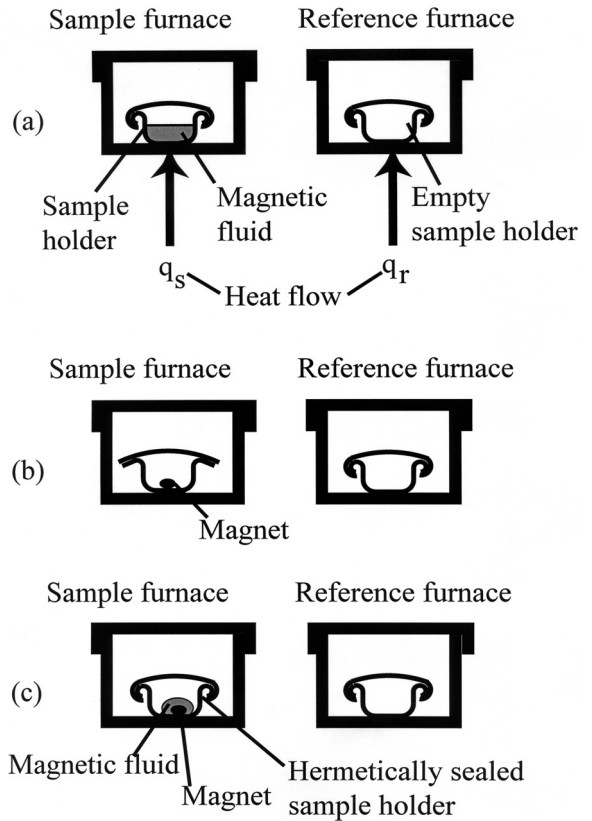
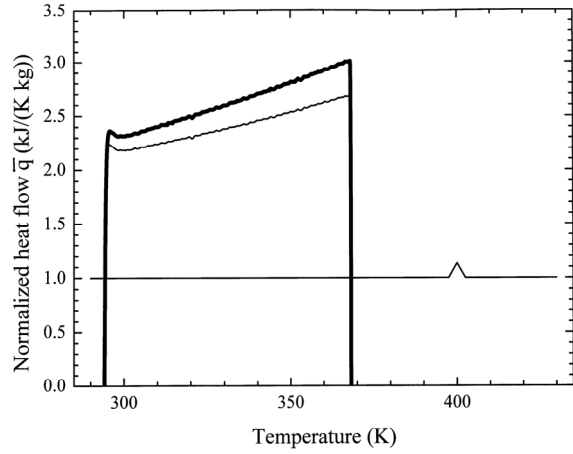


FIG. 13. Schematic construction of Differential Scanning Calorimeter (DSC).

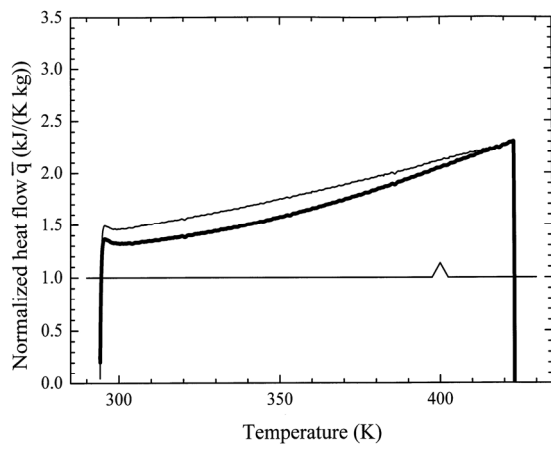
We put these two sample holders in the adiabatically isolated two furnices of a DSC; a sample furnace and a reference furnace, respectively. Heat flows, q_s and q_r , were supplied to the sample holder in which the MF was filled and the empty holder from the heat source of the DSC so that both holders increased their temperature at the same rate of β (K/sec). Of course, the two heat flows, q_s and q_r , were carefully controlled to keep the two sample

holders' temperature rise rate, β , constant. For example, if there occurs a heat discharge from the MF at temperature, T , q_s should be decreased so that both samples' temperature rise rate, β , is constant. In fact, if there is a heat discharge from the MF sample, there should be a new difference between q_s and q_r , in order to keep the two sample holders' temperature increase rates constant. If we measure the heat flow difference, $q = q_s - q_r$, as a function of the sample temperature, T , we can learn whether or not there occurs a heat discharge or absorption from the sample, together with the sample's heat capacity which can be estimated from the gradient of q as a function of T . In this experiment, we measured the heat flow difference, q , in the temperature region from $T = 295\text{K}$ to $T = 423\text{K}$ by increasing T . Three different MF Samples, A, B and E, were used. Their characteristics are tabulated in Table I. The thin solid curves in Figs. 14(a), (b) and (c) are the experimental $\bar{q} - T$ curves for the samples, A, B and E, respectively. Here, $\bar{q} = q / (\beta m)$, where, m is the MF's mass in the holder. In the present experiment, the most important issue was whether or not there were any traces of a peak in the $\bar{q} - T$ curves. If there was a phase transition of first order for the MF sample at a certain temperature, T , and consequently there was a heat discharge or heat absorption, there should be a peak in the $\bar{q} - T$ curve around the temperature T . The upward peaks and the downward peak indicate the heat discharge and absorption of the sample, respectively. The peak area is equal to the heat amount. Although the DSC's principle is simple, it can detect very small heat discharge or heat absorption. For example, a virtual $\bar{q} - T$ curve with a small triangle peak at around $T = 400\text{K}$ is shown in every figure, (a), (b) and (c) in Fig. 14. The triangle area is equal to the absorbed heat of 334 J/kg which is just 10^{-3} times as large as the latent heat between water and ice. In fact, from this prominent peak area, one can detect a very weak heat absorption, the amount of which is 10^{-3} times as large as the water latent heat. There is no peak in every $\bar{q} - T$ curve in Figs. 14(a), (b) and (c). This implies that there was no phase transition of first order in the MF samples in the temperature region $295\text{K} < T < 423\text{K}$.

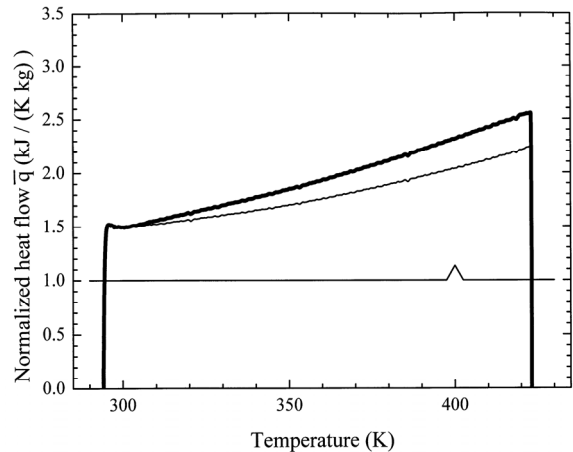
We also performed the experiment under a magnetic field. In this experimental setup, it was not possible to apply the external field to the sample by electromagnets. Instead, we put a fragment of a strong permanent magnet together with the MF in the sample holder, when we performed the calorimetric experiment. In order to remove the calorimetric contribution by the magnet fragment, we put only the magnet fragment in the sample holder and made the measurement to obtain $\bar{q}_1 - T$ curve (Fig. 14(b)). Then, filling the MF in the sample holder and hermetically sealing the MF and the magnet fragment with the lid, the same measurement was made to obtain $\bar{q}_2 - T$ curve (Fig. 14(c)). The difference $\bar{q} = (\bar{q}_2 - \bar{q}_1)$ is the true heat flow due to the MF. A non-uniform magnetic field was applied to the MF samples in this experiment. The average fields for three MF samples, A, B and E, were 8.0 , 8.0 and 9.5 kA/m, respectively. The maximum fields for these samples were 16.0 , 18.0 and 19.0 kA/m, respectively. As the applied field was not uniform, if a phase transition of first order occurred, there was a considerable width in transition temperature from point to point in the MF. However, if there was a phase transition of first order, there should be a peak with a wide width in the $\bar{q} - T$ curve instead of a sharp peak as there would be under the uniform magnetic field. The $\bar{q} - T$ curves obtained by this method are shown with thick solid lines in Figs. 14(a), (b) and (c). Evidently, there was no peak in the three curves. On the other hand, as was mentioned in §II A *Direct Observation of Macro-Clusters by Optical Microscope*, in the MF Sample A, the so-called macro-clusters which can be observed by an optical microscope disappeared with the temperature increase in the same temperature region as the present experiment under the external field. In conclusion, the phase transition from the phase in which the macro-clusters were observed to the phase in which the macro-clusters were not observed, was not a first order phase transition. This experimental conclusion contradicts the theoretical conclusion that the phase transition with the formation of shape anisotropic coagulation with the same direction should be a first order phase transition. This contradiction is to be solved in the last section, §V *Discussion*.



(a)



(b)



(c)

FIG. 14: The heat flow difference, \bar{q} , as a function of temperature, T , for the unit volume of the MF samples: (a), (b) and (c) for the Samples A, B and E, respectively. The thin solid lines are under no field. The thick solid lines are under a magnetic field [48].

C. Mutual Interaction between Magnetic Colloidal Particles in a Magnetic Fluid

The origin of the cluster formation in the MF is believed to be the attractive force between the

magnetic colloidal particles. At room temperature, the two particles in the MF cannot be closer than a certain distance due to the steric hindrance of the surfactant molecules which cover the surface of the particles [56]. Furthermore, the magnetic attractive energy between the two particles is much less than the particle's thermal energy. In fact, the calculation of the magnetic attractive energy and the thermal energy also leads to the same conclusion. We tested whether or not the mutual magnetic attractive interaction between the magnetic colloidal particles in the MF is really negligible. The experimental method is as follows. The three MFs: A, B and E in Table I were used as mother MFs. By diluting these mother MFs with each of their solvents, we obtained about 1000 fold diluted MF samples, H, I and J, respectively. Their characteristics are tabulated in Table I. We measured the $M - H$ curves, the temperature dependence of the initial complex magnetic susceptibilities and the frozen MF's magnetic aftereffect of both the mother MFs and the diluted MFs. If the MF is diluted 1000 times, the average distance between the nearest neighbor's particles increases 10 times as large as that of the mother MF. Of course, this argument implies an implicit assumption that the particles do not make clusters, or the particles distribution is uniform. As the magnetic dipole-dipole interaction energy between the two colloidal particles is proportional to the inverse cube of their distance, the magnetic dipole-dipole energy between the particles in the diluted MF is 10^{-3} times as large as that of the mother MF. Accordingly, if there is a mutual interaction between the particles in the mother MF, that interaction is negligible in the 1000 fold diluted MF. It follows that even if there is a mutual interaction in the mother MF, there is no interaction in the highly diluted MF, and their $M - H$ curves, the temperature dependent curve of the initial complex magnetic susceptibility and time dependent curve of the frozen MFs' remanent magnetization should be different in shape even if the concentration compensation is given. Conversely, if there is no interaction in the mother MF, the graph of the mother MF and that of the diluted one should coincide after concentration compensation. In the following, we show the three different experimental results successively.

1. $M - H$ Curve under Static Magnetic Field Conventional Theory

Conventionally, researchers in this field believe that the MF's magnetization curve is theoretically obtained assuming no interaction between the magnetic colloidal particles. When an external field, H , is applied to the MF, the average magnetic moment of the magnetic colloidal particle of volume ν in the field direction, $m_\nu(H)$, is given by:

$$m_\nu(H) = \nu M_s L\left(\frac{\nu M_s H}{k_B T}\right) \quad (24)$$

where the Langevin function $L(x)$ was expressed by Eq. (5) and M_s , ν , T and k_B are magnetic colloidal particle's saturation magnetization, volume, temperature and Boltzmann constant, respectively. As the colloidal particle's volume in MF is distributed widely, the MF's magnetization, $M(H)$, is given by the integration of $m_\nu(H)$ with weighting function, $f_{dst}(\nu)$, with respect to the particle volume, ν , given by:

$$M(H) = M_s \phi \int_0^\infty L\left(\frac{\nu M_s H}{k_B T}\right) f_{dst}(\nu) d\nu. \quad (25)$$

Here, $f_{dst}(\nu)$ is the distribution function of the magnetic particles in the MF with respect to their volume, ν and ϕ is the volume fraction of the particles. As $f_{dst}(\nu) d\nu$ is the fraction of particles the volume of which falls in $(\nu, \nu + d\nu)$,

$$\int_0^\infty f_{dst}(\nu) d\nu \equiv 1, \quad (26)$$

holds. Chantrell *et al.* [57] assumed the colloidal particle distribution in the MF as a log-normal distribution and assumed $f_{dst}(\nu)$ as:

$$f_{dst}(\nu) = \frac{1}{\sqrt{2\pi}\sigma\nu} \exp\left\{-\frac{\left[\ln\left(\frac{\nu}{\nu_0}\right)\right]^2}{2\sigma^2}\right\}, \quad (27)$$

where σ and ν_0 are positive constants. Inserting Eq. (27) into Eq. (25) and choosing suitable values of σ and ν_0 , they tried to fit the $M-H$ curve calculated from Eq. (25) to the experimentally obtained $M-H$ curve. "Unfortunately", the agreement between the two curves was excellent. Since then almost all the researchers were convinced of the validity of Eq. (25) and naturally convinced with the no

interaction between the magnetic particles in the MF. Even if there was a small deviation between the two curves, it was ascribed to the deviation of the particle distribution from the log-normal distribution.

Experiment Whether or Not the Interaction Exists

In the following, we show the existence of the small interaction between the particles in the MF by comparing the $M - H$ curves of the mother MF and its highly diluted MF [58, 59]. If the magnetic interaction between the magnetic colloidal particles in the mother MF is negligible, Eq. (25) holds. In addition, if we denote the mother MF's $M(H)$ and the diluted MF's $M(H)$ as $M_{moth}(H)$ and $M_{dil}(H)$, respectively, $M_{moth}(H)$ is expressed after Eq. (25) as:

$$\left. \begin{aligned} M_{moth}(H) &\equiv M_s \phi_{moth} \int_0^\infty L\left(\frac{\nu M_s H}{k_B T}\right) f_{dst}(\nu) d\nu. \\ &= \frac{\phi_{moth}}{\phi_{dil}} \cdot M_s \phi_{dil} \int_0^\infty L\left(\frac{\nu M_s H}{k_B T}\right) f_{dst}(\nu) d\nu. \\ &= \frac{\phi_{moth}}{\phi_{dil}} \cdot M_{dil}(H), \end{aligned} \right\} (28)$$

where ϕ_{moth} and ϕ_{dil} are the particles volume fractions of the mother MF and the diluted MF, respectively. If we define a dilution factor, r , by $r = (\phi_{moth} / \phi_{dil})$, Eq. (28) leads to

$$M_{dil}(H) = \frac{1}{r} M_{moth}(H). \quad \text{Here, we used the}$$

important property that $f_{dst}(\nu)$ was invariant even after a high dilution. Therefore, by comparing both the experimental $M_{dil} - H$ curve and the $\frac{1}{r} M_{moth}(H) - H$ curve, if they coincide, it is concluded that there is no interaction in the mother MF.

We used three different mother MF samples, A, B, E and their diluted samples, H, I, J, respectively. We measured their magnetization at magnetic fields from $H = 0$ to as large as $H = 750$ kA/m at room temperature. The values of the dilution factor, r , were 2450, 1300 and 1230, for the couples, (A, H), (B, I) and (E, J), respectively. The MF samples' characteristics are tabulated in Table I. Hereafter, we compare the experimental diluted MF's magnetization, $M_{dil}(H)$, and the mother MF's $\frac{1}{r} M_{moth}(H)$.

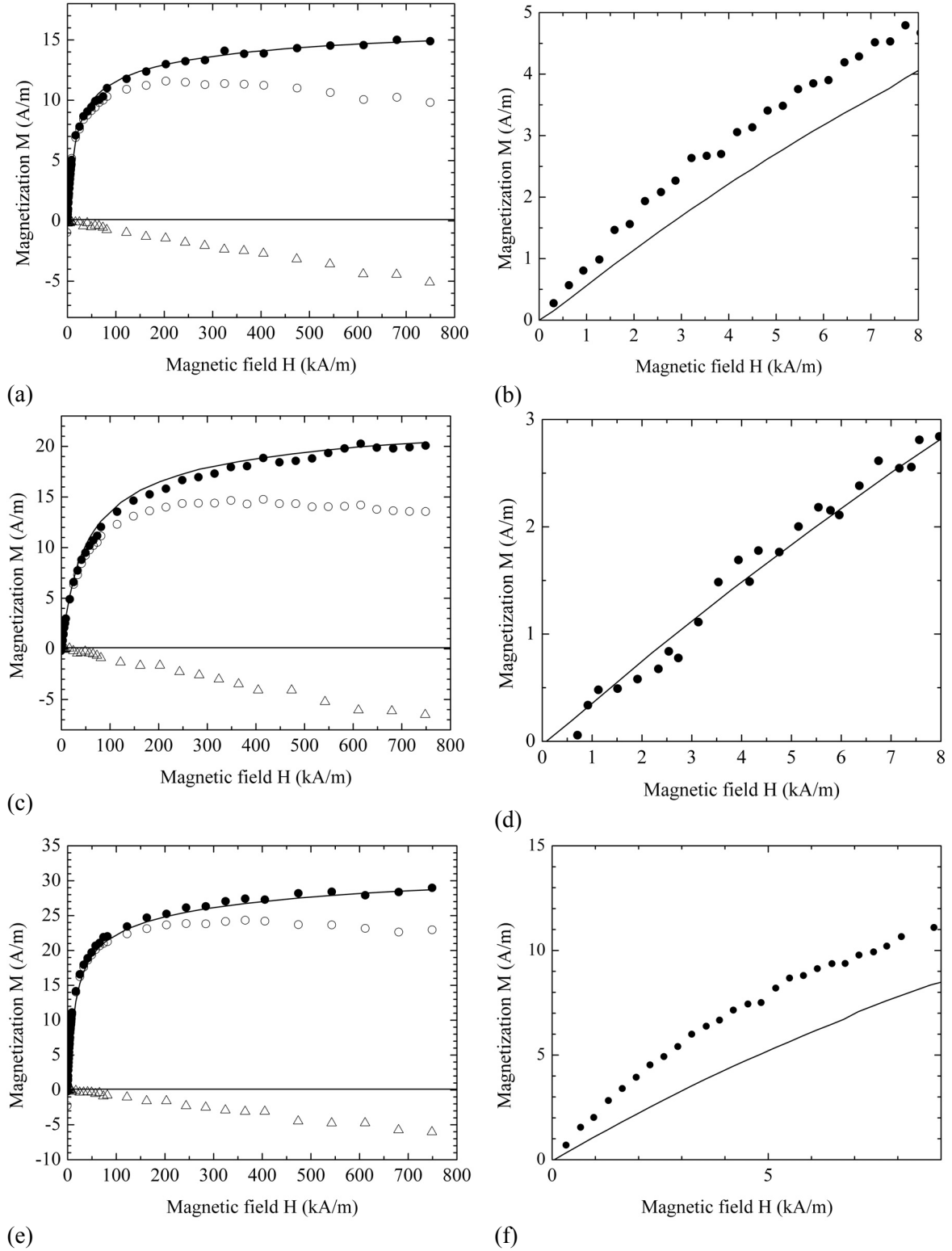


FIG. 15: The $M - H$ curves of the diluted MFs and the mother MFs [58, 59]. The mother MF's magnetization M is divided by the dilution factor r . \circ : raw magnetization of the diluted MF, Δ : magnetization of the MF's solvent, \bullet : revised magnetization of the diluted MF, $M_{dil}(H)$, solid line: the magnetization of the mother MFs divided by the dilution factor, r , i.e., $\frac{1}{r}M_{moth}(H)$, (a): MF samples, A and H and paraffine (solvent), (b): magnified graphs of (a), (c): MF samples, B and I and alkylnaphthalene (solvent), (d): magnified graphs of (c), (e): MF samples, E and J and water (solvent), (f): magnified graphs of (e). The three solvents were all diamagnetic, and in (b), (d) and (f), only $M_{dil}(H)$ and $\frac{1}{r}M_{moth}(H)$ are shown.

Figs. 15(a), (c) and (e) show the $M - H$ curves of the MF couples, (A, H), (B, I) and (E, J), respectively [48]. The empty circles show the raw measured magnetization of the diluted MFs, H, I and J, respectively. The magnetization decreased in the high field region. This is due to the solvent's magnetization. The magnetization due to the magnetic colloidal particles was so small, that the magnetization of the solvent was no longer negligible. The empty triangles in (a), (c) and (e) are the solvents' magnetization. The three solvents: paraffine, alkylnaphthalene and water were all diamagnetic materials. The solid circles show the revised magnetization of the diluted MFs, $M_{dil}(H)$, or the raw magnetization reduced by the solvent's magnetization. The solid curve shows the magnetization of the mother MFs divided by the dilution factor, r , or $\frac{1}{r}M_{moth}(H)$. The solid circles and the solid lines coincide fairly well in the three figures (a), (c) and (e). Figs. 15(b), (d) and (f) are the magnified graphs of (a), (c) and (e), respectively, in the weak field region. The solid circles and solid lines are the same as those in (a), (c) and (e). The solid circles evidently deviate from the solid curve in each graph of (b) and (f). The gradient of the solid circles is greater than that of the solid curve in the weak field region in each figure. On the contrary, the solid circles and the solid curve coincide still in the weak field region in (d). This is not simply due to the existence of the interaction between the particles in MF samples A and E and no interaction in the MF sample B. Perhaps, it is due to the spontaneous coagulation in the MF samples A and E under no external field. In fact, if there is a magnetic interaction between the particles, the particles' magnetic moments are easier to orient in the same direction, and accordingly, the gradient of the solid curve should be greater than that of the solid circles in the weak field region. The experimental result was, however, opposite. In the MFs of paraffin or water solvents, there should exist clusters of the colloidal particles even under no external field, and the magnetic moments of the particles in the same cluster naturally make a closed magnetic circuit. It follows that the magnetic moment of the cluster is zero and it does not contribute to the MF's magnetization. When the external field is applied to the cluster and the field strength is gradually increased, the magnetic moment of each particle in the cluster is gradually oriented to the field direction, and at the same time, the cluster

changes its form to a chain orienting along the field direction. In such a case, the MF's magnetization is less than the magnetization of the MF in which the particles are monodispersed and each particle's magnetic moment independently interacts with the external field. It is the reason for the disagreement between the solid circles and the solid curves in the weak field region of (b) and (f).

Such an interpretation was shown to be correct in another MF by Chantrell *et al.* via computer simulation of a two-dimensional system [60, 61]. They showed that if there is an interaction amongst the magnetic colloidal particles in the two-dimensional case, they form closed chains under zero applied field. These closed chains collapse and gradually line up in the applied field direction with field increase. Therefore, the initial susceptibility of the system with interaction is less than that without interaction.

The fact that the colloidal particles in the water or paraffin solvent MFs are easier to coagulate than that in the alkylnaphthalene solvent MF was confirmed by the optical microscope observation. On the contrary, the solid circles and the solid line coincide even in the weak field region (d). It follows that there is no magnetic interaction between the magnetic colloidal particles in the alkylnaphthalene solvent MF only from this experimental fact. However, the next AC field experiment gives the opposite conclusion.

2. Initial Complex Magnetic Susceptibility

We also performed the following experiment on the MF samples A, B, E and I [62]. Filling the MF in the hermetically sealed nonmagnetic capsule, we put the capsule in the cryostat and cooled it to 4.2 K. Increasing the MF sample's temperature up to room temperature, we measured its initial complex magnetic susceptibility at temperature, T , with a constant temperature interval. Applying an AC magnetic field of amplitude, 79.6 A/m, to the sample at constant temperature, T , we measured the initial complex magnetic susceptibility, $\chi^* = \chi' - i\chi''$ for five different AC frequencies, $f = 0.1, 1, 10, 100$ and 1000 Hz, respectively. Here χ' and χ'' are the real and imaginary parts of the complex magnetic susceptibility, χ^* , respectively. Fig. 16(a) and (b) show the temperature dependence of χ' and χ'' , for the AC frequency $f = 1000$ Hz, respectively. They were normalized by the

colloid volume fraction ϕ . The MF sample B, the mother alkylnaphthalene solvent MF and its highly diluted MF sample I showed evidently different $\chi'/\phi - T$ and $\chi''/\phi - T$ curves. We can apply the same argument of the agreement of $M - H$ curves of the mother and the highly diluted MFs in the $\chi'/\phi - T$ and $\chi''/\phi - T$ curves [59]. It implies that there was magnetic interaction between the magnetic colloidal particles in the mother MF. However, in the static field experiment, or $M - H$ curve coincidence, it was concluded that there is no interaction between the particles in the mother alkylnaphthalene solvent MF. Therefore, it is concluded that the interaction was very weak.

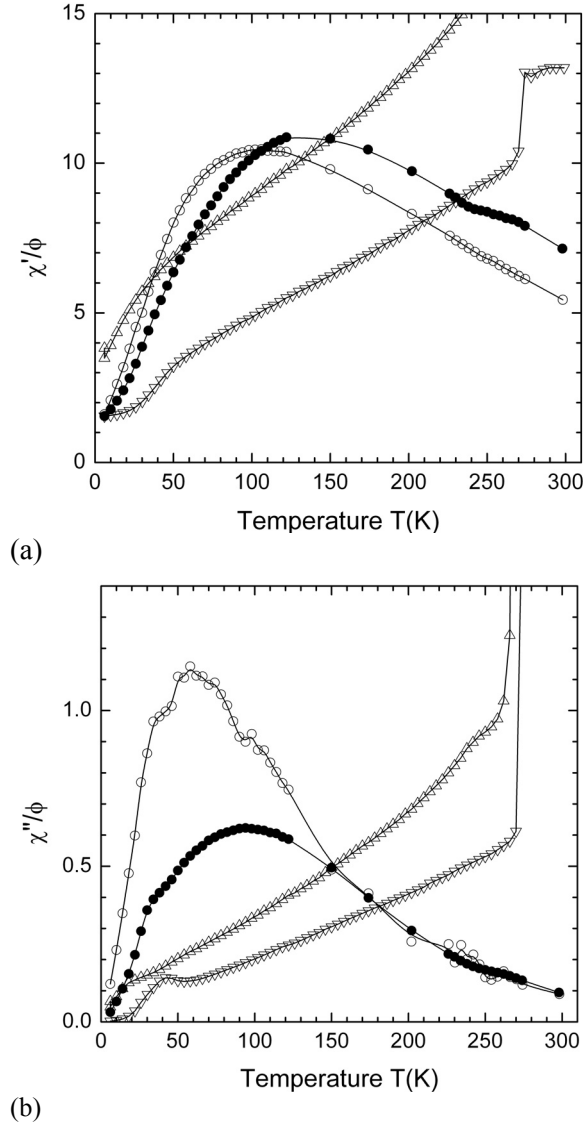


FIG. 16: (a) real part, χ'/ϕ , and (b) imaginary part, χ''/ϕ , of the initial complex magnetic susceptibility divided by the colloid volume fraction, ϕ , at 1000 Hz for the MF Samples, A(Δ), B(\bullet), E(∇) and I(\circ) [62].

The existence of a peak of χ' and χ'' with respect to the temperature, T , for the highly diluted MF sample, I, is explained as follows. As the magnetic interaction between the particles in the highly diluted MF is negligible, the MF is assumed to be superparamagnetic. Accordingly, MF Sample I's magnetic susceptibility, χ , should be proportional to the inverse of T , or χ increases with the decrease of T [63]. On the other hand, while the magnetic moment of the magnetic colloidal particle can rotate freely in the particle at the temperature higher than the temperature, T_B , which satisfies:

$$\frac{K \nu}{k_B T_B} = 1, \quad (29)$$

the magnetic moment is fixed in the particles at the temperature lower than T_B [64]. Here, K is the magnetic anisotropy constant and ν is the colloidal particle's volume. Hereafter, we call T_B a blocking temperature. Accordingly, when the MF's temperature is lower than T_B and also the solvent is frozen, the colloidal particles were imbedded in the solid solvent so that the magnetic moment is fixed in the MF. Therefore, in the low temperature region, when the AC field is applied to the MF, the fixed magnetic moment in the particle does not contribute to χ' . As the particle's volume, ν , is widely distributed in the MF, the blocking temperature, T_B , is also widely distributed. In conclusion, the particles in which the magnetic moments are fixed increase with the temperature decrease, to cause χ' to decrease with the temperature decrease. The two competing factors, χ' decrease due to the magnetic moment blocking and χ' increase due to that χ' is proportional to $1/T$ with decreasing temperature, create the peak in χ' with respect to the temperature. The same scenario explains the peak in χ'' . The small peak in χ'' at around $T = 110$ K must be ascribed to the Verwey transition [65].

On the other hand, the peak in χ' and χ'' of the mother MF is perhaps due to the spinglass interaction between the magnetic colloidal particles in the mother MF. It is well known that if the interaction of the magnetic spin of atoms is not strong enough to create a ferromagnetic state or antiferromagnetic state, but strong enough compared with that of paramagnetic atoms, the material shows a spin-glass state. Some metallic

alloys diluted with ferrous ions show typical spin glass state. This magnetic susceptibility, χ , shows a cusp as a function of temperature [66]. In the present MF Sample B's case, χ shows the cusp as a function of temperature and it also shows the weak interaction between the magnetic colloidal particles. Accordingly, it makes sense that the origin of the MF Sample B's cusp in χ in Fig. 16 is the spin glass state. Chantrell and Wolfath discussed the magnetic fine particle system's spin glass state and they suggested that the Vogel-Fulcher law holds in such a system [67]. If we assume τ as the transition time between the ground state of the magnetic spin in the spin glass state and the nearest excited state, τ obeys the Vogel-Fulcher law:

$$\tau = \tau_0 \exp\left[\frac{E}{k_B(T - T_0)}\right], \quad (30)$$

where τ_0 , E and T_0 are positive constants. Let's denote $f_r \equiv (1/\tau)$ as the resonant frequency of the transition. The imaginary part of the magnetic susceptibility, χ'' , is proportional to the sample's dissipation energy when the AC magnetic field is applied to the sample. Accordingly, when the χ'' is maximum at the temperature, T_p , the AC field's frequency, f , and the resonant frequency, f_p , should be equal and be in a resonant state. As $f_r = f$ at $T = T_p$, Eq. (30) is transformed to:

$$T_p - T_0 = \frac{E}{k_B} \frac{1}{(\ln f_0) - (\ln f)}, \quad (31)$$

where $f_0 \equiv (1/\tau_0)$. Eq. (31) is the typical criterion whether or not the magnetic material is in a spin glass state. Zhang, Boyd and Luo experimentally first found that Eq. (31) holds in dense MF [68]. Fig. 17 shows our experimental results whether or not Eq. (31) holds [62]. Besides the MF samples, B and I, we used other differently diluted samples, K ($\phi = 0.0484$), L ($\phi = 0.00792$) and M ($\phi = 0.00066$). Each sample's experiment was made at different AC field frequencies, $f = 10^{-1}$, 10^0 , 10^1 , 10^2 and 10^3 sec^{-1} , respectively, and the temperature, T_p , at which the χ'' was maximum, was determined. While

$\frac{1}{(\ln f_0) - (\ln f)}$ is scaled in the abscissa, T_p is scaled in the ordinate in Fig. 17 [62]. Here, $f_0 = 1 \times 10^9 \text{ sec}^{-1}$ was adopted. If Eq. (31) holds, the experimental points in Fig. 17 for each sample should fall on the same straight line. The

experimental data, T_p , fall almost on the same straight lines in Fig. 17 for samples B, K, L and M; while those of sample I evidently deviate from a straight line. This means that the Vogel-Fulcher law holds for the MF sample when the colloid's volume fraction, ϕ , is equal to or larger than 0.00066, while it no longer holds for the MF sample whose ϕ is equal to or less than 0.000080. In other words, the magnetic colloidal particles in the dense MF make a spin glass state; while they no longer make it when ϕ of the MF becomes as small as 0.000080. However, as mentioned many times, there should be no interaction between the magnetic colloidal particles in the MF from the theoretical viewpoint. This contradiction is to be solved in the last section, §V Discussion.

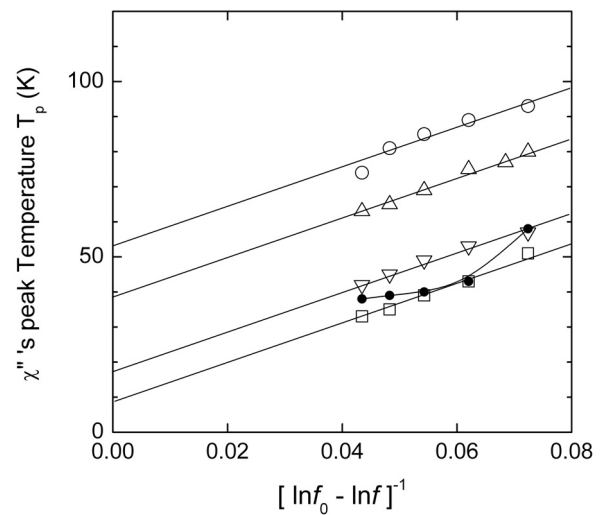


FIG. 17. T_p vs $(\ln f_0 - \ln f)^{-1}$ relations. $(\ln f_0 - \ln f)^{-1}$ is scaled in the abscissa; while T_p is scaled in the ordinate [62].

$$f_0 = 1 \times 10^9 \text{ sec}^{-1}$$

○: Sample B, $\phi = 0.1044$. △: Sample K, $\phi = 0.0484$.

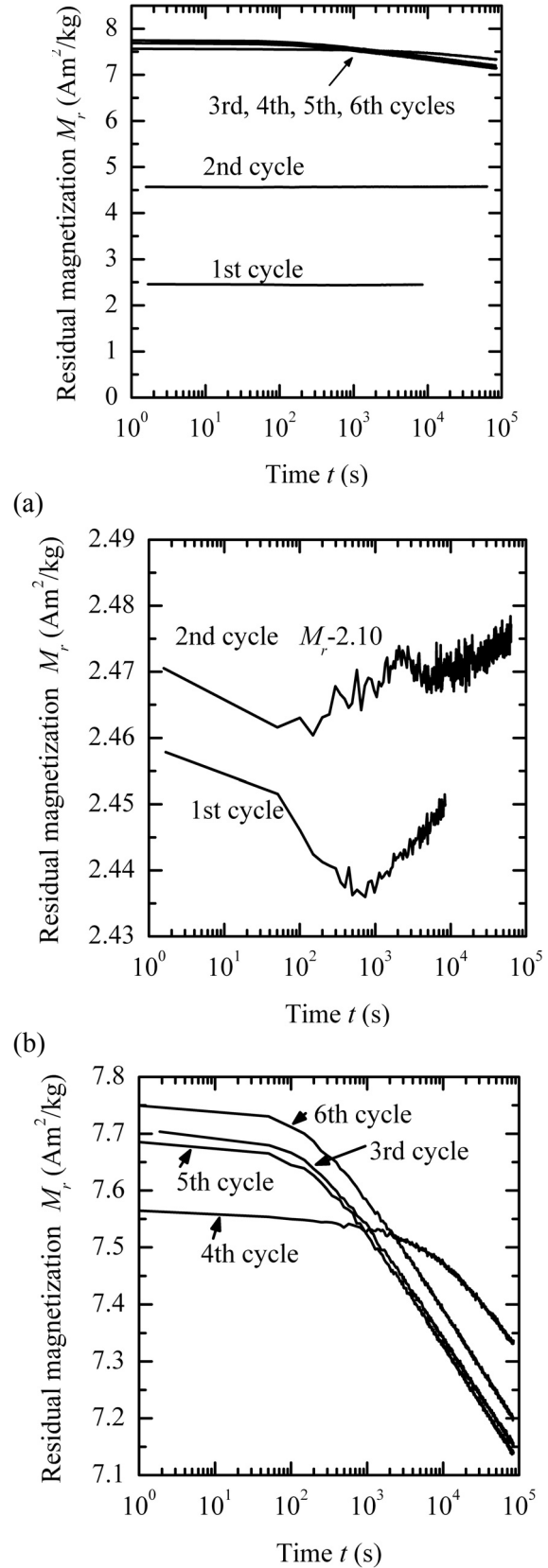
▽: Sample L, $\phi = 0.00792$. □: Sample M, $\phi = 0.00066$.

•: Sample I, $\phi = 0.000080$.

There are no peaks in χ' or χ'' with respect to temperature, T , for the paraffin-solvent MF (sample A) and the water-solvent MF (sample E) in Fig. 16. This can be explained as follows. There are spontaneous agglomerates or clusters of the magnetic particles in these MFs even under no external magnetic field. The spontaneous cluster's magnetic moment is so gigantic that the resonant frequency is very low which is far less than the ac frequency range which was used in the experiment. That was the reason why the peak did not appear in Fig. 16 for these MF samples, A and E.

3. Frozen Magnetic Fluid's Magnetic Aftereffect

The magnetic aftereffect experiments also give much interesting knowledge with respect to the magnetic particles' mutual interaction in the MF. After cooling the MF to the frozen state under zero magnetic field, we applied a strong magnetic field to the MF and made the magnetic moment's direction of all the MF's magnetic colloid to the applied field direction. After removing the external magnetic field, we measured the time dependence of the frozen MF's residual magnetization. This tells us whether or not there is an interaction between the magnetic colloidal particles in the MF by measuring the residual magnetization's time dependence. If there is no mutual interaction, the remanent magnetization converges rapidly to a half value of the MF's saturation magnetization. It is because each particle's magnetic moment's direction converges to its easy axis direction in the applied field direction's hemisphere by rotational thermal fluctuation, and the easy axis directions of the particles were randomly distributed. But, if there is a magnetic mutual interaction between the particles, the rotational thermal fluctuation should be prevented by the interaction and the residual magnetic moment converges slowly or does not converge to a constant magnetization. Measuring the converging rate of the residual magnetization, one can know whether or not the mutual interaction exists, and if it exists, how strong the interaction is. The experimental result was far from our expectation [69, 70]. The experimental procedure was as follows. We made a sample by filling a glass tube with the MF followed by hermetically closing it with a glass lid and epoxy glue. We set the sample in a cryostat followed by evacuating the cryostat under vacuum. Then, the sample was cooled to 10 K and we applied an external magnetic field of 2.86 MA/m to the sample with a superconducting magnet for 300 sec. Quenching the superconducting magnet, we removed the field from the sample and measured the frozen MF's residual magnetization in the sample as a function of time. The reason why quenching was adopted instead of stopping the current in the superconducting magnet was that if quenching was not made, there remained magnetic fluxons in the superconducting magnet even when the current was zero and there still remained a residual field applied to the sample.



(c) FIG. 18. Residual magnetization, M_r , as a function of time, t , for the MF sample B [69, 70]. (a) for cycles 1 through 6, (b) magnified for cycle 1 and cycle 2 (reduced by 2.1 Am^2/kg) and (c) magnified for cycles 3 through 6.

The most important procedure in our experiment was that we conducted the same experiment many times with the same samples. We obtained a different experimental result for each experiment. Figs. 18(a), (b) and (c) show the experimental result of the frozen MF's residual magnetization, $M_r(t)$, as a function of time, t , for the MF Sample B. Its characteristics are tabulated in Table I. Hereafter, we show the residual magnetization, $M_r(t)$, for unit mass (Am^2/kg) instead of unit volume (A/m). We do this because we measured the sample's magnetic moment but did not measure the sample's volume change. We performed the same experiment with the same sample six times. We designate the first experiment, the second experiment,..., as the first cycle, the second cycle,..., and so on, respectively. The average $M_r(t)$, increased with the cycles and $M_r(t) - t$ curves converged to a certain universal curve in Fig. 18. The other important point is that $M_r(t)$ increased with time in a certain time region in the early cycle experiment.

Therefore, we performed a different experiment. We left the MF sample B under a vacuum (0.133Pa) for one hour, we call this MF sample as MF sample N. Its characteristics are tabulated in Table I. We performed the similar experiment with the MF sample N. The experimental result is shown in Fig. 19. $M_r(t) - t$ curves almost coincide with the universal curve from the first cycle in this experiment.

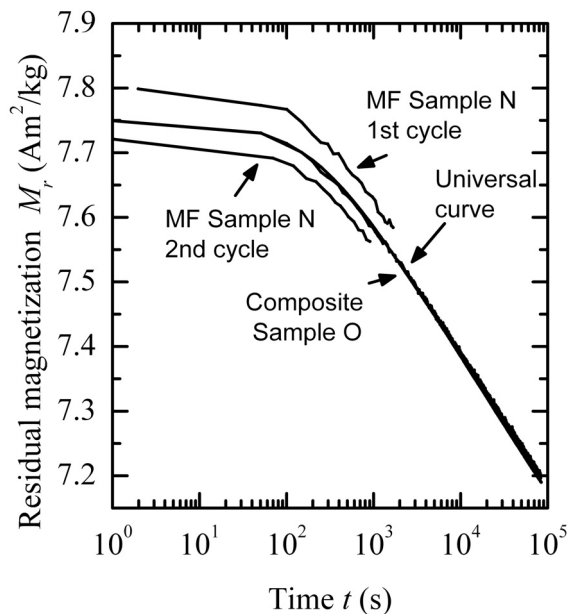


FIG. 19. Residual magnetization, M_r , as a function of time, t , for the MF sample N and MF-epoxy composite sample O [69].

In order to examine the resembling frozen MF's case, we prepared the following sample. Mixing the MF sample B and epoxy glue fiercely, we left the mixture until it solidified. In this case, the alkyl-naphthalene solvent dissolved in the epoxy matrix and the composite itself was solidified. We call this solidified composite Sample O.

Fig. 20 is the scanning-electron micrograph of the Sample O's cross section. The dark area is the epoxy matrix. The brighter regions are the magnetic fluid dispersed in the epoxy matrix. As the alkyl-naphthalene solvent was dissolved in the epoxy glue, the black circles were also solidified. Accordingly, the magnetic colloids in the MF were also embedded in the epoxy matrix. We performed the same experiments with the composites. The experimental result is shown in Fig. 19. The $M_r(t) - t$ curves precisely coincide with the universal curve.

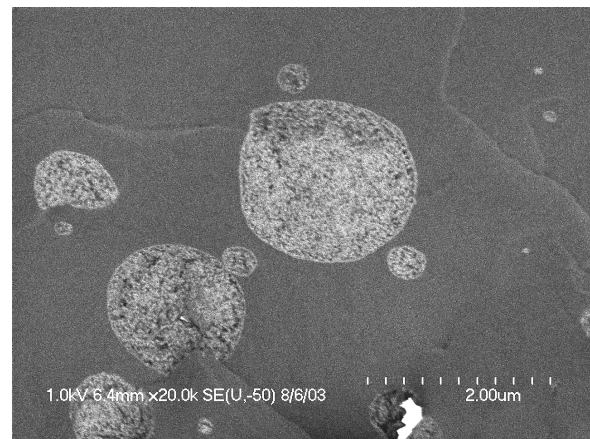
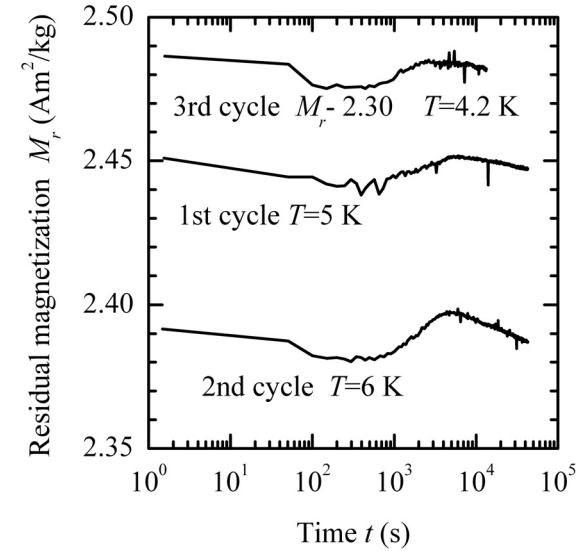
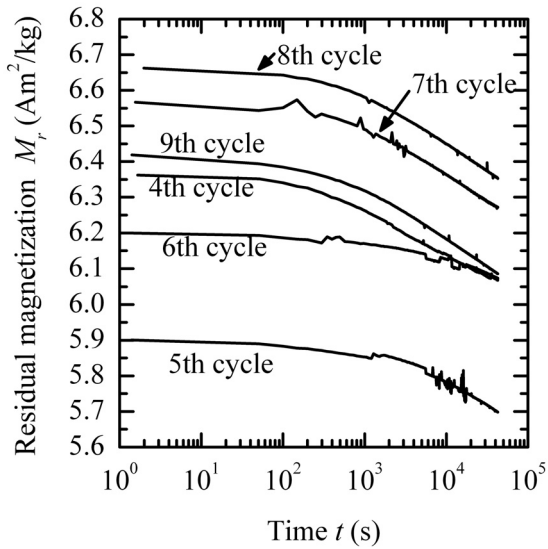


FIG. 20. The scanning-electron micrograph of the magnetic fluid-epoxy composite's cross section [71].

Fig. 21 shows the experimental results for the extremely diluted MF, the MF sample I. For convenience, we multiplied the true residual magnetization by the dilution factor, 819.7, with respect to the unit mass of the MF. The dilution factor, 1300, in Table I was with respect to the unit volume of the MF. To our surprise, it shows results similar to that for the mother MF, the MF sample B. In conclusion, the experimental results for the frozen MF's magnetic aftereffect suggest that it occurs due to some structural or organized change in the MF during the freezing process. In the next section, we propose a special micelle formation model to explain the present peculiar experimental results.



(a)



(b)

FIG. 21. Residual magnetization, M_r , as a function of time, t , for the diluted MF, sample I, (a) for cycles 1, 2 and 3 (reduced by $2.3 \text{ Am}^2/\text{kg}$), and (b) for cycles 4 through 9. M_r is the measured residual magnetization multiplied with the dilution factor, 819.7. The temperatures, $T(K)$, and field application times, t_H (s), (T, t_H), for the individual cycles are as follows: 1st cycle-(5, 0), 2nd cycle-(6, 0), 3rd cycle-(4.2, 0), 4th cycle-(4.2, 0), 5th cycle-(6, 0), 6th cycle-(5, 0), 7th cycle-(4.2, 300), 8th cycle-(5, 300) and 9th cycle-(5,300) [70].

V. Discussion

A. Micelle Model

In practice, when an MF is prepared, a very little excess amount of surfactant over that theoretically needed remains in the MF so that there is a minimal chance for coagulation of colloidal magnetic particles. Theoretically, the required amount of surfactant is that amount

which is needed to exactly cover the surface of all the colloidal particles with one-molecular layer. Accordingly, though the excess amount is small, there are a considerable number of excess surfactant molecules (isolated and monodispersed in the solvent) in a conventional MF (Fig. 22).

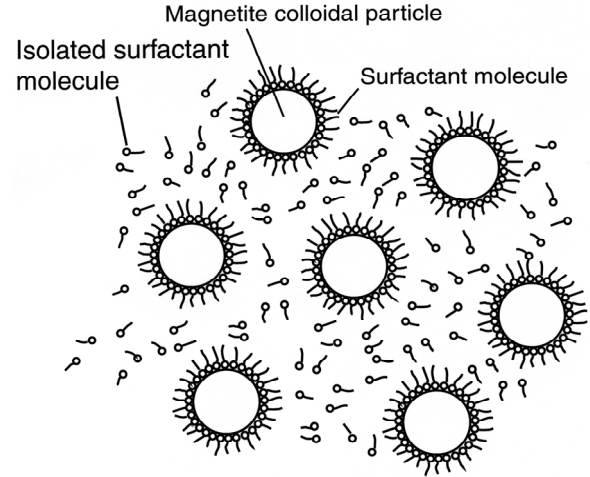


FIG. 22. Schematic figure of the magnetic fluid structure showing the magnetic colloid's monodispersed phase. There are not only attached surfactant molecules on the colloid surface, but also isolated surfactant molecules in the solvent.

We feel that these isolated and monodispersed extra surfactant molecules play an important role. In order to interpret the paradox of the so-called MFs' temporary agglomeration which has confused many researchers for many decades, we propose the following physical model which takes the extra surfactant molecules into account.

The MF's magnetic colloidal particles are monodispersed and the excess surfactant molecules are also dispersed in the solvent at room temperature as shown in Fig. 22. However, when the temperature of the MF is decreased, the isolated surfactant molecules trigger the generation of special surfactant micelles. In addition, because of their mutual interaction, a considerable amount of the colloidal magnetic particles sticks to the surface of the micelles. These particle-coated micelles somewhat resemble aggregates of particles.

In other words, with a temperature decrease, there occurs a phase transition from a phase of monodispersed magnetic colloids to a magnetic colloid micelle phase. Fig. 23 shows the schematic construction of the micelle covered with the magnetic colloidal particles whose magnetic dipoles make a closed magnetic circuit.

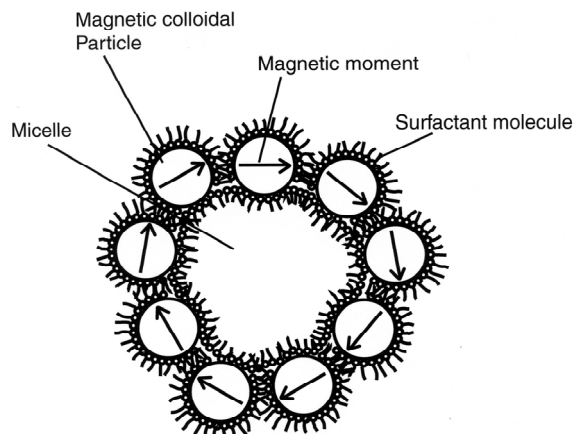


FIG. 23. Schematic figure of the special micelle made of the isolated surfactant molecules covered with the magnetic colloidal particles whose magnetic moments make a closed magnetic circuit.

When the MF's temperature is decreased lower than a critical temperature, the isolated surfactant molecules in the solvent spontaneously make special micelles on the surface to which the magnetic colloidal particles are stuck.

This micelle possesses a spherical shape though the micelle in Fig. 23 looks like a circle. This process is reversible, i.e., when the temperature is increased, the micelles collapse and the particles are once again monodispersed in the solvent together with the isolated excess monodispersed surfactant molecules. This phase transition or the special micelle formation is induced not only by temperature decrease, but also by the application of an external magnetic field. The special micelle formation occurs with the application of the external field forming elongated micelles along the field direction. It will be discussed later.

B. Frozen Magnetic Fluid's Magnetic Aftereffect

The peculiar phenomena of the frozen MF's magnetic aftereffect in §IV. C. 3 are explained by this physical model. In fact, this physical model was obtained by the analysis of the frozen MF's magnetic aftereffect [69, 70]. In order to conduct the frozen MF's magnetic aftereffect experiment, the sample MF's temperature is decreased from room temperature. The special micelles are formed in the MF at a certain temperature. With the further temperature decrease, the solvent freezes and the micelles themselves are embedded in the frozen solvent and they are fixed in the solvent. Fig. 24(a) shows the micelle together with the magnetic colloids' ring which makes the closed magnetic circuit on the micelle surface.

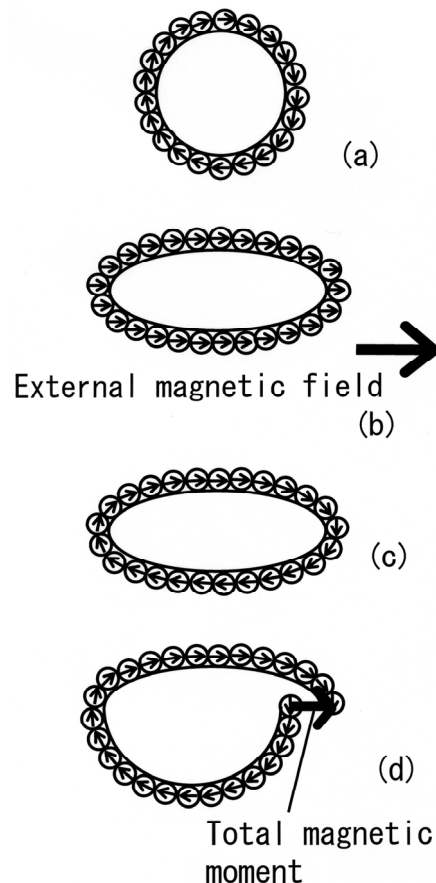


FIG. 24. Change of the micelle with the colloids' magnetic moment before and after the application of the external magnetic field. (a) Special spherical micelle on the surface to which the magnetic colloidal particles are attached and their magnetic moments forming a closed magnetic circuit. (b) Shape distorted micelle under a strong external magnetic field. The particles' magnetic moments are directed parallel to the field direction. (c) After removal of the external field, the magnetic moments once again form a closed magnetic circuit. (d) After a certain time, the micelle gets broken spontaneously due to the distorted energy and a non-zero magnetic moment is generated for the micelle.

When a strong external magnetic field is applied to the MF for a certain duration, the field makes the direction of the magnetic moments of all the particles which make the ring on the micelle in the field direction together with distorting the micelle shape by the magnetic force (Fig. 24(b)). After the removal of the external field, the magnetic particles' magnetic moments once again make the closed magnetic circuit, however, with the distorted shape left (Fig. 24(c)). This is the reason why the residual magnetization was anomalously small compared with the theoretical value in Fig. 18. If all the magnetic particles were monodispersed in the

frozen solvent, the residual magnetization should amount to $7\text{Am}^2/\text{kg}$. However, the experimental value of the residual magnetization was as small as $3\text{Am}^2/\text{kg}$. The fact that the residual magnetization was not zero means that not all the magnetic particles contributed to form the micelle but a considerable amount of the particles remained monodispersed in the frozen solvent. After the removal of the external field, the distorted micelle held its shape with the distorted energy for some time, but after some duration, the micelle breaks by discharging the distorted energy. The particles' ring which made the closed magnetic circuit also breaks the circle and a finite magnetic moment is generated in the broken micelle (Fig. 24(d)). The duration time of the micelle breaking is distributed widely from micelle to micelle, and the apparent increase of the residual magnetization with time appears in a certain time range.

When the same magnetic aftereffect experiment was carried out many cycles with the same MF sample, the MF sample was exposed under a vacuum for a long time. Though the MF was encapsulated in a glass tube with a glass lid hermetically sealed with epoxy glue, the isolated surfactant molecules in the MF gradually evaporated from the MF sample under vacuum at room temperature. The decrease in the isolated surfactant molecules in the MF decreases the formation of the micelles in the MF when the temperature is decreased. This implies that after many cycles of magnetic aftereffect experiments, there remained more monodispersed magnetic colloids in the MF than in the MF of the first cycle experiment under low temperature. This is the reason why the residual magnetization of the MF in the magnetic aftereffect experiment increased with the experimental cycles. After many cycles of the experiment, there are few isolated surfactant molecules and no micelles are formed causing the residual magnetization curve with time to converge to a universal function. Hereafter, it will be mentioned how the micelle model can explain the MF's other peculiar physical phenomena.

C. Macro-Cluster Formation under the External Magnetic Field

The micelles generated by the temperature decrease are spherical in shape and contain magnetic dipoles of the colloidal particles which form a closed magnetic circuit (Fig. 23), while the micelles induced by the application of an

external field are elongated in shape and the particles' magnetic dipoles do not form a closed circuit in accordance with lowering the magnetic energy. In addition, if there are many isolated surfactant molecules in the MF under no external field, many elongated micelles are generated when the external field is applied and these elongated micelles make a bundle. Fig. 25 shows the schematic structure of the bundle made of the elongated micelles.

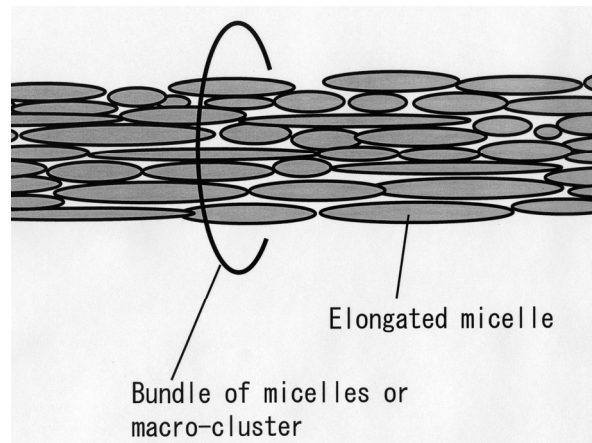


FIG. 25. Schematic structure of the bundle which is made of many elongated micelles under the external magnetic field. This bundle is the so-called macro-cluster which can be observed by an optical microscope as is shown in Fig. 1.

This bundle is the so-called macro-cluster which is large enough to be observed by an optical microscope as shown in Fig. 1. The macro-cluster in the MF is not really the agglomeration of the magnetic colloids, but the bundle of the elongated special micelles. Therefore, it easily appears and disappears with the application and removal of the external magnetic field because it is due to the micelle formation but not due to the agglomeration.

D. Anomalous Burst Pressure of the Magnetic Fluid's Shaft Seal

In §III. A, we assumed that once the magnetic colloidal particles in the MF entered into the area where the magnetic field was maximum in the sealing area of the MF shaft seal, they were trapped in this area, and the number density of the particles increased with time in this area. However, the true answer is that it is not the particles but instead the special micelles that were trapped in this area. In fact, when the gas pressure was applied to the seal from the left side in Fig. 3, the MF shifted to the right side (See Figs. 3(a), (b)). If the particles were simply trapped in the top of the projection area before

the pressure was applied, they would be shifted to the right side by the movement of the MF's solvent when the pressure was applied. As the particles were trapped in the highest field region as the special micelles, the micelles themselves clung to the projection's top area even when the MF was shifted to the right side.

E. Acoustic Properties, Magneto-Optical Effects, Latent Heat Measurement, Scaling Law and Satellite Peak in Nmr

Previously, we ascribed the spatial anisotropies of the MF's acoustic and magneto-optical properties under the magnetic field to the formation of the magnetic colloids' elongated agglomeration, or the so-called micro-clusters and macro-clusters. However, here we obtained the correct answer that the micro-clusters and macro-clusters are replaced with the special micelles and the huge bundles of the special micelles, respectively.

The contradiction of the Landau criterion which annoyed us for a long time is also clearly solved. Landau criterion claims that if phase transition occurs from one phase to the other with two phases belonging to different space symmetry groups in a physical system, the phase transition is of first order. On the other hand, the MF's magneto-optical effects were thought to be due to the formation of the elongated colloids' clusters by the applied magnetic field. This means that the MF's magneto-optical effects were induced by the phase transition from the phase in which the colloidal particles were monodispersed to the other phase in which there were clusters elongated parallel to the external field direction. Apparently, the two phases belong to the different space symmetry groups and accordingly this phase transition should be first order phase transition from Landau criterion. On the contrary, the phase transition of the MF's magneto-optics is apparently a second order phase transition as mentioned in §III. C. 4. This contradiction is now clearly solved. The origin of the MF's magneto-optical effect is not due to the elongated agglomeration of the magnetic colloidal particles, but due to the formation of the elongated special micelles which not only the colloidal particles but also the excess surfactant molecules construct. Therefore, the Landau criterion cannot be applicable to the MF's magneto-optical phenomena.

The different field dependences of the magnetic birefringence, Δn , in a weak magnetic field region mentioned in §III. C. 1, is also clearly explained. The fresh MF's Δn was proportional to H , while it was proportional to H^2 after the MF was under vacuum for several minutes before the magneto-optical experiment. The origin of the magneto-optical effect of the fresh MF was mainly due to the formation of the special micelles and, accordingly, Δn was proportional to H . However, when the MF was under vacuum, the excess surfactant molecules in the MF were removed from the MF, and the magneto-optical effect was induced not by the special micelle formation but by the shape anisotropy of the colloidal particles of the MF. That was the reason why the field dependence of the Δn was proportional to H^2 , which was known as Majorana effect a long time ago.

The origin of the scaling law is perhaps due to the following reason. When an external magnetic field, H , is applied to the MF, some of the magnetic colloids make the special micelles in the MF. Increasing H , as strong as H_m , all the magnetic colloids make the special micelles and there are no monodispersed colloids in the MF. We say that the MF is in a critical state at $0 < H < H_m$. In general, when the scaling law holds for a physical quantity, A , in the critical state, the physical quantity, A , is a function of one parameter, ξ , which is usually a typical length representing the critical state [72]. For example, the average Cooper pair length is ξ for the critical region between the superconducting state and the normal state [73]. Another example is the phase transition between the paramagnetic phase and the ferromagnetic phase. The average size of the germs of ferromagnetic phase in the paramagnetic phase, is ξ for the critical region between the ferromagnetic state and the paramagnetic state. Therefore, A is expressed by:

$$A = f_A(\xi), \quad (32)$$

where $f_A(x)$ is the function of x , and ξ represents a typical size which represents the special micelles' length. Now, we assume for any MFs, that ξ is generally expressed by:

$$\xi = g_\xi \left(\frac{H}{H_0} \right), \quad (33)$$

where $g_\xi(x)$ is a function of x , and H_0 is a constant which is characteristic to each MF. From Eq. (32) and Eq. (33), one obtains:

$$A = f_A(\xi) = f_A \left(g_\xi \left(\frac{H}{H_0} \right) \right), \quad (34)$$

which is equivalent with the scaling law.

In §IV. A, we assumed that the satellite peaks in the water-solvent MF's NMR experiment were due to the formation of the macrocluster. However, the true answer is that it was due to the special micelle formation which made the magnetization greater than in the rest of the area.

F. $M - H$ Curves for the Static Magnetic Field

In §IV. C. 1, we showed the deviation between the normalized $M - H$ curve of the mother MF and that of the highly diluted solution for the static magnetic field in the weak field region. This deviation was found for the water solvent and paraffin solvent MFs but not for the alkylnaphthalene solvent MF. We ascribed this deviation to the spontaneous agglomeration of the magnetic colloids under no magnetic field. However, the correct answer is not the agglomeration but the spontaneous special micelle formation even under no magnetic field.

G. Initial Complex Magnetic Susceptibility

In §IV. C. 2, we showed that the frozen MF's initial complex magnetic susceptibility, $\chi' - i\chi''$, possessed a spin-glass-like temperature dependence. Especially, the ac magnetic field's frequency, f , and the peak temperature, T_p , at which the off-time magnetic susceptibility, χ'' , obeyed the Vogel-Fulcher law, formed the decisive evidence that the frozen MF possessed a spin-glass nature. When we performed this experiment, we made a vague conclusion that the magnetic colloids in the frozen MF had a spin-glass-like configuration. However, we now realize that the correct interpretation is that the spin-glass nature was due to the special micelle formation. However, we still do not yet have a reason for the Vogel-Fulcher law behaviour. We can speculate that this effect is due to the similar mechanism of glass viscosity, η , which also typically obeys the Vogel-Fulcher law in temperature dependence. When the glass temperature is increased over the temperature, T_g , it begins to possess fluidity and its viscosity, η , is expressed by:

$$\eta = \eta_0 \exp \left[\frac{E}{k_B (T - T_g)} \right], \quad (35)$$

where η_0 and E are positive constants. The origin of the Vogel-Fulcher law in this case is ascribed to the generation of the voids around the glass molecules. The void sizes are widely distributed and the free volume space which the voids make is thought to be the origin of the Vogel-Fulcher law [74]. In the frozen MF's case, the special micelle's inner space can possibly play the role of the voids. However, this problem is also open to questions at the present stage as the spin-glass nature of the frozen MF.

VI. Conclusions

Magnetic fluid (MF) is a colloidal solution of stably dispersed ferromagnetic or ferrimagnetic colloidal particles in a solvent. Soon after the invention of the MF, needle-like agglomeration of about 1 micron thickness was found in some MFs under an external magnetic field by optical microscope observation. We call these agglomerate-like objects macro-clusters. The macro-cluster was not a simple precipitation of the colloidal particles because it disappeared when the external field was removed. This paper reviewed not only the macro-cluster's nature but also its composing elements, special micelles which are much more fundamental in the MFs nature. In §2, the macro-cluster's observation by the optical microscope and its nature was explained. In §3, MF shaft seal's burst pressure experiment, MF's acoustic anisotropy in an external field and MF's magneto-optical effect were explained. These peculiar phenomena appeared not only in the MF in which the macro-clusters were observed, but also in the MF in which the macro-clusters were not observed. Therefore, in order to explain these peculiar phenomena, it was necessary that we should assume the formation of sub-micron agglomerations in all the MFs under external field. We call these sub-micron agglomerations micro-clusters. The fresh MF showed that its birefringence, Δn , was proportional to the applied field, H , while the MF which was under vacuum for a few minutes before the magneto-optical experiment showed that its Δn was proportional to H^2 in a weak field region. In addition, the temperature dependence of Δn experiment revealed that the origin of the MF's magneto-optical effect was ascribed to the generation of the elongated micro-clusters in the MF, and the generation of the microclusters in the MF was a second order phase transition from the monodispersed phase of the colloidal

particles to the phase which contained the micro-clusters which were directed along the external field. However, if we took only the colloidal particles dispersing status into account, the two phases belonged to different symmetry groups with respect to the colloidal particles, leading to the conclusion that, from the theoretical viewpoint, the phase transition should be a first order transition, which apparently contradicted the experimental conclusion. In §4, proton-NMR experiment for water-solvent MF revealed that though the local magnetization in the cluster was higher than that of the rest of the area, it was less than twice that of the rest of the area. Therefore, it is denied that the macro-cluster was the precipitation of the magnetic colloidal particles. There was neither heat discharge nor heat absorption accompanying the MF's phase transition which was confirmed by Differential Scanning Calorimetry (DSC). Therefore, it was confirmed that the MF's phase transition was of second order. In order to determine whether or not there was an interaction among the magnetic colloidal particles in the MF, we prepared the conventional MF (mother MF) and approximately 1000 fold diluted MF from the mother MF. We measured both MF's $M - H$ curves, the temperature and AC magnetic field frequency dependences of the initial complex magnetic susceptibility, and the magnetic aftereffect. By comparing both MF's experimental results, we determined whether or not there was an interaction among the magnetic particles. It was found from the $M - H$ curve experiment, that there were already spontaneous micro-clusters even under zero external field in the MF in which the macro-clusters were found by optical microscope. There was a cusp present in the temperature dependence of the complex magnetic susceptibility graph for the MF which showed no interaction between the particles from the $M - H$ curve experiment. The Vogel-Furche law was also found between the peak temperature of the cusp and the AC magnetic field frequency. It meant that this frozen MF was under spin-glass state due to very weak magnetic interactions among the magnetic colloidal particles. Cooling the same MF down to as low as 10K, and keeping this temperature during the experiment, we performed the following experiment. First, a strong external magnetic field was applied to the frozen MF sample for a certain time. Then, after removing the external field, the MF's residual magnetization, $M_r(t)$, was measured as a function of the elapsed time,

t , from the removal of the external field. We performed the same experiment many cycles for the same sample. The $M_r(0)$'s values at $t = 0$ in the initial few cycles experiment were very small compared with the theoretically expected value. In addition, in some time region, $M_r(t)$ increased with t . However, after many cycles, not only the $M_r(0)$'s values converged to the theoretically expected value, but also the whole $M_r - t$ curves converged to a certain universal curve. In §5, we proposed a special micelle model and proved that with this physical model all the MF's mysterious experimental results were interpreted. In the conventional MF, there were not only the surfactant molecules which cover the magnetic colloidal particles to prevent the particles' coagulation, but also extra isolated surfactant molecules dispersed in the solvent. With the decrease of the MF temperature, the isolated surfactant molecules suddenly formed special spherical micelles at a transition temperature. The magnetic colloidal particles attached to the surface of this special micelle and particles on the surface made a ring. The magnetic moment of the particles which construct the ring also made a closed magnetic circuit. With further temperature decrease, the special micelles were embedded in the solidified frozen solvent. When a strong external magnetic field was applied to the micelle, the magnetic moments of the particles on the micelle were all directed to the field direction together with the micelle shape's deformation by the magnetic force. After removal of the external field, the particles' magnetic moment once again made the closed magnetic circuit leaving the micelle's shape deformed. Since the magnetic moments of the colloidal particles which construct the ring made a closed magnetic circuit, they did not contribute to the MF's residual magnetization, $M_r(t)$. The magnetic moment of the colloidal particles which did not attached to the micelles only contributed to $M_r(t)$. That was the reason why $M_r(0)$ in the initial few cycles' experiment was very small compared with the theoretically expected value. With the time elapsed, the deformation energy in the micelle was suddenly released at time t with the breaking of the micelle. The breaking of the micelle induced the breaking of the particles' ring and consequently the breaking of the closed magnetic circuit. Accordingly, a finite non-zero magnetic moment was generated in the broken micelle. The micelle's breaking time was widely distributed. That is the reason why $M_r(t)$ increased with time

in a certain time region. When the magnetic aftereffect experiments were conducted many cycles for the same MF sample, the MF sample in a capsule was exposed under vacuum in the room-temperature's cryostat for a long time. The isolated free surfactant molecules in the MF of the sample evaporated gradually through the sample capsule even though it hermetically sealed the MF. The decrease of the free surfactant in the MF meant the decrease of the micelle when the temperature decreased. It implies that the increase of the monodispersed magnetic colloidal particles in the MF and $M_i(0)$ also increased and $M_i(t)$ curves converged to the universal curve after many experimental cycles. The special micelles are generated not only with the temperature decrease but also when an external magnetic field is applied to the MF. However, in this case, the magnetic moments of the colloidal particles attached to the micelle are directed along the field, and in order to decrease a static magnetic energy, the micelle itself is elongated to the field direction. In fact, this elongated micelle is equivalent with the micro-cluster assumed in the preceding sections. The elongated micro-cluster is a complex physical system consisting of not only the colloidal particles but also of the surfactant molecules which were not attached to the surface of the particles in advance. Therefore, the Landau's phase transition argument that as the colloidal particles' monodispersed phase and the phase in which particles make elongated agglomerates in the field's direction belong to different space symmetry groups implying that the phase transition should be of first order, is no longer applicable to the present MF phase transition. Accordingly, it is not contradictory that the MF phase transition is a second order phase transition. The origin of the fresh MF's magnetic birefringence was due to the elongated micelles and accordingly Δn was proportional to H . On the contrary, after leaving the MF under vacuum, there were no excess free surfactant molecules in the solvent of the MF and no elongated micelles were formed in that MF under the external field. That was the reason why the MF which was once under vacuum did not show Δn proportional to H , instead proportional to H^2 , which was caused by the shape anisotropy of the colloidal particles themselves. The macro-cluster shown in Figs. 1(a) and (b) was the bundle of the many elongated micro-clusters directed parallel to the external field.

Appendix: Derivation of H^2 Dependence of Δn for Ordinary Material and Theory's Limit

In ordinary magneto-optical materials, Δn due to Cotton-Mouton effect is proportional to H^2 . But this Appendix shows that it does not hold for magneto-optics of the MF. The starting theory for the ordinary magneto-optical material is:

$$\varepsilon_{ij}(H) = \varepsilon_{ji}(-H), \quad (\text{A1})$$

where $\varepsilon_{ij}(H)$ is the (i, j) component of the permittivity matrix under a magnetic field H [46]. It leads to:

$$\varepsilon_{ii}(H) = \varepsilon_{ii}(-H), \quad (\text{A2})$$

and $\varepsilon_{xx}(H)$ and $\varepsilon_{yy}(H)$ can be expressed, respectively, as:

$$\varepsilon_{xx}(H) = \varepsilon_1 + a_2 H^2 + a_4 H^4 + \dots, \quad (\text{A3})$$

$$\varepsilon_{yy}(H) = \varepsilon_1 + b_2 H^2 + b_4 H^4 + \dots, \quad (\text{A4})$$

where ε_1 , a_2 , a_4 , b_2 and b_4 are positive constants. As the birefringence Δn is expressed by:

$$\left. \begin{aligned} \Delta n &= \sqrt{\frac{\varepsilon_{yy}(H)\mu_0}{\varepsilon_0\mu_0}} - \sqrt{\frac{\varepsilon_{xx}(H)\mu_0}{\varepsilon_0\mu_0}} \\ &\propto \sqrt{\varepsilon_{yy}(H)} - \sqrt{\varepsilon_{xx}(H)} \\ &= \frac{\varepsilon_{yy}(H) - \varepsilon_{xx}(H)}{\sqrt{\varepsilon_{yy}(H)} + \sqrt{\varepsilon_{xx}(H)}} \\ &\approx \frac{(b_2 - a_2)H^2}{2\varepsilon_1} \\ &\propto H^2, \end{aligned} \right\} \quad (\text{A5})$$

where ε_0 and μ_0 are permittivity and magnetic permeability in vacuum, respectively, and $a_2 H^2$, $b_2 H^2 \ll \varepsilon_1$ was used. This condition seems to be a strong condition. But it does not hold for all cases. The condition Eq. (A1) is derived from the so called linear response theory or Kubo formula [45, 46]. In a physical system, if some field, h , is applied to a physical system, there is a generated response, g . Here, concretely speaking, h is an electric field, E , a magnetic field, H , a force, f , ... etc. The corresponding responses are an electric polarization, P , a magnetization, M , a displacement x , ... etc. If:

$$g = \chi h \quad (\text{A6})$$

holds, the linear response theory is applicable and Eq. (A1) holds. Consequently, Eq. (A5) holds. Here, χ is the generalized susceptibility

corresponding to the electric susceptibility χ_e , magnetic susceptibility χ_m , stiffness, G , and etc. But χ diverges ∞ as the system approaches a critical state. So, in the critical state and in the vicinity of the critical state, the linear response theory cannot be applicable and Eq. (A5) no longer holds in this region. The magneto-optics

of the magnetic fluids in the vicinity of $H = 0$ is some kind of critical phenomena. The spontaneous microcluster generation at zero field, mentioned in §IV C 1, suggests this relation.

References

- [1]Hayes, C.F., J. Colloid Interface Sci. 52 (1975) 239.
- [2]Bitter, F., Phys. Rev. 38 (1931) 1903.
- [3]Elmore, W. C., Phys. Rev. 51 (1937) 982.
- [4]McTague, J.P., J. Chem. Phys. 51 (1969) 133.
- [5]Taketomi, S., Takahashi, H., Inaba, N. and Miyajima, H., J. Phys. Soc. Jpn. 60 (1991) 1689.
- [6]Sano, K. and Doi, M., J. Phys. Soc. Jpn. 52 (1983) 2810.
- [7]Cebers, A.O., Magnetohydrodynamics, 18 (1982) 137.
- [8]Cernak, J. and Macko, P., J. Mag. Mag. Mater. 123 (1993) 107.
- [9]Bar'yakhtar, F.G., Gorobets, Yu.I., Kosachevskii, L.Ya., Il'chishin, O. V. and Khizhenkov, F.K., Magnitnaya Gidrodinamika, No. 3 (1981) 120 (in Russian).
- [10]Jones, G.A. and Niedoba, H., J. Magn. Magn. Mat. 73 (1988) 33.
- [11]Jones, G.A. and Belfield, D.G., J. Magn. Magn. Mat. 85 (1990) 37.
- [12]Hong, C.Y., Horng, H.E., Kuo, F.C., Yang, S.Y., Yang, H.C. and Wu, J.M., Appl. Phys. Letters, 75 (1999) 2196.
- [13]Rosensweig, R.E. and Popplewell, J., Int. J. Appl. Electromagn. in Materials, 2 Suppl. (1992) 83.
- [14]Haas, W.E. and Adams, J.E., Appl. Phys. Letters, 27 (1975) 571.
- [15]Yusuf, N.A., J. Phys. D, Appl. Phys. 22 (1989) 1916.
- [16]Donselaar, L.N., Frederik, P.M., Bomans, P., Buining, P.A., Humbel, B.M. and Philipse, A.P., J. Magn. Magn. Mat. 201 (1999) 58.
- [17]Rosensweig, R.E., Miskolczy, G. and Ezekiel, F. D., Machine Design, 40 (1968) 145.
- [18]Taketomi, S., Jpn. J. Appl. Phys. 19 (1980) 1929.
- [19]Taketomi, S. and Chikazumi, S., "Magnetic Fluids— Principle and Application", Chapter 2, (Nikkan Kogyo Shinbun Publishing, Tokyo, 1988), in Japanese, Russian Version, (Mir Publisher, Moscow 1993).
- [20]Parsons, J.D., J. Phys. D, 8 (1975) 1219.
- [21]de Gennes, P.G., "The Physics of Liquid Crystals", Chapt. 5, (Oxford University Press, London, 1974).
- [22]Chung, D.Y. and Isler, W.E., J. Phys. Lett. 61A (1977) 373.
- [23]Chung, D.Y. and Isler, W.E., J. Appl. Phys. 49 (1978) 1809.
- [24]Gotoh, K. and Chung, D.Y., J. Phys. Soc. Jpn. 53 (1984) 2521.
- [25]Taketomi, S., J. Phys. Soc. Jpn. 55 (1986) 838.
- [26]Kasparkova, M., "Abstract Booklet", Fifth International Conf. on Magnetic Fluids, Riga, Latvia, (1989) pp.134-135.
- [27]Skumiel, A., Jozefczak, A., Hornowski, T. and Labowski, M., J. Phys. D, 36 (2003) 3120.
- [28]Motozawa, M. and Sawada, T., Int'nat. J. Appl. Electromag. Mech. 28 (2008) 143.
- [29]Yusuf, N.A. and Abu-Aljarayesh, I.O., Jordan J. Phys. 2 (2009) 1.
- [30]Majorana, O., Phys. Zeitschr. 4 (1902) 145.
- [31]Papell, S., US Patent No.3215572 (1965).
- [32]Mehta, R.V., J. Colloid and Sci. 42 (1973) 165.
- [33]Martinet, P.A., Rheol. Acta, 13 (1974) 260.
- [34]Voigt, W., Ann. der Physik, 8 (1902) 880.
- [35]Cotton, A. and Mouton, H., Compt. Rend. 141 (1905) 317, *ibid.*, 349.
- [36]Sakhnini, L. and Popplewell, J., J. Magn. Magn. Mat. 122 (1993) 142.

- [37] Davies, H.W., Llewellyn, J.P., *J. Phys. D, Appl. Phys.* 12 (1979) 311.
- [38] Taketomi, S., Inaba, N., Takahashi, H. and Miyajima, H., *J. Phys. Soc. Jpn. Letters*, 59 (1990) 3077.
- [39] Abu-Safia, H., Abu-Aljarayesh, I., Mahmood, S. and Yusuf, N.A., *J. Mag. Mag. Mater.* 87 (1990) 333.
- [40] Taketomi, S., Takahashi, H., Inaba, N., Miyajima, H. and Chikazumi, S., *J. Phys. Soc. Jpn.* 59 (1990) 2500.
- [41] Taketomi, S., Ukita, M., Mizukami, M., Miyajima, H. and Chikazumi, S., *J. Phys. Soc. Jpn.* 56 (1987) 3362.
- [42] Scholten, P.C., *IEEE Trans. Magn. MAG-16* (1980) 221.
- [43] Taketomi, S., *Jpn. J. Appl. Phys.* 22 (1983) 1137.
- [44] Scholten, P.C., *IEEE Trans. Magn. MAG-11* (1975) 1400.
- [45] Kubo, R., *Rep. on Progress in Physics* (London) 29, Part 1 (1966) 255.
- [46] Landau, L.D. and Lifshitz, E.M., “*Electromagnetics of Continuous Media*”, Chapters 11 and 13, (Pergamon Press, Oxford, 1960).
- [47] Taketomi, S., Ogawa, S., Miyajima, H. and Chikazumi, S., *IEEE Translational J. Magnetics in Jpn.* 4 (1989) 384.
- [48] Taketomi, S., Sorensen, C.M. and Klabunde, K.J., *Phys. Rev. E*, 68 (2003) 021501.
- [49] Landau, L.D. and Lifshitz, E. M., “*Statistical Physics*”, Chapter 14, (Pergamon Press, Oxford, 1960).
- [50] Chapter 2 of Ref. [21].
- [51] Bissell, P.R., Bates, P.A., Chantrell, R.W., Raj, K. and Wyman, J.E., *J. Mag. Mag. Mater.* 39 (1983) 27.
- [52] Taketomi, S. and Saito, S., *J. Appl. Phys.* 87 (2000) 6929.
- [53] Kittel, C., “*Introduction to Solid State Physics*”, Third Edition, Chap.12, (John Wiley and Sons, Inc. 1953). In this chapter, if an electric field is replaced with a magnetic field, the present discussion is obtained.
- [54] Abragam, A., “*The Principles of Nuclear Magnetism*”, Chapter 3, (Clarendon Press, Oxford, 1961).
- [55] Saitou, Y., “*Principle of Thermal Analysis*”, (Kyoritsu Shuppan, Tokyo, 1990). in Japanese.
- [56] Rosensweig, R.E., Nestor, J.W. and Timmings, R.S., *Ame. Inst. Chem. Eng.-Int. Chem. Eng. Sympo. Series No. 5* (1965) 104.
- [57] Chantrell, R.W., Popplewell, J. and Charles, S.W., *IEEE Trans. on Magn. MAG-14* (1978) 975.
- [58] Taketomi, S. and Shull, R.D., *J. Appl. Phys.* 91 (2002) 8546.
- [59] Taketomi, S. and Shull, R.D., *J. Magn. Magn. Mat.* 266 (2003) 207.
- [60] Chantrell, R.W., Bradbury, A., Popplewell, J. and Charles, S.W., *J. Phys. D*, 13 (1980) L119.
- [61] Chantrell, R.W., Popplewell, J. and Charles, S.W., *J. Appl. Phys.* 53 (1982) 2742.
- [62] Taketomi, S., *Phys. Rev. E*, 57 (1998) 3073, *ibid. E*, 58 (1998) 1175.
- [63] Chapter 14 of Reference[53].
- [64] Chikazumi, S., “*Physics of Ferromagnetism*”, §20, (Oxford University Press, New York, 1997).
- [65] Verway, E.J.W. and Haayman, P.W., *Physica*, 8 (1941) 979.
- [66] Binder, K. and Young, A.P., *Rev. Mod. Phys.* 58 (1986) 801.
- [67] Chantrell, R.W. and Wohlfarth, E.P., *J. Magn. Magn. Mat.* 40 (1983) 1.
- [68] Zhang, J., Boyd, C. and Luo, W., *Phys. Review Lett.* 77 (1996) 390.
- [69] Taketomi, S., Drew, R.V. and Shull, R.D., *IEEE Trans. Magn. MAG-40* (2004) 3039.
- [70] Taketomi, S., Drew, R.V. and Shull, R.D., *J. Magn. Magn. Mat.* 307 (2006) 77.
- [71] Taketomi, S., Shapiro, A. and Shull, R.D., unpublished.
- [72] Ma, S., “*Modern Theory of Critical Phenomena*”, Chapter 4, (The Benjamin / Cummings Pub. Co. Inc., Reading, Massachusetts, 1976).
- [73] de Gennes, P.G., “*Superconductivity of Metals and Alloys*”, Chapter 6, (W. A. Benjamin, Inc., New York, 1966).
- [74] Cohen, M.H. and Turnbull, D., *J. Chem. Phys.* 31 (1959) 1164, *ibid.* 34 (1961) 120.

Jordan Journal of Physics

ARTICLE

Motion of a Charged Particle in a Strong Magnetic Field as a Lagrangian Linear in Velocities

Khaled I. Nawafleh

Department of Physics, Mu'tah University, Al-Karak, Jordan.

Received on: 29/9/2010; Accepted on: 21/2/2011

Abstract: The motion of a charged particle in a magnetic field as a Lagrangian system that varies linearly with the velocities is analyzed using the Hamilton-Jacobi method. The equations of motion are derived as a result of considering the integrability conditions of the action function in the limit of a strong field.

Keywords: Electrodynamics; Lagrangian; Action integral; Hamilton-Jacobi.

PACS No.: 11.10.Ef.

Introduction

The study of singular Lagrangians with linear velocity has been dealt with within the past 50 years by Dirac's Hamiltonian formalism [1, 2]. In this formalism, Dirac distinguishes between the two types of constraints: first-class and second-class constraints. The first-class constraints are those that have zero Poisson brackets with all other constraints in the subspace of phase space in which constraints hold; constraints which are not first-class are by definition second-class ones.

Despite the success of Dirac's approach in studying singular systems, which is demonstrated by the wide number of physical systems to which this formalism has been applied, it is always instructive to study singular systems through other formalisms; since different procedures will provide different views for the same problem, even for nonsingular systems.

Lagrangians that are linear in velocity are important in physics because their Euler-Lagrange equations become systems of first-order differential equations, appearing as constraints, instead of systems of second-order as it would happen with regular Lagrangians. So, they will play a relevant role in many cases, not

only in physics, where many equations are of first order as in Dirac equation, but also in other fields as in biology dynamics and chemistry. There are various methods for treating this kind of Lagrangians [3-7]. Some authors [8, 9] investigated this problem using Dirac's method. Furthermore, a general treatment of singular Lagrangians with linear velocities is given elsewhere [10, 11].

Another model for solving mechanical problems of singular Lagrangian with linear velocities using the Hamilton-Jacobi formulation has been proposed in reference [12]. The authors have obtained the integrable action directly without considering the total variation of constraints. This new method of analysis has been successfully used by several authors [13-16], and is by now a standard technique to deal with Lagrangians linear in velocities.

The aim of this work is to analyze the motion of a charged particle in a strong magnetic field by using the concepts of the above-mentioned model [12].

Review of the Model

Now, a brief discussion for recovering the action integral from Lagrangians that are linear in velocities is introduced. Considering the following linear Lagrangian:

$$L = a_i(q_j)\dot{q}_i - V(q_j), \quad (1)$$

the generalized momenta corresponding to this Lagrangian read:

$$p_i = a_i \equiv -H_i. \quad (2)$$

From the above equation it is possible to obtain the primary constraints as:

$$H'_i = p_i - a_i = 0. \quad (3)$$

The canonical Hamiltonian H_0 is given by:

$$H_0 = \dot{q}_i p_i - L = V(q_j). \quad (4)$$

The corresponding Hamilton-Jacobi partial differential equations are:

$$H'_0 = p_0 + H_0 = \frac{\partial S}{\partial t} + V(q_j) = 0, \quad (5)$$

$$H'_i = p_i + H_i = \frac{\partial S}{\partial q_i} - a_i = 0. \quad (6)$$

The principal Hamilton function S can be found from the above equations as:

$$S = \frac{1}{2} a_i q_i - \frac{1}{2} \int (q_j da_j - a_i dq_i + 2V dt). \quad (7)$$

Assuming that the functions $a_i(q)$ and $V(q)$ satisfy the following conditions:

$$\left. \begin{aligned} q_j \frac{\partial a_i}{\partial q_j} &= a_i, \\ q_j \frac{\partial V}{\partial q_j} &= 2V, \end{aligned} \right\} \quad (8)$$

we finally obtain:

$$\left. \begin{aligned} S &= \frac{1}{2} a_i q_i \\ &- \frac{1}{2} \int q_j \left(da_j - \frac{\partial a_i}{\partial q_j} dq_i + \frac{\partial V}{\partial q_j} dt \right) \end{aligned} \right\} \quad (9)$$

However, in order for S to be an integrable function, the terms inside the brackets must be zero;

$$da_j - \frac{\partial a_i}{\partial q_j} dq_i + \frac{\partial V}{\partial q_j} dt = 0. \quad (10)$$

In fact, Eq. (10) is the main result in this formalism. It represents the equation of motion of the j^{th} generalized coordinate, q_j . Accordingly, Eq. (9) reduces to:

$$S = \frac{1}{2} a_i q_i + \text{const}. \quad (11)$$

Motion of a Charged Particle in a Strong Magnetic Field

The well-known example in classical mechanics is a particle with charge q and mass m moving in the x - y plane subject to a constant homogeneous magnetic field in the z -direction with strength B_0 . The Lagrangian of the system is:

$$L = \frac{m}{2} v^2 + \frac{q}{c} \vec{A} \cdot \vec{v} - V(\vec{r}), \quad (12)$$

where V is some external potential, and we set:

$$\vec{A} = \frac{1}{2} (\vec{B} \times \vec{r}) = \frac{B_0}{2} (x\hat{j} - y\hat{i}). \quad (13)$$

Then the Lagrangian becomes:

$$\left. \begin{aligned} L &= \frac{m}{2} (\dot{x}^2 + \dot{y}^2) \\ &+ \frac{qB_0}{2c} (xy - yx) - V(x, y). \end{aligned} \right\} \quad (14)$$

Now, consider the limit where $\frac{qB_0}{mc} \gg 1$;

which corresponds to a very large magnetic field. In such a case, one can neglect the usual kinetic energy term in the Lagrangian and obtains a Lagrangian that is linear in velocities:

$$L = \frac{qB_0}{2c} (xy - yx) - V(x, y). \quad (15)$$

The first order Euler's Lagrange-equations of motion will be as follows:

$$\left. \begin{aligned} \dot{y} &= \frac{c}{qB_0} \frac{\partial V}{\partial x}, \\ \dot{x} &= -\frac{c}{qB_0} \frac{\partial V}{\partial y}. \end{aligned} \right\} \quad (16)$$

Following the Hamiltonian procedure, the canonical momenta associated with the linear Lagrangian are:

$$p_x = \frac{\partial L}{\partial \dot{x}} = -\frac{qB_0}{2c} y, \quad (17)$$

$$p_y = \frac{\partial L}{\partial \dot{y}} = \frac{qB_0}{2c} x, \quad (18)$$

which are unusual in that they are not invertible to the velocities. A Legendre transformation produces the Hamiltonian:

$$H_0 = \dot{x}p_x + \dot{y}p_y - L \equiv V(x, y). \quad (19)$$

Note that this Hamiltonian has no dependence on the momenta; which means that equations of motion from Hamilton's equations are inconsistent. Thus, the Hamiltonian procedure has broken down.

Let us now analyze the dynamics of the constraint system by using the method illustrated previously. Choose $q_1 = x$ and $q_2 = y$, then from Equations (1) and (15), one obtains:

$$\left. \begin{aligned} a_1 &= -\frac{qB_0}{2c} y, \\ a_2 &= \frac{qB_0}{2c} x. \end{aligned} \right\} \quad (20)$$

Making use of Eq. (10), the equations of motion for the generalized coordinates x and y can be respectively determined as:

$$\left. \begin{aligned} -\frac{qB_0}{c} dy + \frac{\partial V}{\partial x} dt &= 0, \\ \frac{qB_0}{c} dx + \frac{\partial V}{\partial y} dt &= 0. \end{aligned} \right\} \quad (21)$$

This set of equations can easily be written as:

$$\left. \begin{aligned} \dot{y} &= \frac{c}{qB_0} \frac{\partial V}{\partial x}, \\ \dot{x} &= -\frac{c}{qB_0} \frac{\partial V}{\partial y}. \end{aligned} \right\} \quad (22)$$

These results are in exact agreement with those obtained from Euler's equations of motion (16).

Finally, one can use equations (11) and (20) to get the action function as:

$$S = \text{const}. \quad (23)$$

Conclusion

In this work, a brief review of the basic concepts and results of the Hamilton-Jacobi method for Lagrangian systems with linear velocities is presented. Then, the method is applied to analyze the motion of a charged particle in a uniform magnetic field. The equations of motion are recovered as a result of applying the integrability conditions on the action integral. It is shown that the results are found to be in exact agreement with those obtained by Euler-Lagrange equations of motion. Indeed, the solutions of the investigated example are restricted to the limit $qB_0 \gg mc$ which corresponds to a very large magnetic field. In such a case, the Lagrangian is linear in velocities.

The advantage of using the method presented in this paper, is that it is easy to obtain the action function which plays an important role for obtaining the WKB or path integral quantization for any mechanical Lagrangian system. The action is obtained directly as an integration over the independent dynamic variables without any need to use functions as given in the Faddeev and Jackiw method [4]. This topic is now undergoing further investigation.

References

- [1]Dirac, P.A.M., Can. J. Math. 2 (1950) 129.
- [2]Dirac, P.A.M., “Lectures on Quantum Mechanics”, (Belfer Graduate School of Science, Yeshiva University, New York, 1964).
- [3]Carinena, J.F., Lopez, C. and Ranada, M.F., J. Math. Phys. 29 (1988) 1134.
- [4]Faddeev, L. and Jackiw, B., Phys. Rev. Lett. 60 (1988) 1692.
- [5]Carinena, J.F., Forts. Phys. 38 (1990) 641.
- [6]Guler, Y., Il Nuovo Cimento, B107 (1992) 1143.
- [7]Rabei, E.M. and Guler, Y., Phys. Rev. A, 46 (1992) 3513.
- [8]Corichi, A., J. Math. Phys. 33 (1992) 4066.
- [9]Kulshreshtha, V., J. Math. Phys. 33 (1992) 633.
- [10]Rabei, E.M., Il Nuovo Cimento, B112 (1997) 1447.
- [11]Baleanu, D. and Guler, Y., Il Nuovo Cimento, B115 (2000) 319.
- [12]Rabei, E.M. *et al.*, Mod. Phys. Lett. A, 18 (2003) 1591.
- [13]Baleanu, D. and Avkar, T., Il Nuovo Cimento, 119B (2004) 73.
- [14]Muslih, S.I. and Baleanu, D., J. Math. Anal. Appl. 304 (2) (2005) 599.
- [15]Muslih, S.I. *et al.*, Int. J. Theor. Phys. 44 (8) (2005) 64.
- [16]Jarad, F. and Baleanu, D., Reports on Mathematical Physics, 59 (1) (2007) 33.

Two-Segment Electrophysiological Model of Excitable Membrane of *Paramecium*

Abdul-Rahman A. Al-Rudainy

Faculty of Science and Engineering, University of Science and Technology, Sana'a, Yemen.

Received on: 20/10/2010; Accepted on: 16/3/2011

Abstract: Our goal in this paper is to design a two-segment electrophysiological model for *Paramecium* based on the work of Hook and Hildebrand (1979, 1980). This model considers *Paramecium* divided into two segments. Both segments are assumed to obey Hook and Hildebrand equations. The aim of constructing this model is to consider theoretically how the free-swimming *Paramecium* responds to the external electric stimulation, involving whether the organism is facing the anode or the cathode during the application of the electric pulse. We assume that there is an irregular distribution of Ca^{2+} and K^+ channels on both segments.

We have designed a computer program to illustrate the relationship between the distribution channels and swimming reversal time of the *Paramecium*. It is found that the reversal time depends on the precise distribution of Ca^{2+} and K^+ channels. The relevant ratio of ionic channels distribution is found to be 74.8% and 25.2% for K^+ and Ca^{2+} , respectively over the cell anterior and *vice versa* for posterior.

Keywords: *Paramecium*; Potassium and calcium currents; Membrane potential; Ionic conductance; Ca^{2+} and K^+ channels; Reversal time.

Introduction

Paramecium is covered with cilia which form an integral part of the cell and are enclosed within the cell membrane. *Paramecium* ordinarily swims in a forward left-handed spiral path. It has an ability to turn smoothly and swim towards the cathode when an electric current is passed through the cell suspension (galvanotaxis) [1-6].

The electric properties of *Paramecium* have become of interest because of the emerging role of membrane potential and conductance in the control of ciliary activity [7-9]. Experiments indicate that ciliary responses are coupled to a membrane potential by membrane regulated calcium fluxes, and ciliary reversal is associated with depolarization of the membrane [10-14].

The experimental results described in previous work [15] need to be interpreted in terms of a physiological model of the cell

membrane. The model outlined by Hook and Hildebrand [16, 17] is ideally suited for this purpose. It describes ion flow across the ciliary membrane of *Paramecium* in terms of potassium and calcium channels whose conductivities depend upon the instantaneous membrane potential, and also takes into account the effects of changes in the surface charge on the ciliary membrane as external cation concentrations (e.g. of K^+) are varied; this is excluded in the following analysis, however, since the ionic concentrations in the electric field experiments were always kept constant.

One immediate deduction, which may be made from experimental results on *Paramecium*, is that the membrane is not functionally the same over the whole cell surface. Since the response depends on whether the cell is facing the cathode or the anode during the pulse, it follows that the front and rear halves of the cell are

physiologically different. It is therefore desirable to modify Hook and Hildebrand's model to incorporate, if possible, the functional differences between the cell membrane at the front and rear sides of the cell.

In this paper, the modifications of Hook and Hildebrand's model will be discussed. Account is given of how a membrane asymmetry can be incorporated into the model leaving the whole body responses unchanged whilst permitting different responses to asymmetric stimulation to occur.

Outlines of Hook and Hildebrand's Model

In this section, we review some equations of Hook and Hildebrand's model [16, 17] because of their importance as a basis for our two-segment model.

The Hook and Hildebrand's model is based on Ca^{2+} influx mechanism. It assumed that Ca^{2+} channels are built up by subunits extending through the lipid phase of the membrane. Both subunit ends contain a twice negatively charged binding site. The degree of cation binding (of Ca^{2+} and K^+) to these negative sites is supposed to be high. There are four possible states of cation binding which may be denoted X_1 to X_4 .

The subunit X_1 can undergo a conformational change to an active state, X_1^* , at a rate which depends exponentially on the transmembrane potential. A single Ca^{++} channel is assumed to require some number of subunits N in an active state X_1^* in order to open.

The conservation of subunit molecule gives:

$$\sum_{i=1}^4 X_i + X_1^* = X_0 = \text{constant} \quad (1)$$

This may be normalized with respect to the overall concentration X_0 .

$$\sum_{i=1}^4 x_i + x_1^* , \quad (2)$$

where $x_i \equiv X_i / X_0$ $i = 1, 2, 3, 4$.

The quantity x_1^* may be considered to be the probability of a subunit being in the active state, X_1^* . Because each subunit is independent of its neighbors, the probability that N such units will

come together to form an open Ca^{2+} - channel is therefore $(X_1^*)^N$.

If the potential-dependent conformational changes are rapid compared with the binding rate of the cations, then $X_1 \rightarrow X_1^*$ can be treated as a quasi steady - state process:

$$X_i^* = c \cdot X_1 , \quad (3)$$

where:

$$c = c_0 \cdot \exp(\varepsilon \cdot V_m), \quad (4)$$

$$\varepsilon = \varepsilon_0 \cdot F / RT , \quad (5)$$

where c_0 is a constant, ε_0 is the effective valency of the gating charge; F is Faraday's constant = 96485.34 C/mol of electrons (i.e., electric charge carried on one mole of electrons); R is the gas constant = 8.314 J.K⁻¹.mol⁻¹; and T is the absolute temperature.

Eq. (2) can be written in the form:

$$x_1^* = \frac{c}{c+1} (1 - x_2 - x_3 - x_4) \quad (6)$$

The calcium current can be introduced as:

$$i_{\text{Ca}} = \bar{g}_{\text{Ca}} \cdot (x_1^*(t))^N \cdot (V_m - E_{\text{Ca}}) + P_{\text{Ca}} , \quad (7)$$

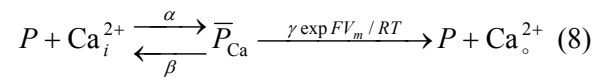
where i_{Ca} is the Ca^{2+} current (ions / s); \bar{g}_{Ca} is the maximum possible Ca^{2+} - conductivity per cilium (1 / mV.s); V_m is the membrane potential (mV); E_{Ca} is the Nernst potential of Ca^{2+} given by:

$$E_{\text{Ca}} = \frac{RT}{2F} \ln \frac{[\text{Ca}^{2+}]_0}{[\text{Ca}^{2+}]_i}$$

P_{Ca} is the rate of active Ca^{2+} - extrusion (Ca^{2+} - pump), ions / s.

The calcium current is taken to be positive outward; thus the calcium pump is positive.

Because Ca^{2+} - channels are known to be located in the cilia, it is suggested that the Ca^{2+} - pump is also located in the vicinity of the cilia [16]. The membrane is considered to be a potential barrier for Ca^{2+} - carrying proteins, with the potential peak placed halfway across the lipid matrix, and the following simplified substrate kinetic for active Ca^{2+} - transport:



So, Ca^{2+} - extrusion depends on the membrane potential. \bar{P}_{Ca} is an intermediate complex formed by Ca^{2+} bound to the ligand P (an ion, a molecule or a molecular group that binds to another chemical entity to form a larger complex). The binding reaction of P and Ca_i^{2+} is treated as fast as compared with actual Ca^{2+} transport across the membrane, so the association of Ca^{2+} and P is a quasi steady – state reaction. The conservation law is given by:

$$P + P_{\text{Ca}}^- = P_0 = \text{constant} . \quad (9)$$

The overall electric current (in amperes) is then given by:

$$I_{\text{Ca}} = z n i_{\text{Ca}} , \quad (10)$$

where z is the cation valency (being 2 for calcium).

Turning next to the case of potassium ions, the transmembrane flux of K^+ (K^+ - current) is given by:

$$I_K = \bar{g}_K \cdot X_K (V_m - E_K) + P_K , \quad (11)$$

where \bar{g}_K is the effective K^+ - conductance (1 / mV. s); X_K is the ratio of the open – channels; P_K is the pump rate of K^+ $P_K < 0$ (1 / s).

It is assumed that $[\text{K}^+]_i$ is independent of time, as it is highly compared with $[\text{K}^+]_o$.

($[\text{K}^+]_i = 20 \text{ mmol dm}^{-3}$). At steady – state, $I_K = 0$, $V_m = V_m$; thus from Eq. (11):

$$\frac{\bar{g}_K \cdot X_K}{P_K} = - \frac{1}{V_m - E_K} . \quad (12)$$

The complete K^+ - current is:

$$I_K = \bar{g}_K \cdot (V_m - E_K) \cdot \sum_{i=1}^3 X_{Ki} + P_K . \quad (13)$$

The total current across the *Paramecium* membrane is:

$$I = C \cdot \frac{dV}{dt} + I_{\text{Ca}} + I_K , \quad (14)$$

where $C \cdot \frac{dV}{dt}$ is the capacitive current and C is the overall capacitance of the membrane (in e / mV).

The model describes ciliary reversal on a short-time scale. In order to make the model describe long-lasting changes in the Ca^{2+} - influx system, the reaction scheme of Ca^{2+} - channel

was extended by assuming an additional slow reaction coupled to the conformation X_4 [17].



where d and f are the rates of reaction on a long time scale ($>10 \text{ sec.}$). So, Eq. 1 is no longer valid, and it must be written in a new form:

$$\sum_{i=1}^5 X_i + X_1^* \equiv X_0^- = \text{constant} \quad (16)$$

and then normalized with respect to X_0^- .

Hook and Hildebrand (1979) estimated the parameters of their model for *Paramecium* in the following way.

As a fixed point, the steady-state membrane potential V_m is -30 mV, and the ionic concentrations are as follows: The intracellular Ca^{2+} - concentration is $10^{-8} \text{ mol. dm}^{-3}$, $[\text{K}]_i$ is $20 \times 10^{-3} \text{ mol. dm}^{-3}$, at given external Ca^{2+} and K^+ - concentrations $[\text{Ca}^{2+}]_o$ is $10^{-8} \text{ mol. dm}^{-3}$ and $[\text{K}^+]_o$ is $2 \times 10^{-3} \text{ mol. dm}^{-3}$.

The overall membrane capacitance of $1 \mu\text{F/cm}^2$ together with an estimated total area of ciliary and intraciliary membrane of about 10^{-3} cm^2 , yield a value of membrane capacitance, C , of $6.5 \times 10^6 \text{ (e/mV)}$.

For the probability of Ca - channel being open (X_1^*)^N, it was found that the steepness of the current-voltage relationship requires a value of $N = 10$. The effective valency of the gating charge is $\epsilon_0 = 2$.

The number of cilia is $n = 10^4$, with a respective volume of $\Delta_i = 3 \times 10^{-13} \text{ cm}^3$ (area of cilia $A_i = 3 \times 10^{-10} \text{ cm}^2$, length = 10 μm) and an effective volume of the *Paramecium* body $\Delta_c = 10^{-5} \text{ cm}^3$. The choice of effective K^+ and Ca^{2+} channel conductivity is as follow:

$$\bar{g}_K = 2.5 \times 10^8 \text{ (1/mV. s)},$$

$$\bar{g}_{\text{Ca}} = 3.75 \times 10^5 \text{ (1/mV. s)} \cdot C_o = N = 10.$$

With respect to the extended reaction system (Eq. 15), f was chosen to be equal to $5 \times 10^{-4} \text{ s}^{-1}$. The relaxation from a high adapted state (high X_5) to a normal excitability is:

$$\frac{d}{dt} X_5^- \equiv -f \cdot X_5^- . \quad (17)$$

The relaxation time $t_r = 1/f$, so that t_r lies in the range of 30 min. d was estimated to be 0.1 s^{-1} .

In Hook and Hildebrand's model, the simulated membrane responses to depolarizing and hyperpolarizing current pulses were in good agreement with the measured response [16-18].

So, the advantage of Hook and Hildebrand's model is that it has the ability to fit any cell response expression, because there are enough arbitrary constants from which values can be chosen to make the model to provide a satisfactory fit.

A Two-Segment Ionic Model

When a membrane covered cell, which is freely swimming, is exposed to an external electric field, that part of the cell facing the cathode becomes depolarized (resulting in ciliary reversal), while the part facing the anode becomes hyperpolarized (making the cilia increase their beating in the normal direction; i.e., toward the cell's rear side). A middle area between these two regions is unaffected and the cilia are partially inactivated [3].

In order to solve the Hook and Hildebrand's equations in these circumstances, it is necessary to divide the organism into several segments, the membrane potential perturbation within each segment being constant. Faced with the problem of inordinately long computation times, however, it was decided to utilize a two-segment model, the membrane perturbation in each segment being constant over its surface, and being equal and opposite in the two segments. Thus, no degree of inaccuracy is being tolerated in the interest of obtaining realistic execution times on the computer.

Both segments are assumed to obey the Hook and Hildebrand's equations, the linking conditions being (a) the algebraic sum of the membrane currents entering and leaving each segment is zero (Kirchhoff's first law), and (b) the electrical potentials inside each segment are always equal.

The total currents through each membrane segment, if leakage currents are ignored, are given by:

$$I_1 = I_{Ca1} + I_{K1} + C_1 \cdot dV/dt, \quad (18)$$

$$I_2 = I_{Ca2} + I_{K2} + C_2 \cdot dV/dt, \quad (19)$$

where I_{Ca} and I_K are outward calcium and potassium currents (in amperes) through each membrane segment, and C_1 and C_2 are the membrane capacitances (in Farad).

The two linking conditions then yield:

$$\frac{dV}{dt} = (I_{Ca1} + I_{Ca2} + I_{K1} + I_{K2}) \cdot \frac{1}{C}, \quad (20)$$

where $C = C_1 + C_2$ is the total membrane capacitance.

In these calculations, the electric potentials in various regions are given relative to a point just outside the cell, in the external medium and lying in the mid-plane of the cell.

During a pulse, the potentials outside the two segments are taken to be V_p and $-V_p$, respectively, while before and after the pulse these potentials are taken to be zero. Eq. 20 permits the change in internal potential dV to be calculated during time dt once the various ionic currents are given.

The membrane potential V_m during the pulse is given by:

$$V_m = V_{in} - V_p, \quad (21)$$

where V_{in} is the potential inside the cell. In a resting cell, $V_{in} = -30 \text{ mV}$.

It is clear from the experimental results that the membranes at the front and rear sides of the organism are different. A two-segment asymmetric model is therefore required to interpret the experimental results. Such an asymmetry may be reduced in two different ways. First, the ionic channels (Ca^{2+} and K^+) may be non-uniformly distributed over the cell. Second, the characteristics of the ionic channels (e.g. ionic conductance, g_{Ca} and g_K or ionic pump rates) may be different in the two halves of the cell.

It is found that the mutant of *Paramecium* is defective in the stimulus response pathway [20]. The "pawn" mutant; i.e., the cell which cannot swim backward, does not deflect the passive electrical properties (resting potential and input impedance) of the membrane and it also shows no change in delayed rectifying active electrical properties. The important result is that the "Pawns" are defective in their inward current mechanism; i.e., affect Ca^{2+} - channels' mechanism, since they show a different degree of ciliary reversal [20-22]. This means that the membrane is not depolarized enough to induce a

reversal. Such evidence of an existence of a difference in the ionic channels' mechanisms in any part of the wild type is not available. So, it is suggested that the only relevant reason so far to cause asymmetry in the two-segment model is to assume that the ionic channels are non-uniformly distributed over the cell's membrane.

One of the observations made in the present study is that ciliates never reverse when swimming towards the cathode, but usually do

when swimming initially towards the anode. The present two-segment model was used to find out whether or not a non-uniform distribution of ion channels could account for this phenomenon. Cells were deemed to reverse if the intraciliary calcium concentration exceeded 5×10^{-7} mol. dm^{-3} . The table below (Table 1) shows the effect on reversal time of redistributing the Ca^{2+} and K^{+} channels between the two segments such that the total number of channels remains constant.

TABLE 1. The distribution ratio of Ca^{2+} and K^{+} channels and ciliary reversal time

Y_1 Ratio of Ca^{2+} channels	Y_2 Ratio of K^{+} channels	T_{SR} ciliary reversal time (ms)
0.735	0.265	10
0.745	0.255	120
0.746	0.254	135
0.747	0.253	220
0.748	0.252	450
0.750	0.250	$H > 20$ s
0.850	0.150	$H > 20$ s

Y_1 and Y_2 are the distribution ratios of the Ca^{2+} and K^{+} channels, respectively, over the posterior segment and *vice versa* for the anterior segment. The total number of Ca^{2+} and K^{+} channels for the cell is assumed to be 10^4 . T_{SR} is the ciliary reversal time in ms. H signifies a ciliary reversal time of more than 20s. The pulse duration is 0.6 ms and its voltage is 100 mV with the anterior segment towards the anode. No reversal occurs when the polarity of the pulse is reversed. X_5^- is 0.1449.

The reversal time is clearly very dependent on the precise channel distribution. For the purposes of this study, it was found that the value of X_5^- affects the period of ciliary reversal, if X_5^- increases or decreases, the ciliary reversal time decreases or increases, respectively. The optimum ionic channels' distribution was found to be 74.8% and 25.2% for K^{+} and Ca^{2+} channels, respectively over the cell's anterior and *vice versa* for posterior. The reasons for this choice are: First, it is found that the longest relevant period of ciliary reversal is 450 ms, at $X_5^- = 0.1449$, 74.8% and 25.2% of ionic channels' distribution. This ciliary reversal time is followed by a predictable return to a normal ciliary beating. Second, the symbol H in the above table means that the reversal time produced by the model of 75% and 25% or that of 85% and 15% of ionic channels is more than 20 s. At this situation, the model predicts no

return to normal beating, and the reason for this is unknown. So, for that reason, this ciliary reversal time, H , is considered as an irrelevant time and is excluded as a criterion for choosing the ratio of ionic channel distribution. Third, there were no significant differences in the values of these ratios; i.e., 74.8% and 25.2%, as X_5^- changed; for example, if $X_5^- = 0.1842$, the ratios of ionic channels' distribution, Y_1 and Y_2 , are 71.6% and 28.4%, which also produced a ciliary reversal time of about 400 ms as the longest relevant time. This model exhibits reversal when the posterior segment is depolarized, but not when the anterior segment is depolarized. Thus, a non-uniform ion channel distribution can account for the asymmetry of the electric pulse response if the correct channel distribution is chosen. With this choice of channel distribution, the two- segment model can now be characterized by the following equations. The calcium and potassium currents through the posterior segment are given by:

$$I_{\text{Ca}1} = 0.748 I_{\text{Ca}} \quad , \quad (22)$$

$$I_{\text{K}1} = 0.252 I_{\text{K}} \quad , \quad (23)$$

where I_{Ca} and I_{K} are the total calcium and potassium currents, respectively, through the whole cell (Eq.18 and Eq. 19). Similarly, the currents through the anterior segment are given by:

$$I_{\text{Ca}2} = 0.252 I_{\text{Ca}} \quad , \quad (24)$$

$$I_{\text{K}2} = 0.748 I_{\text{K}} \quad . \quad (25)$$

The diffusion of cytoplasmic calcium within the two segments is given by:

$$\frac{d}{dt} [Ca^{2+}]_c = v' \cdot ([Ca^{2+}]_{i1} + [Ca^{2+}]_{i2} - 2[Ca^{2+}]_c), \quad (26)$$

where $[Ca^{2+}]_{i1}$ and $[Ca^{2+}]_{i2}$ are the intraciliary Ca^{2+} in cilia over posterior and anterior segments, respectively.

It is assumed that Ca^{2+} ions can diffuse freely from one segment to the other, so the intracellular calcium concentration is always equal in the two segments.

The one other parameter which needs adjustment in the two-segment model is the degree of long-term adaptation of the individual cell represented by the parameter X_5^- .

Hook and Hildebrand's (1980) estimates for the rate constants were $d = 0.1 \text{ s}^{-1}$ and $f = 5 \times 10^{-4} \text{ s}^{-1}$, corresponding to $X_5^- = 0.2315$. This value of X_5^- produces no reversal at all in the two-segment model, and presumably corresponds to cells in a state of high adaptation as voltage clamped specimens would be. By adapting the new values of $f = 7.6 \times 10^{-4} \text{ s}^{-1}$ with d unchanged, the value of X_5^- becomes about 0.145 and corresponds more closely to cells which have not reversed for some time.

The computer program for the two-segment model is designed to solve, as a function of time, the change in *Paramecium* membrane parameters (e.g.; V_m , $[Ca^{2+}]_i$, I_{Ca} , I_K , ... etc.), when the cell is exposed to an external electric field. The program consists of a subroutine loop, inside which are all the membrane parameters, which, apart from the membrane potential and cytoplasmic calcium concentration, are solved with respect to whether the segment is an anterior or a posterior segment.

Discussion

Hook and Hildebrand's model has been adapted to deal with asymmetrical excitation, due to external electric pulses, for the freely swimming paramecia, according to their swimming direction before the pulse. This adaptation has been achieved by dividing the cell into two segments and by assuming that the ionic channels are non-uniformly distributed over the cell.

The two-segment model is based on the assumption that all the cells are identical, but this seems likely to be not true, because the experimental results show an opposite finding to this assumption. It is found for a given electric pulse, that some cells swimming in the direction of the cathode do reverse, while others do not. This asymmetrical response may be caused by one or more of the following suggestions: (1) Larger cells may have more ionic elements (especially Ca^{2+} - levels) than smaller cells, so the effect of a pulse will depend upon the cell size; thus the probability of reversing may depend upon cell size; (2) Cells of an identical size, but having differences in the lengths of cilia, may also have different numbers of ionic channels, leading to asymmetric responses; (3) The other possibility which may lead to an asymmetrical response is that the ionic conductance values are different among the cell population, so those cells which have a high ionic conductance, especially calcium conductance, before the pulse may reverse due to a given pulse are more readily than those which have low calcium conductance; (4) It is found that the steady-state value of X_5^- (the slow reaction) has affected the ciliary reversal time when the two-segment model is simulated. As X_5^- is low, the cell reverses for longer than one which has high X_5^- , and as X_5^- is higher, there is no reversal produced by the model. Since there is no evidence to support the suggestions in points 1, 2 and 3, I considered that the difference in the steady-state values of X_5^- among cell population is a reasonable cause to make the two-segment model explain the percentage of cell reversing. Not enough is known about the percentage reversal, but my analysis is a first attempt to address the problem.

Many researchers proposed dynamic and physical models for *Paramecium* cells, to analyze their swimming behavior, geotaxis, thigmotaxis and gravikinesis, and their responses to different stimuli to utilize microorganisms as micro-robots in many applications [5, 6, 23, 24, 25, 26, 27, 28].

In a future work, I will try to make a comparison of experimental results and computer predictions of the two-segment model.

Summary

In this paper, I proposed a two-segment physical model of *Paramecium* based on Hook and Hildebrand's model (1979, 1980). This two-

segment model is the first attempt to investigate the behavior of free-swimming *Paramecium* due to electrical stimulation.

References

- [1]Machemer, R., Machemer, H. and Brauker, R. Journal of Comparative Physiology A, 179 (1996) 213.
- [2]Eckert, R. and Naitoh, Y., J. Gen. Physiol. 55 (1970) 467.
- [3]Machemer, H. and Peyer, J., "Swimming Sensory Cells: Electrical Membrane Parameters, Receptor Properties and Motor Control in Ciliate Protozoa", (Verhandlungen der deutschen, zoologischen Gesellschaft, G. Fischer Verlag, Stuttgart, 1977) 86-110.
- [4]Clark, K.D. and Nelson, D.L., Cell Motile Cytoskeleton, 19(2) (1991) 91.
- [5]Ogawa, N., Oku, H., Hashimoto, K. and Ishikawa, M., "Dynamics Modelling and Real-time Observation of Galvanotaxis in *Paramecium caudatum*". (Bio-Mechanisms of Swimming an Flying, Springer, Japan, 2008) 29-40.
- [6]Ogawa, N., Oku, H., Hashimoto, K. and Ishikawa, M., Journal of Theoretical Biology, 242 (2006) 314.
- [7]Yamaguchi, T., J. Fac. Sci., Tokyo Univ. IV, 8 (1960) 573.
- [8]Okumura, H. and Yamaguchi, T., Zool. Mag. 71 (1962) 157.
- [9]Naitoh, Y. and Eckert, Z. Vergl. Physiol. 161 (1968) 427.
- [10]Doughty, J.M., Comp. Biochem. Physiol. 61c (1978) 369.
- [11]Doughty, J.M., Comp. Biochem. Physiol. 61c (1978) 375.
- [12]Doughty, J.M., Comp. Biochem. Physiol. 63c (1979) 183.
- [13]Machemer, H., "Motor Control of Cilia", In: (Görtz, H.D., ed). (Paramecium, Springer Verlag, Berlin, Heidelberg, New York, Tokyo, 1988) 216-235.
- [14]Machemer, H., J. Protozool. 3 (1989) 463.
- [15]Al-Rudainy, A., Dirasat Journal, 36 (2) (2009) 105.
- [16]Hook, C. and Hildebrand, E., J. Math. Biol. 8 (1979) 197.
- [17]Hook, C. and Hildebrand, E., J. Math. Biol. 9 (1980) 347.
- [18]Hill, T.L., J. Theor. Biol. 10 (1966) 442.
- [19]Kung, C., Chang, SY., Satow, Y., Houten, J.V. and Hansma, H., Science, 188 (4191) (1975) 898.
- [20]Stanley, J., Bennet, M.V. and Katz, G.M., J. Exp. Biol. 65 (1976) 699.
- [21]Browning, J.L., Nelson, D.L. and Hansma, H., Nature, 259 (1976) 491.
- [22]Satow, Y. and Kung, C., J. Exp. Biol. 84 (1980a) 57.
- [23]Blake, J., Journal of Biomechanics, 6 (2) (1973) 133.
- [24]Fukui, K. and Asai, H., Biophysical Journal, 47 (4) (1985) 479.
- [25]Sikora, J., Braranowski, Z. and Zajaczkowska, M., Experientia, 48 (8) (1992) 789.
- [26]Hasegawa, T., Ogawa, N., Oku, H. and Ishikawa, M., IEEE International Conference on Robotics and Automation, ICRA (2008).
- [27]Jana, S., Bulletin of American Physics Society APs, 55 (2) (2010).
- [28]Takeda, A., Mogami, Y. and Shoji, A.B., Biological Sciences in Space (BSS), 20 (2) (2006) 44.

IBM-1 Calculations of Low-Lying Excited Levels and Electric Transition Probabilities B(E2) on the Even-Even $^{174-180}\text{Hf}$ Isotopes"

K. A. Al-Maqtary, M. H. Al-Zuhairy, M. N. Al-Sharaby and N. A. Shamlan

Physics Department, Faculty of Science, Ibb University, Ibb, Yemen.

Received on: 21/10/2010; Accepted on: 3/4/2011

Abstract: In this paper, the interacting boson model (IBM-1) is discussed and employed for calculating the energy levels and the electromagnetic transition probabilities B(E2) of the even – even $^{174-180}\text{Hf}$ isotopes". These isotopes have been investigated based on two different arrangements; i.e., the dynamical symmetry of $^{176-180}\text{Hf}$ isotopes", SU(3) (deformed nuclei) and the dynamical symmetry of ^{174}Hf isotope" in transition region SU(3)-O(6). The determined values using the IBM-1 Hamiltonian showed significant agreement with the experimentally reported energy levels and B(E2) values. The model provides a fast and accurate prediction method of energy levels and B(E2) values.

Keywords: Hafnium isotopes; Energy levels; Interacting boson model.

Introduction

The nucleus consists of many nucleons (protons and neutrons). Each nucleon is interacting with all others and moving within a complex structure. This structure could be described by the analytical solution of their wave function. As a consequence, the excitation energies of collective quadrupole excitations in nuclei near a closed shell are strongly dependent on the number of nucleons outside the closed shell. The interacting boson model of Arima and Iachello [1-6] has become widely accepted as a tractable theoretical scheme of correlating, describing and predicting low-energy collective properties of complex nuclei. In this model, it was assumed that low-lying collective states of even-even nuclei could be described as states of a given (fixed) number N of bosons. Each boson could occupy two levels; one with angular momentum $L = 0$ (s-boson) and the other, usually with higher energy, with $L = 2$ (d-boson). In the original form of the model known as the Interacting Boson Model (IBM-1), proton- and neutron-boson degrees of freedom are not distinguished. The model has an inherent group

structure, which is associated with it in terms of s- and d- boson operators.

The even-mass Hafnium $^{174-180}\text{Hf}$ isotopes" have been extensively investigated experimentally using a wide variety of reactions. From these studies, the excited states in the $^{174-180}\text{Hf}$ isotopes" have been investigated from (γ, γ') , (d, p) , $(\alpha, 2n\gamma)$, $(\alpha, 4n\gamma)$, (n, γ) , $(n, n'\gamma)$ and coulomb excitation reactions which gave information about the experimental energy levels and the electromagnetic transition probabilities B(E2) in these isotopes [7-16].

The aim of the present work is to investigate the dynamical symmetry of $^{176-180}\text{Hf}$ isotopes" and study the energy levels and the electromagnetic transition probabilities B(E2) of these isotopes (proton number 72) within the framework of the (IBM-1) model.

Theoretical Basics of Interacting Boson Model (IBM-1)

The IBM-1 Hamiltonian can be expressed as [5, 17]:

$$\begin{aligned}
H = & \varepsilon_s s^+ s + \varepsilon_d (d^+ d) \\
& + \sum_{L=0,2,4} c_L [(d^+ d^+)^{(L)} \cdot (dd)^{(L)}] \\
& + \frac{1}{2} v_0 [(d^+ d^+)^{(0)}_0 s^2 + (s^+)^2 (dd)^{(0)}_0] \\
& + \sqrt{\frac{1}{2}} v_2 \left[[(d^+ d^+)^{(2)} ds]^{(0)}_0 + [s^+ d^+ (dd)^{(2)}]^{(0)}_0 \right] \\
& + \frac{1}{2} u_0 (s^+)^{(2)} s^+ + \frac{1}{\sqrt{5}} u_2 s^+ s (d^+ d)
\end{aligned} \quad (1)$$

This Hamiltonian contains 2 terms of one-body interactions, (ε_s and ε_d), and 7 terms of two-body interactions [c_L ($L = 0,2,4$), v_L ($L = 0,2$), u_L ($L = 0,2$)], where ε_s and ε_d are the single-boson energies, and c_L , v_L and u_L describe the two-boson interactions. However, it turns out that for a fixed boson number N , only one of the one-body terms and five of the two-body terms are independent, as it can be seen by noting $N = n_s + n_d$.

The IBM-1 Hamiltonian equation (1) can be written in general form as [3,18,19,,20,21]:

$$\begin{aligned}
\hat{H} = & \varepsilon (\hat{n}_s + \hat{n}_d) + a_0 \hat{P}^+ \cdot \hat{P} + a_1 \hat{L} \cdot \hat{L} \\
& + a_2 \hat{Q} \cdot \hat{Q} + a_3 \hat{T}_3 \cdot \hat{T}_3 + a_4 \hat{T}_4 \cdot \hat{T}_4
\end{aligned} \quad (2)$$

where ε is the bosons energy, and the operators are:

$$\begin{aligned}
\hat{n}_s = & \hat{s}^+ \cdot \hat{s} \quad , \quad \hat{n}_d = \hat{d}^+ \cdot \hat{d} \\
\hat{P} = & \frac{1}{2} (\hat{d} \cdot \hat{d}) - \frac{1}{2} (\hat{s} \cdot \hat{s}) \\
\hat{L} = & \sqrt{10} \left[\hat{d}^+ \times \hat{d} \right]^{(1)} \\
\hat{Q} = & \sqrt{5} \left[(\hat{d}^+ \times \hat{s}) + (\hat{s}^+ \times \hat{d}) \right]^{(2)} + \chi \left[\hat{d}^+ \times \hat{d} \right]^{(2)} \\
\hat{T}_3 = & \left[\hat{d}^+ \times \hat{d} \right]^{(3)} \\
\hat{T}_4 = & \left[\hat{d}^+ \times \hat{d} \right]^{(4)}
\end{aligned} \quad (3)$$

The phenomenological parameters a_0 , a_1 , (a_2, χ), a_3 , a_4 , represent the strengths of the pairing, angular momentum, quadrupole,

octupole and hexadecupole interaction between bosons, respectively.

The Hamiltonian equations (1, 2) can be rewritten in terms of the Casimir operators of U(6) group. In that case, one says that the Hamiltonian H has three dynamical symmetries. These symmetries are called SU(5) vibrational, SU(3) rotational and O(6) γ -unstable. The three dynamical symmetries of IBM-1 are:

Group Chin I: The Vibrational Symmetry SU(5)

This dynamical symmetry group describes the vibrational nuclei which have a spherical shape. The Hamiltonian of this symmetry can be written as [18, 20]:

$$\begin{aligned}
\hat{H}^{(I)} = & \varepsilon (\hat{n}_s + \hat{n}_d) \\
& + a_1 \hat{L} \cdot \hat{L} + a_3 \hat{T}_3 \cdot \hat{T}_3 + a_4 \hat{T}_4 \cdot \hat{T}_4
\end{aligned} \quad (4)$$

$\varepsilon (\hat{n}_s + \hat{n}_d)$ is the energy of s and d boson, a_1 is the angular momentum, a_3 is the octupole and a_4 the hexadecupole parameters.

Group Chin II: The Rotational Symmetry SU(3)

This symmetry is used to describe the rotational spectra of nuclei that possess axial symmetrical rotor. The Hamiltonian of this symmetry used the angular momentum and the quadrupole parameters (a_1 , a_2). This Hamiltonian is given by [18, 20]:

$$\hat{H}^{(II)} = a_1 \hat{L} \cdot \hat{L} + a_2 \hat{Q} \cdot \hat{Q} \quad (5)$$

Group Chin III: The Γ - Unstable Symmetry O(6)

This symmetry is used to describe the asymmetric (γ -soft) deformed rotor of nuclei. The Hamiltonian parameters of this symmetry are the strengths of the pairing a_0 , angular momentum a_1 and octupole a_3 . The Hamiltonian equation of this symmetry is [18,20]:

$$\hat{H}^{(III)} = a_0 \hat{P}^+ \cdot \hat{P} + a_1 \hat{L} \cdot \hat{L} + a_3 \hat{T}_3 \cdot \hat{T}_3 \quad (6)$$

Table 1 shows the typical conditions of the energy ratios for these three dynamical symmetries.

TABLE 1. The typical conditions of the energy ratios for three dynamical symmetries in IBM-1 [18, 20]

symmetry	$E\left(\frac{4_1^+}{2_1^+}\right)$	$E\left(\frac{6_1^+}{2_1^+}\right)$	$E\left(\frac{8_1^+}{2_1^+}\right)$
SU(5)	2	3	4
O(6)	2.5	4.5	7
SU(3)	3.33	7	12

The interferences between these three dynamical symmetries give three transitional regions. These regions are as follows *SU(3)* - *SU(5)*: This transitional region can be treated by breaking *SU(3)* symmetry in the direction of *SU(5)* by adding $\varepsilon(\hat{n}_s + \hat{n}_d)$, $a_3\hat{T}_3 \cdot \hat{T}_3$, $a_4\hat{T}_4 \cdot \hat{T}_4$ terms. The Hamiltonian of this region can be written as [18, 20]:

$$\left. \begin{aligned} \hat{H} = \varepsilon(\hat{n}_s + \hat{n}_d) + a_1\hat{L} \cdot \hat{L} \\ + a_2\hat{Q} \cdot \hat{Q} + a_3\hat{T}_3 \cdot \hat{T}_3 + a_4\hat{T}_4 \cdot \hat{T}_4 \end{aligned} \right\} \quad (7)$$

SU(3) - *O(6)*: The nuclei in this transitional region can be treated by breaking *SU(3)* symmetry in the direction of *O(6)* by adding $a_0\hat{P}^+ \cdot \hat{P}$, $a_3\hat{T}_3 \cdot \hat{T}_3$ terms. The Hamiltonian of this region can be written as [18, 20]:

$$\hat{H} = a_0\hat{P}^+ \cdot \hat{P} + a_1\hat{L} \cdot \hat{L} + a_2\hat{Q} \cdot \hat{Q} + a_3\hat{T}_3 \cdot \hat{T}_3 \quad (8)$$

O(6) - *SU(5)*: The nuclei in this transitional region can be treated by a Hamiltonian containing $\varepsilon(\hat{n}_s + \hat{n}_d)$ and $a_0\hat{P}^+ \cdot \hat{P}$ terms as [18, 20]:

$$\left. \begin{aligned} \hat{H} = \varepsilon(\hat{n}_s + \hat{n}_d) + a_0\hat{P}^+ \cdot \hat{P} \\ + a_1\hat{L} \cdot \hat{L} + a_3\hat{T}_3 \cdot \hat{T}_3 + a_4\hat{T}_4 \cdot \hat{T}_4 \end{aligned} \right\} \quad (9)$$

The Electromagnetic Transitions' Operator

The general form of the electromagnetic transitions' operator in IBM-1 is [18, 20, 21]:

$$\left. \begin{aligned} \hat{T}^{(L)} = \gamma_0 [\hat{S}^+ \times \tilde{\hat{S}}]^{(0)} \\ + \alpha_2 [\hat{d}^+ \times \tilde{\hat{S}} + \hat{S}^+ \times \tilde{\hat{d}}]^{(2)} \\ + \beta_L [\hat{d}^+ \times \tilde{\hat{d}}]^{(L)} \end{aligned} \right\} \quad (10)$$

where γ_0 , α_2 and β_L ($L = 0, 1, 2, 3, 4$) are parameters specifying the various terms in the corresponding operators. Equation (10) yields transition operators for E0, M1, E2, M3 and E4 transitions with appropriate values of the corresponding parameters. The electric quadrupole operator E2 has a widespread application in the analysis of γ -ray transitions and it is deduced from equation (10) as [18, 20, 21]:

$$\left. \begin{aligned} \hat{T}^{(E2)} = \alpha_2 [\hat{d}^+ \times \tilde{\hat{S}} + \hat{S}^+ \times \tilde{\hat{d}}]^{(2)} \\ + \beta_2 [\hat{d}^+ \times \tilde{\hat{d}}]^{(2)} \end{aligned} \right\} \quad (11)$$

It is clear that, for the E2 polarity, two parameters, α_2 and β_2 , are needed in addition to the wave functions of initial and final states.

The electric transition probabilities' B(E2) values are defined in terms of reduced matrix elements by Iachello and Arima (1987) as [20, 21]:

$$\left. \begin{aligned} B(E2; L_i \rightarrow L_f) = \\ \frac{1}{2L_i + 1} \left| \langle L_f || \hat{T}^{(E2)} || L_i \rangle \right|^2 (eb)^2 \end{aligned} \right\} \quad (12)$$

Results and Discussion

The obtained results can be discussed separately for both energy levels and the electric transition probabilities B(E2) as follows:

Energy Levels

The IBM-1 model has been used in the calculation of the energy levels of the ¹⁷⁴⁻¹⁸⁰Hf isotopes", using the experimental energy ratios:

$$E\left(\frac{4_1^+}{2_1^+}\right) = 3.3, 3.29, 3.3, 3.3,$$

$$E\left(\frac{6_1^+}{2_1^+}\right) = 6.76, 6.77, 7, 6.88 \text{ and}$$

$$E\left(\frac{8_1^+}{2_1^+}\right) = 11.21, 11.33, 11.67, 11.645,$$

respectively. It has been found that the ¹⁷⁶⁻¹⁸⁰Hf isotopes" are rotational (deformed nuclei) and that they have a dynamical symmetry *SU(3)* and the ¹⁷⁴Hf isotope" is found in the transitional region *SU(3)*-*O(6)* respecting to IBM-1.

According to the Hamiltonian of the IBM-1 model, the energy levels of the " ^{174}Hf isotope" (total number of bosons 15 in the transitional region $\text{SU}(3) - \text{O}(6)$, Eq. 8) and the " $^{174-180}\text{Hf}$ isotopes" (total number of bosons 16, 15 and 14, respectively, in dynamical symmetry $\text{SU}(3)$, Eq. 5) have been calculated using the angular momentum, quadrupole and octupole parameters [a_1 , (a_2, χ) and a_3]. The best fit values of these parameters are given in Table 2, which shows the values of the relevant parameters. These values are obtained by fitting to get results of the energy levels that match with the experimentally reported data [22-25], whereas, the first two terms and the last term in Eq. 2 have now been included because they are irrelevant to the case of fully and weakly deformed nuclei (rotational nuclei).

TABLE 2. The best fit values of the Hamiltonian parameters for " $^{174-180}\text{Hf}$ isotopes"

Isotopes	a_1	a_2	a_3	χ
	MeV	MeV	MeV	
^{174}Hf	0.0450	-0.0105	0.0640	-0.06
^{176}Hf	0.0097	-0.1130	0.000	-0.6
^{178}Hf	0.0960	-0.0146	0.000	-0.11
^{180}Hf	0.0100	-0.0140	0.000	-0.26

The obtained results by this process are given in Table 3; this table shows the ground state, β and γ bands of the experimental and the IBM-1 calculations energy levels of " $^{174-180}\text{Hf}$ isotopes". It shown that there is a good agreement between experimental energy values and the IBM-1 calculations.

TABLE 3. The experimental and calculated energy levels of $^{174-180}\text{Hf}$ isotopes

^{174}Hf Isotope								
g-band			β band			γ - band		
E (Mev)			E (Mev)			E (Mev)		
L^π	Exp	IBM-1	L^π	Exp	IBM-1	L^π	Exp	IBM-1
$^+0$	0	0	$^+0$	0.828	0.808	2^+	1.226	1.220
$^+2$	0.090	0.090	$^+2$	0.900	0.903	3^+	1.336	1.343
$^+4$	0.297	0.294	$^+4$	1.062	1.110	4^+	1.448	1.478
$^+6$	0.608	0.602	$^+6$	1.307	1.419	5^+	1.658	1.667
$^+8$	1.009	1.004						
$^+10$	1.485	1.492						
^{176}Hf Isotope								
g-band			β band			γ band		
E (Mev)			E (Mev)			E (Mev)		
L^π	Exp	IBM-1	L^π	Exp	IBM-1	L^π	Exp	IBM-1
$^+0$	0	0	$^+0$	1.149	1.152	2^+	1.341	1.331
$^+2$	0.088	0.085	$^+2$	1.226	1.237	3^+	1.445	1.415
$^+4$	0.29	0.283	$^+4$	1.39	1.435	4^+	1.54	1.528
$^+6$	0.596	0.595	$^+6$	1.628	1.747	5^+	1.727	1.67
$^+8$	0.997	1.02						
$^+10$	1.481	1.558						
^{178}Hf Isotope								
g-band			γ band			β band		
E (Mev)			E (Mev)			E (Mev)		
L^π	Exp	IBM-1	L^π	Exp	IBM-1	L^π	Exp	IBM-1
$^+0$	0	0	2^+	1.17	1.18	$^+0$	1.19	1.18
$^+2$	0.09	0.09	3^+	1.26	1.27	$^+2$	1.27	1.27
$^+4$	0.30	0.30	4^+	1.38	1.39	$^+4$	1.45	1.48
$^+6$	0.63	0.63	5^+	1.53	1.54	$^+6$	1.73	1.82
$^+8$	1.05	1.08						
$^+10$	1.57	1.65						

¹⁸⁰ Hf Isotope								
g-band			β band			γ -band		
E (Mev)			E (Mev)			E (Mev)		
L $^{\pi}$	Exp	IBM-1	L $^{\pi}$	Exp	IBM-1	L $^{\pi}$	Exp	IBM-1
+0	0	0	+0	1.102	1.102	2 $^{+}$	1.199	1.193
+2	0.093	0.090	+2	1.183	1.169	3 $^{+}$	1.291	1.260
+4	0.308	0.302	+4	1.369	1.381	4 $^{+}$	1.409	1.405
+6	0.640	0.632	+6	1.703	1.715	5 $^{+}$	1.557	1.533
+8	1.083	1.089						
+10	1.630	1.664						

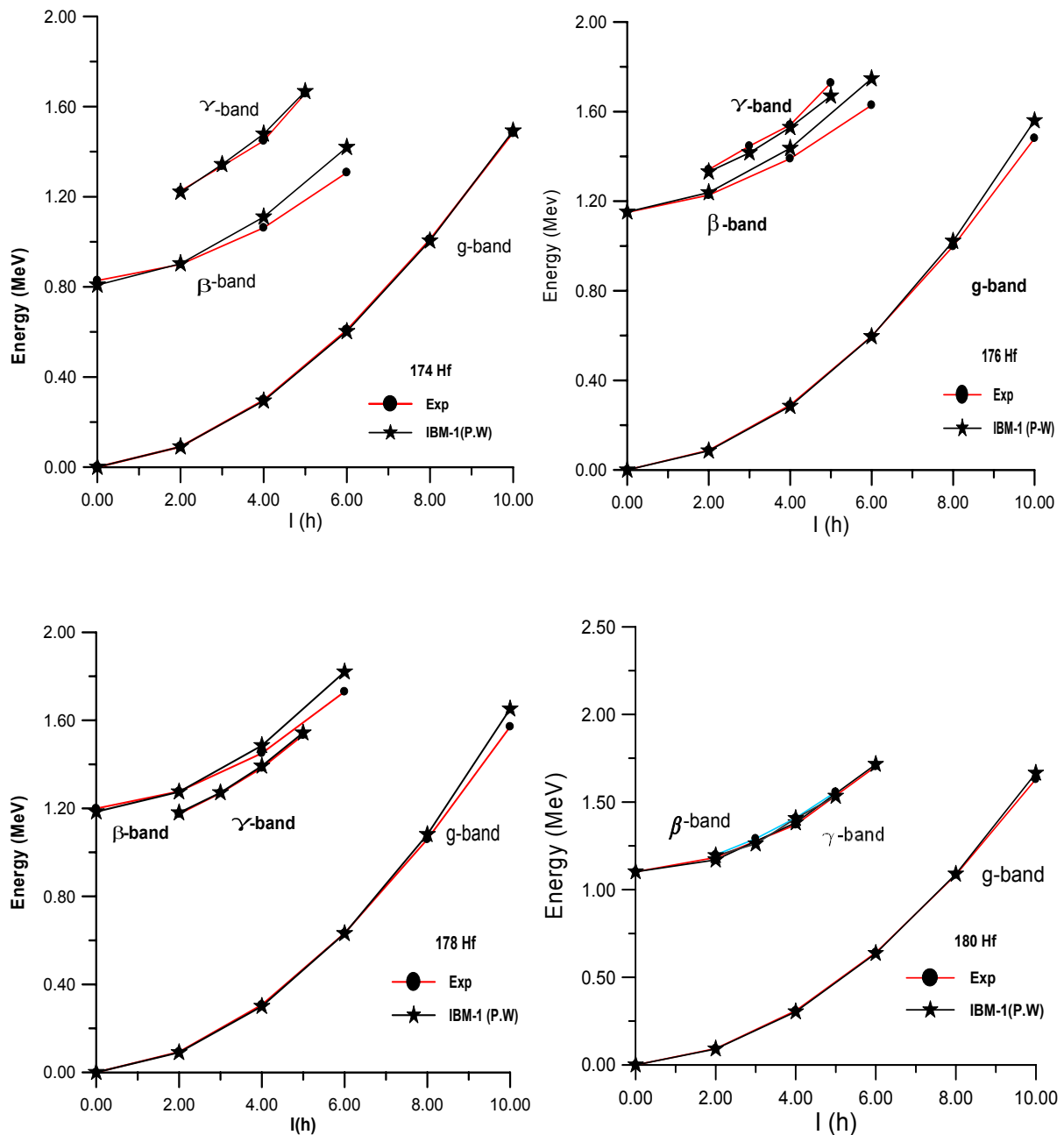


FIG.1. Variation of energy levels with the angular momentum for "¹⁷⁴⁻¹⁸⁰Hf isotopes".

The root mean square deviation [26]

$$RMSD = \left[\frac{1}{N} \sum (E_{cal} - E_{Exp})^2 \right]^{\frac{1}{2}}$$

is used to compare experimental and calculated energy levels (N is the number of levels), Table 4. In the ground state bands the best agreement was found in ^{174}Hf where the smallest value of RMSD is equal to 0.0045 and equal to 0.01 for γ -bands in ^{178}Hf . However, $RMSD = 0.011$ for β -bands in ^{180}Hf .

TABLE 4. The root mean square deviation RMSD between experimental and calculated energy levels

Isotopes	RMSD		
	g- band	β - band	γ -band
^{174}Hf	0.0045	0.062	0.016
^{176}Hf	0.033	0.064	0.033
^{178}Hf	0.035	0.048	0.010
^{180}Hf	0.015	0.011	0.020

A very good agreement has been obtained between the experimentally reported and the calculated energy level variations with the angular momentum as depicted in Fig.1. This figure shows that the experimental and the theoretical energy levels of the ground state, β and γ bands in " $^{174-180}\text{Hf}$ isotopes" increase with increasing angular momentum. The very good agreement was also found between the experimental and the theoretical energy levels of the ground state bands in all studied isotopes, and good agreement was achieved in energy levels of β and γ bands. In general, the experimental and the IBM-1 calculated energy levels in " $^{174-180}\text{Hf}$ isotopes" increase with angular momentum as I(I+1) because these isotopes are of rotational nuclei (deformed nuclei). Comparison between the ground state, β and γ bands of the experimentally determined energy levels and the IBM-1 calculations is shown in Fig. 2.

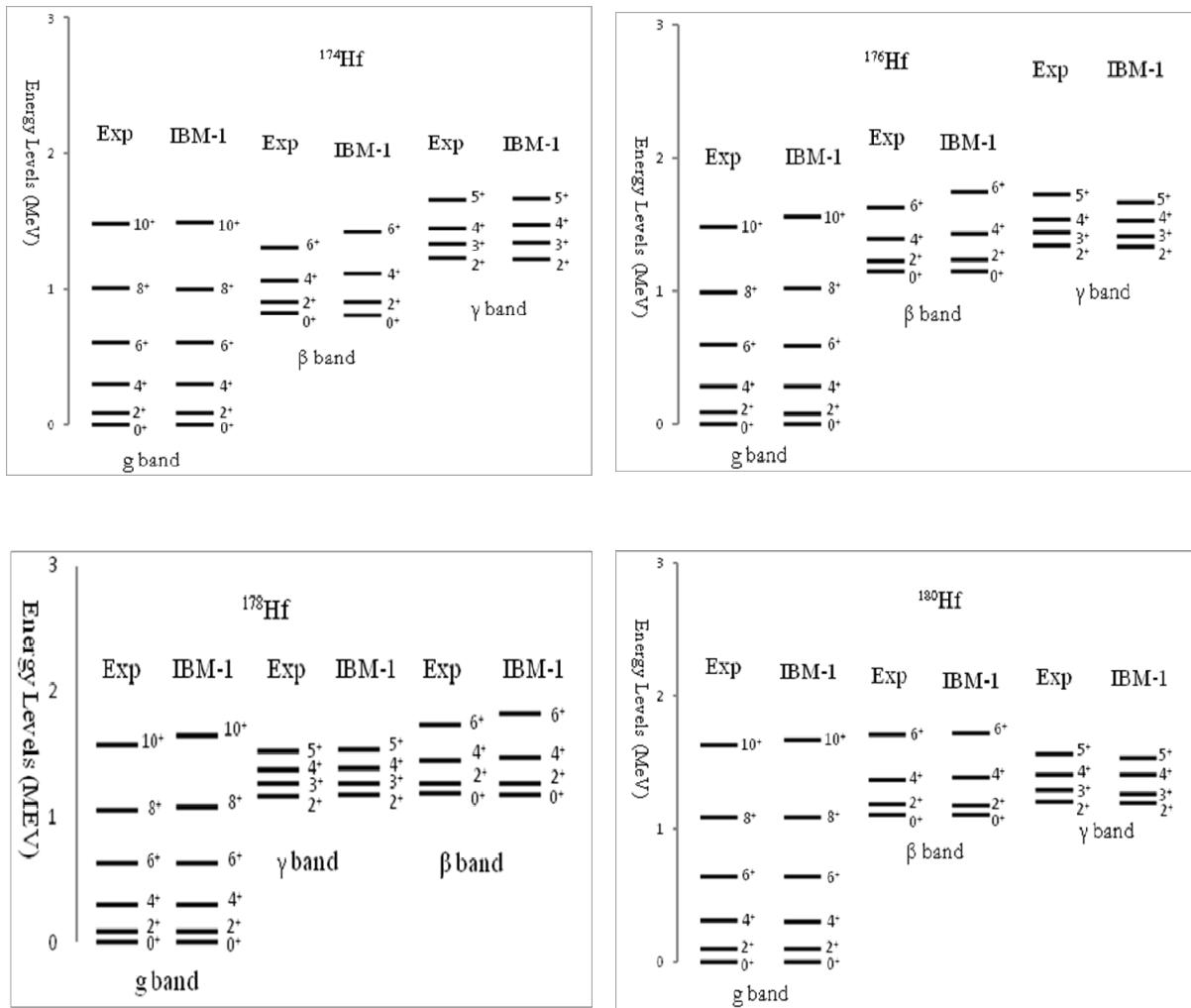


FIG. 2. The ground state, β and γ bands of the experimental and calculated energy levels of " $^{174-180}\text{Hf}$ isotopes".

Electric Transition Probabilities B(E2)

Once the wave functions have been fixed by fitting the energy levels, one could determine the electric transition probabilities B(E2) between these levels. The calculated B(E2) values for transitions in ¹⁷⁴⁻¹⁸⁰Hf isotopes" were obtained by employing Eq. 12. The used T^(E2) parameters of ¹⁷⁴⁻¹⁸⁰Hf isotopes" are given in Table 5.

TABLE 5. The used T^(E2) parameters α_2 and β_2 for ¹⁷⁴⁻¹⁸⁰Hf isotopes"

Isotopes	α_2 (eb)	β_2 (eb)
¹⁷⁴ Hf	0.043	-0.3000
¹⁷⁶ Hf	0.128	-0.0560
¹⁷⁸ Hf	0.129	-0.0381
¹⁸⁰ Hf	0.140	-0.0352

A comparison between the experimentally determined values of B(E2) [22-25] and those calculated by the IBM-1 model is given in Table 6, which shows that the B(E2) transitions between β -band and g-band and between γ -band and g-band are smaller than the B(E2) transitions between g-band and g-band, and this table shows also that, in general, there is a good agreement between the experimentally reported and calculated B(E2) values in ground state bands in ¹⁷⁴⁻¹⁸⁰Hf isotopes" except the transition

6_g^+ to 4_g^+ in ¹⁷⁸⁻¹⁸⁰Hf isotopes", where the experimental and calculated B(E2) values of this transition are weak in agreement. The experimental and calculated B(E2) transitions between β -band and g-band and between γ -band and g-band in general are weakly in agreement except the transitions 2_β^+ to 0_g^+ in ¹⁷⁶Hf isotope and 2_γ^+ to 0_g^+ in ¹⁷⁸Hf isotope which gave a very good agreement. The weak agreement between the experimental and calculated values in some B(E2) in those isotopes can be explained by the fact that many small components of the initial and final wave functions contribute coherently to the value of this reduced E2 transition probability, since these small components are not stable enough against small changes in the model parameters [17]. There is no available experimental transition data to many transitions in Table 6; therefore, it has been predicted by using IBM-1.

Table 6 shows that in general there is a good agreement between the experimentally reported B(E2) values and the theoretically calculated ones.

TABLE 6. Experimental and calculated B(E2) values of g-band to g-band, β -band to g-band and γ -band to g-band transitions in ¹⁷⁴⁻¹⁸⁰Hf isotopes"

I _i I _f	¹⁷⁴ Hf		¹⁷⁶ Hf		¹⁷⁸ Hf		¹⁸⁰ Hf	
	B(E2)(e ² b ²)		B(E2)(e ² b ²)		B(E2)(e ² b ²)		B(E2)(e ² b ²)	
	Exp	IBM-1	Exp	IBM-1	Exp	IBM-1	Exp	IBM-1
2_g^+ 0_g^+	0.877	0.870	1.07	1.06	0.95	0.95	0.936	0.939
4_g^+ 2_g^+	-	1.218	-	1.50	-	1.34	1.38	1.33
6_g^+ 4_g^+	-	1.290	-	1.63	1.30	1.45	1.32	1.43
8_g^+ 6_g^+	-	1.750	-	1.66	1.41	1.48	1.50	1.45
10_g^+ 8_g^+	-	1.215	-	1.65	1.51	1.48	1.44	1.43
2_β^+ 0_g^+	0.012	0.0013	0.00057	0.00057	0.0043	0.002	-	0.0073
2_β^+ 2_g^+	-	0.018	-	0.0091	-	0.0031	-	0.04
2_γ^+ 0_g^+	0.027	0.104	0.023	0.012	0.023	0.023	0.023	0.0033
2_γ^+ 2_g^+	0.042	0.113	-	0.019	0.026	0.037	0.031	0.006

Conclusions

Theoretical calculations using IBM-1 model were performed for $^{174-180}\text{Hf}$ isotopes" with proton number of 72. The ^{174}Hf isotope" has a total number of 15 bosons and is considered as weakly rotational (weakly deformed). This nucleus is located within the transitional region $\text{SU}(3) - \text{O}(6)$ with respect to the IBM-1 model. The $^{176-180}\text{Hf}$ isotopes" have bosons' total numbers of 16, 15 and 14, and are considered fully rotational (fully deformed) nuclei, and the dynamical symmetry of these isotopes is $\text{SU}(3)$. The low-lying positive parity states (energy levels) and the theoretically obtained values of

electric transition probabilities $B(E2)$ for these isotopes using IBM-1 model are compared with the experimentally reported values. A very good agreement was obvious. Therefore, it is possible to describe the energy levels of $^{176-180}\text{Hf}$ isotopes" by using the IBM-1 model. Moreover, it is worth mentioning that more experimental investigation on $^{176-180}\text{Hf}$ isotopes" $B(E2)$ values is required in order to identify the strength of $E2$ transitions within the ground state band, from β -band to ground band and from γ -band to ground band.

References

- [1] Arima, A. and Iachello, F., *Phys. Rev. Lett.* 35 (1975) 1069.
- [2] Arima, A. and Iachello, F., *Ann. Phys.* 99 (1976) 253.
- [3] Arima, A. and Iachello, F., *Ann. Phys.* 111 (1978) 201.
- [4] Arima, A. and Iachello, F., *Phys. Rev. Lett.* 40 (1978) 385.
- [5] Arima, A. and Iachello, F., *Ann. Phys.* 123 (1979) 468.
- [6] Arima, A. and Iachello, F., *Ann. Rev. Nucl. Part. Sci.* 31 (1981) 75.
- [7] Eckert, R., Fischer, C., Fransen, R.D., Herzberg, D., Jäger, R.V., Jolos, U., Kneissl, B., Krischok, J., Margraf, H., Maser, A., Nord, H.H., Pitz, M., Rittner, A.S. and Zilges, A., *Nucl. Phys. A*, 618(1-2) (1971) 141.
- [8] Raymond, K., Sheline, D., Burke, G., Michael, M.M. and Sood, P.C., *Phys. Rev. C*, 48 (1993) 911.
- [9] Zaitz, J.I. and Sheline, R.K., *Phys. Rev. C*, 6 (1972) 506.
- [10] Ejiri, H. and Hagemann, G.B., *Nucl. Phys. A*, 161 (2) (1971) 449.
- [11] Khoo, T.L., Bernthal, F.M., Robertson, R.G.H. and Warner, R.A., *Phys. Rev. Lett.* 37 (1976) 823.
- [12] Hague, A.M.I., Casten, R.F., Förster, I., Gelberg, A., Rascher, R., Richter, R., Von Brentano, P., Berreau, G., Börner, H.G., Kerr, S.A., Schreckenbach, K. and Warner, D.D., *Nucl. Phys. A*, 455(2) (1986) 231.
- [13] Bushnell, D.L., Buss D.J. and Smither, R.K., *Phys. Rev. C*, 10 (1974) 2483.
- [14] Kondurov, I.A., Korotkikh, E.M., Petrov, Yu.V. and Shuljak, G.I., *Phys. Lett. B*, 106 (5) (1981) 383.
- [15] Morikawa, T., Gono, Y., Morita, K., Kishida, T., Murakami, T., Ideguchi, E., Kumagai, H., Liu, G.H., Ferragut, A., Yoshida, A., Zhang, Y.H., Oshima, M., Sugawara, M., Kusakari, H., Ogawa, M., Nakajima, M., Tsuchida, H., Mitarai, S., Odahara, A., Kidera, M., Shibata, M., Kim, J.C., Chae, S.J., Hatsukawa, Y. and Ishih, M., *Phys. Lett. B*, 350 (2) (1995) 169.
- [16] Raman, S., Malarkey, C.H., Milner, W.T., Nestor, C.W. and Stelson, P.H., *Atm. Data Ncl. Data Tables*, 36 (1) (1987) 1.
- [17] Atalay, K. and Kaan, M., *Math. Comp. App.* 10 (1) (2005) 9.
- [18] Casten, R.F. and Warner, D.D., *Rev. Mod. Phys.* 60 (1988) 389.
- [19] Harun, R., Yazar, S., Ihsan, U., Volkan, U. and Sinan, Y., *Chi. J. Phys.* 48(3) (2010) 314.
- [20] Iachello, F. and Arima, A., "The Interacting Boson Model". (Cambridge University Press, Cambridge, England, 1987).
- [21] Yazar, H.R. and Erdem, U., *Chi. J. Phys.* 46 (3) (2008) 270.
- [22] Browne, E. and Huo, J., *Nucl. Data Sheets*, 87 (1999) 94.
- [23] Basuni, A.M.S., *Nucl. Data Sheets*, 107 (2006) 865.
- [24] Achterberg, E., Capurro, O.A. and Marti, G.V., *Nucl. Data Sheets*, 110 (2009) 1506.
- [25] Wu, S.C. and Niu, H., *Nucl. Data Sheets*, 100 (2003) 493.
- [26] Xu, F.X., Wu, C.S. and Zeng, J.Y., *Phys. Rev. C*, 40 (5) (1989) 2337.

Authors Index

Al-Maqtary K. A.	51
Al-Rudainy A. A.	43
Al-Sharaby M. N.	51
Al-Zuhairy M. H.	51
Nawafleh K. I.	39
Shamlan N. A.	51
Taketomi S.	1

Subject Index

Action integral	39
Aggregation	1
Ca ²⁺ and K ⁺ channels.....	43
Electrodynamics.....	39
Energy levels.....	51
Ferrofluid	1
Hafnium isotopes.....	51
Hamilton-Jacobi.....	39
Interacting boson model.....	51
Ionic conductance	43
Lagrangian	39
Landau criterion.....	1
Magnetic colloidal particle	1
Magnetic fluid.....	1
Magnetic nanoparticle.....	1
Membrane potential.....	43
Micelle	1
<i>Paramecium</i>	43
Phase transition of second order	1
Potassium and calcium currents.....	43
Reversal time	43

المناقشة: يجب أن تكون موجزة وتركز على تفسير النتائج.

الاستنتاج: يجب أن يكون وصفا موجزا لأهم ما توصلت إليه الدراسة ولا يزيد عن صفحة مطبوعة واحدة.

الشكر والعرفان: الشكر والإشارة إلى مصدر المنح والدعم المالي يكتبان في فقرة واحدة تسبق المراجع مباشرة.

المراجع: يجب طباعة المراجع بأسطر مزدوجة ومرقمة حسب تسلسلها في النص. وتكتب المراجع في النص بين قوسين مربعين. ويتم اعتماد اختصارات الدوريات حسب نظام Wordlist of Scientific Reviewers.

الجدول: تعطى الجداول أرقاماً متسلسلة يشار إليها في النص. ويجب طباعة كل جدول على صفحة منفصلة مع عنوان فوق الجدول. أما الحواشي التفسيرية، التي يشار إليها بحرف فوقي، فتكتب أسفل الجدول.

الرسوم التوضيحية: يتم ترقيم الأشكال والرسومات والرسومات البيانية (المخططات) والصور، بصورة متسلسلة كما وردت في النص.

تقبل الرسوم التوضيحية المستخرجة من الحاسوب والصور الرقمية ذات النوعية الجيدة بالأبيض والأسود، على أن تكون أصيلة وليست نسخة عنها، وكل منها على ورقة منفصلة ومعرفة برقمها بالمقابل. ويجب تزويد المجلة بالرسومات بحجمها الأصلي بحيث لا تحتاج إلى معالجة لاحقة، وألا تقل الحروف عن الحجم 8 من نوع Times New Roman، وألا تقل سماكة الخطوط عن 0.5 وبكثافة متجانسة. ويجب إزالة جميع الألوان من الرسومات ما عدا تلك التي ستنتشر ملونة. وفي حالة إرسال الرسومات بصورة رقمية، يجب أن تتوافق مع متطلبات الحد الأدنى من التمايز (1200 dpi Resolution) لرسومات الأبيض والأسود الخطية، و 600 dpi للرسومات باللون الرمادي، و 300 dpi للرسومات الملونة. ويجب تخزين جميع ملفات الرسومات على شكل (jpg)، وأن ترسل الرسوم التوضيحية بالحجم الفعلي الذي سيظهر في المجلة. وسواء أرسل المخطوط بالبريد أو عن طريق الشبكة (Online)، يجب إرسال نسخة ورقية أصلية ذات نوعية جيدة للرسومات التوضيحية.

مواد إضافية: تشجع المجلة الباحثين على إرفاق جميع المواد الإضافية التي يمكن أن تسهل عملية التحكيم. وتشمل المواد الإضافية أي اشتقاقات رياضية مفصلة لا تظهر في المخطوط.

المخطوط المنقح (المعدل) والأقراص المدمجة: بعد قبول البحث للنشر وإجراء جميع التعديلات المطلوبة، فعلى الباحثين تقديم نسخة أصلية ونسخة أخرى مطابقة للأصلية مطبوعة بأسطر مزدوجة، وكذلك تقديم نسخة إلكترونية تحتوي على المخطوط كاملاً مكتوباً على Microsoft Word for Windows 2000 أو ما هو استجد منه. ويجب إرفاق الأشكال الأصلية مع المخطوط النهائي المعدل حتى لو تم تقديم الأشكال إلكترونياً. وتخزن جميع ملفات الرسومات على شكل (jpg)، وتقدم جميع الرسومات التوضيحية بالحجم الحقيقي الذي ستظهر به في المجلة. ويجب إرفاق قائمة ببرامج الحاسوب التي استعملت في كتابة النص، وأسماء الملفات على قرص مدمج، حيث يعلم القرص بالاسم الأخير للباحث، وبالرقم المرجعي للمخطوط للمراسلة، وعنوان المقالة، والتاريخ. ويحفظ في مغلف واق.

الفهرسة: تقوم المجلة الأردنية للفيزياء بالإجراءات اللازمة لفهرستها وتلخيصها في جميع الخدمات الدولية المعنية.

حقوق الطبع

يُشكّل تقديم مخطوط البحث للمجلة اعترافاً صريحاً من الباحثين بأن مخطوط البحث لم يُنشر ولم يُقدّم للنشر لدى أي جهة أخرى كانت وبأي صيغة ورقية أو إلكترونية أو غيرها. ويُشترط على الباحثين ملء نموذج يُنصّ على نقل حقوق الطبع لتصبح ملكاً لجامعة اليرموك قبل الموافقة على نشر المخطوط. ويقوم رئيس التحرير بتزويد الباحثين بإنموذج نقل حقوق الطبع مع النسخة المُرسلة للتنقيح. كما ويُمنع إعادة إنتاج أي جزء من الأعمال المنشورة في المجلة من دون إذن خطي مُسبق من رئيس التحرير.

إخلاء المسؤولية

إن ما ورد في هذه المجلة يعبر عن آراء المؤلفين، ولا يعكس بالضرورة آراء هيئة التحرير أو الجامعة أو سياسة اللجنة العليا للبحث العلمي أو وزارة التعليم العالي والبحث العلمي. ولا يتحمل ناشر المجلة أي تبعات مادية أو معنوية أو مسؤوليات عن استعمال المعلومات المنشورة في المجلة أو سوء استعمالها.

معلومات عامة

المجلة الأردنية للفيزياء هي مجلة بحوث علمية عالمية مُحكمة تصدر عن اللجنة العليا للبحث العلمي، وزارة التعليم العالي والبحث العلمي، عمان، الأردن. وتقوم بنشر المجلة عمادة البحث العلمي والدراسات العليا في جامعة اليرموك، إربد، الأردن. وتُنشر البحوث العلمية الأصلية، إضافة إلى المراسلات القصيرة Short Communications، والملاحظات الفنية Technical Notes، والمقالات الخاصة Feature Articles، ومقالات المراجعة Review Articles، في مجالات الفيزياء النظرية والتجريبية، باللغتين العربية والإنجليزية.

تقديم مخطوط البحث

تُرسل نسخة أصلية وثلاث نسخ من المخطوط، مُرفقة برسالة تغطية من جانب الباحث المسؤول عن المراسلات، إلى رئيس التحرير:

أ.د. ابراهيم أبو الجرايش،

رئيس التحرير، المجلة الأردنية للفيزياء،

عمادة البحث العلمي والدراسات العليا،

جامعة اليرموك، إربد، الأردن.

هاتف : 00 962 2 72 11 111 / فرعي: 2075

فاكس : 00 962 2 72 11 121

بريد إلكتروني : jjp@yu.edu.jo

تقديم المخطوطات إلكترونياً: اتبع التعليمات في موقع المجلة على الشبكة العنكبوتية.

ويجري تحكيم البحوث الأصلية والمراسلات القصيرة والملاحظات الفنية من جانب مُحكمين اثنين في الأقل من ذوي الاختصاص والخبرة. وتُشجّع المجلة الباحثين على اقتراح أسماء المحكمين. أما نشر المقالات الخاصة في المجالات الفيزيائية النشطة، فيتم بدعوة من هيئة التحرير، ويُشار إليها كذلك عند النشر. ويُطلب من كاتب المقال الخاص تقديم تقرير واضح يتسم بالدقة والإيجاز عن مجال البحث تمهيداً للمقال. وتُنشر المجلة أيضاً مقالات المراجعة في الحقول الفيزيائية النشطة سريعة التغير، وتُشجّع كاتبها مقالات المراجعة أو مُستكثبيها على إرسال مقترح من صفحتين إلى رئيس التحرير. ويُرفق مع البحث المكتوب باللغة العربية ملخص (Abstract) وكلمات دالة (Keywords) باللغة الإنجليزية.

ترتيب مخطوط البحث

يجب أن تتم طباعة مخطوط البحث ببنط 12 نوعه Times New Roman، ويسطر مزدوج، على وجه واحد من ورق A4 (21.6 × 27.9 سم) مع حواشي 3.71 سم، باستخدام معالج كلمات ميكروسوفت وورد 2000 أو ما استُجد منه. ويجري تنظيم أجزاء المخطوط وفق الترتيب التالي: صفحة العنوان، الملخص، رموز التصنيف (PACS)، المقدمة، طرق البحث، النتائج، المناقشة، الخلاصة، الشكر والعرفان، المراجع، الجداول، قائمة بدليل الأشكال والصور والإيضاحات، ثم الأشكال والصور والإيضاحات. وتُكتب العناوين الرئيسية بخط غامق، بينما تُكتب العناوين الفرعية بخط مائل.

صفحة العنوان: وتشمل عنوان المقالة، أسماء الباحثين الكاملة وعناوين العمل كاملة. ويكتب الباحث المسؤول عن المراسلات اسمه مشاراً إليه بنجمة، والبريد الإلكتروني الخاص به. ويجب أن يكون عنوان المقالة موجزاً وواضحاً ومعبراً عن فحوى (محتوى) المخطوط، وذلك لأهمية هذا العنوان لأغراض استرجاع المعلومات.

الملخص: المطلوب كتابة فقرة واحدة لا تزيد على مائتي كلمة، موضحة هدف البحث، والمنهج المتبع فيه والنتائج وأهم ما توصل إليه الباحثون.

الكلمات الدالة: يجب أن يلي الملخص قائمة من 4-6 كلمات دالة تعبر عن المحتوى الدقيق للمخطوط لأغراض الفهرسة.

PACS: يجب إرفاق الرموز التصنيفية، وهي متوافرة في الموقع <http://www.aip.org/pacs/pacs06/pacs06-toc.html>.

المقدمة: يجب أن توضّح الهدف من الدراسة وعلاقتها بالأعمال السابقة في المجال، لا أن تكون مراجعة مكثفة لما نُشر (لا تزيد المقدمة عن صفحة ونصف الصفحة مطبوعة).

طرائق البحث (التجريبية / النظرية): يجب أن تكون هذه الطرائق موضحة بتفصيل كاف لإتاحة إعادة إجرائها بكفاءة، ولكن باختصار مناسب، حتى لا تكون تكراراً للطرائق المنشورة سابقاً.

النتائج: يستحسن عرض النتائج على صورة جداول وأشكال حيثما أمكن، مع شرح قليل في النص ومن دون مناقشة تفصيلية.

Jordan Journal of

PHYSICS

An International Peer-Reviewed Research Journal

Published by the Deanship of Research & Graduate Studies, Yarmouk University, Irbid, Jordan

Name: الأسم:
 Specialty: التخصص:
 Address: العنوان:
 P.O. Box: صندوق البريد:
 City & Postal Code: المدينة/الرمز البريدي:
 Country: القطر:
 Phone: رقم الهاتف:
 Fax No: رقم الفاكس:
 E-mail: البريد الإلكتروني:
 No. of Subscription: عدد الاشتراكات:
 Method of Payment: طريقة الدفع:
 Amount Enclosed: المبلغ المرفق:
 Signature: التوقيع:

Cheques should be paid to Deanship of Research and Graduate Studies - Yarmouk University.

I would like to subscribe to the Journal
For

- / One Year
- / Two Years
- / Three Years

One Year Subscription Rates

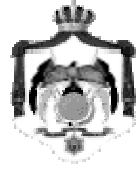
	Inside Jordan	Outside Jordan
Individuals	JD 8	€ 40
Students	JD 4	€ 20
Institutions	JD 12	€ 60

Correspondence**Subscriptions and Sales:**

Prof. Ibrahim O. Abu-AlJarayesh
 Deanship of Research and Graduate Studies
 Yarmouk University
 Irbid – Jordan
Telephone: 00 962 2 711111 Ext. 2075
Fax No.: 00 962 2 7211121



جامعة اليرموك



المملكة الأردنية الهاشمية

المجلة الأردنية
للفيزياء
مجلة بحوث علمية عالمية محكمة

المجلد (4)، العدد (1)، 2011م / 1432هـ

المجلة الأردنية
للفيزياء
مجلة بحوث علمية عالمية محكمة

المجلد (4)، العدد (1)، 2011م / 1432هـ

المجلة الأردنية للفيزياء: مجلة بحوث علمية عالمية محكمة أسستها اللجنة العليا للبحث العلمي، وزارة التعليم العالي والبحث العلمي، الأردن، وتصدر عن عمادة البحث العلمي والدراسات العليا، جامعة اليرموك، إربد، الأردن.

رئيس التحرير:

ابراهيم عثمان أبو الجرايش

قسم الفيزياء، جامعة اليرموك، إربد، الأردن.

ijaraysh@yu.edu.jo

هيئة التحرير:

ضياء الدين محمود عرفة

قسم الفيزياء، الجامعة الأردنية، عمان، الأردن.

darafah@ju.edu.jo

نديل يوسف أيوب

قسم الفيزياء، جامعة اليرموك، إربد، الأردن.

nayoub@yu.edu.jo

هشام بشارة غصيب

جامعة الأميرة سمية للتكنولوجيا، عمان، الأردن.

ghassib@psut.edu.jo

جميل محمود خليفة

قسم الفيزياء، الجامعة الأردنية، عمان، الأردن.

jkalifa@ju.edu.jo

سامي حسين محمود

قسم الفيزياء، الجامعة الأردنية، عمان، الأردن.

s.mahmood@ju.edu.jo

مروان سليمان موسى

قسم الفيزياء، جامعة مؤتة، الكرك، الأردن.

mmousa@mutah.edu.jo

نهاد عبد الرؤوف يوسف

قسم الفيزياء، جامعة اليرموك، إربد، الأردن.

nihadyusuf@yu.edu.jo

خلف عبد العزيز المساعيد

قسم الفيزياء التطبيقية، جامعة العلوم والتكنولوجيا الأردنية، إربد، الأردن.

khalaf@just.edu.jo

سكرتير التحرير: مجدي الشناق

ترسل البحوث إلى العنوان التالي:

الأستاذ الدكتور إبراهيم عثمان أبو الجرايش
رئيس تحرير المجلة الأردنية للفيزياء
عمادة البحث العلمي والدراسات العليا، جامعة اليرموك
إربد، الأردن

هاتف 00 962 2 7211111 فرعي 2075

E-mail: jjp@yu.edu.jo

Website: <http://Journals.yu.edu.jo/jjp>

